Electrochemical Synthesis of Functional Nanowires

Mirette Fawzy

Supervised by Professor Mark Blumenthal
Department of Physics
University of Cape Town

A thesis submitted for the degree of Master of Science

February 2016

Acknowledgements

I would like to express my gratitude to my supervisor Professor Mark Blumnethal for his valuable comments, remarks and assistance. His continuous encouragement, understanding, and support helped me a lot at the frustrating and stressful times. I am also indebted to Dr. Pieter Levecque at the Chemical Engineering Department for providing me with the required equipment and platform for the electrochemical synthesis work. Without his help and enthusiasm towards establishing this new field of work within the university, this project could not have been possible. Furthermore, I am thankful to Miranda Waldron and Mohamed Jaffer from the Centre of Imaging and Analysis for their assistance with thermal evaporations, SEM, and TEM measurements. I also thank Dr. Franscious Cummings, Earl McDonald and Adrian Josephs from the University of Western Cape for allowing me to use their facilities for SEM and TEM measurements. And from iThemba LABS, I would like to extend my gratitude to Zakhele Khumalo for the XRD measurements and Dr. Godfrey for the optical characterizations. I am also very grateful to Dr. Dave English and Dr. Hume Howe from the University of College London for the assistance in electrical and photoconductivity measurements. Many thanks to Marija Ojdanic for the help during the annealing process and all the work on single-nanowire devices with Dr. Alexey Ilin at the Kotelnikov Institute of Radiotechnology and Electronics of Russian Academy of Science. Additional thanks to Niels Luchters and Waldo Koorts for the assistance with the gas chromatography measurements.

Abstract

Semiconducting, metal, and multi-segmented nanowires of 200 nm diameters with lengths up to 10 μm were synthesized through electrochemical deposition in the pores of anodic aluminium oxide (AAO) and polycarbonate track-etched (PCTE) templates. With the work focusing on CdSe nanowires, results from the cyclic electrodeposition/stripping method was reported with different deposition conditions (potential range, solution, and scan rate). The stoichiometric deposition of CdSe nanowires was confirmed by energy dispersive spectroscopy (EDS) analysis, with an average Cd:Se atomic percentage of 0.92. Structural characterizations were done on the synthesized nanowires via scanning electron microscopy (SEM), transmission electron microscopy (TEM), and X-ray diffraction (XRD) measurements. Devices with a single CdSe nanowire were made by standard electron beam lithography techniques. Electrical transport measurements were performed on the nanowire arrays as well as single contacted CdSe nanowires. Photo response measurements were also carried out on the samples in the dark and under illumination. The nanowire arrays showed pronounced visible light photoconductivity. As a direct application, a preliminary proof-of-concept photoelectrochemical activity test for water splitting using the synthesized CdSe nanowires was performed in a water/methanol mixture.

Declaration

I, the undersigned, hereby declare that the work contained in this thesis is my original work, and that any work done by others or by myself previously has been acknowledged and referenced accordingly.

Signed by candidate

signature Removed

Mirette Fawzy, February 2016

Contents

Abbreviations

AAO	Anodic Aluminum Oxide
CB	Conduction Band
CE	Counter Electrode
CV	Cyclic Voltamm (etry/ogram)
CVD	Chemical Vapour Deposition
EDS/EDX	Energy Dispersive Xray Spectroscopy
ESED	Electrochemical Step Edge Decoration
FTO	Fluorine-doped Tin Oxide
GC	Gas Chromatography
HOPG	Highly Oriented Pyrolytic Graphite
ITO	Indium Tin Oxide
LPNE	Lithographically Patterned Nanowire Electrodeposition
NHE	Normal Hydrogen Electrode
P3HT	Poly(3-hexylthiophene)
PAO	Porous Aluminium Oxide
PCTE	Polycarbonate Track-Etched
PEDOT:PSS	Poly(3,4-ethylenedioxythiophene) poly-(styrenesulfonate)
RE	Reference Electrode
SAED	Selected Area Electron Diffraction
SCE	Saturated Calomel Electrode
SEM	Scanning Electron Microscop(e/y)
SLS	Solution-Liquid-Solid
TEM	Transmission Electron Microscop(e/y)
UV-VIS	Ultraviolet-Visible
VB	Valence Band
VLS	Vapour-Liquid-Solid
WE	Working Electrode
XRD	X-Ray Diffraction

1. Introduction

Nanowires are a type of one-dimensional nanostructure, which are extremely small in diameter (few to hundreds of nanometers) and large in surface-to-volume ratio. The physical properties of the nanowires differ from their bulk counterparts, due to their unique density of electronic states. Other forms of one-dimensional nanostructures are nanorods, nanotubes, and nanobelts. The remarkable increase in one-dimensional research field was triggered by the discovery of carbon nanotubes in the early 1990s (Iijima, 1991). Since then, many researchers have explored various chemical and physical methods to synthesize one-dimensional structures with controlled size and composition (Hu et al., 1999; Xia et al., 2003). Several important sub-fields have emerged in the research of nanowires such as nanowire photonics (Yan et al., 2009), nanowires for energy conversion and storage (Hochbaum and Yang, 2009), nanowire electronics (Thelander et al., 2006), and nanowire biochemical sensing (García et al., 2014).

In particular, semiconducting nanowires have attracted much attention due to their distinctive physical properties (Lu and Lieber, 2006) and their potential role in future electronic and optoelectronic devices. Among the promising functions of semiconducting nanowires is their utilization in solar energy harvesting and conversion (Dasgupta and Yang, 2014; Qu and Duan, 2012). The high density and large surface area of these nanowires makes them ideal candidates for photoelectrochemical applications as a significant fraction of atoms or molecules can participate in the desired surface redox reactions, thus enhancing the efficiency of the photocatalytic process.

1.1 Motivation

While fossil fuels such as coal, oil and natural gas are the main sources of generating energy currently, their impact on the environment and their contribution to global warming and climate change have increased concerns of procuring an alternative source that is cleaner and more abundant. The world is becoming united in using more renewable energy as it is generally unlimited and has minimal impact on the environment. If properly harnessed, renewable energy is capable of providing the whole world with its needs of energy for the foreseeable future.

One of the rapidly growing fields of research and most abundant natural source of renewable energy is solar energy which, unlike other renewable sources such as wind, biomass or nuclear energy, is more feasible to harness and more efficient in producing electricity on a large scale. Furthermore, its limited impact on the environment makes it the most preferable source of green energy as the production of energy process does not require any fossil fuels and it does not leave any kind of waste. Every year the earth receives about 1.2×10^5 TW of solar energy, such large amount of energy that only 0.02% is enough to provide equivalent energy to all fossil fuels and nuclear plants combined. However, harnessing such a relatively small percentage of solar energy seems to be one of the most difficult challenges for three reasons; namely, harvest, conversion into usable electric energy and storage of solar energy for later usage. The most commonly used technique of harvesting solar energy is by using a photovoltaic cell that, when irradiated, absorbs sunlight and uses it to excite electrons of a semiconductor material to move freely generating electrical current. With relatively low efficiency (20-35%) and the need for external storage units such as batteries or supercapacitors, the need for another technique has risen. The photocatalytic solar fuel generation technique aims to address the three problems of harvest, conversion and storage of solar energy at the same time. One of the currently used strategies is to attempt to split water into hydrogen and oxygen and store the solar energy as a chemical fuel inside a carrier

(in this case, the hydrogen) thus solving the three main challenges at once. Hydrogen generation via photocatalytic water splitting provides a promising route because it utilizes two renewable resources, sunlight and water. Moreover, when hydrogen is used in fuel cells to produce energy, the only byproduct of the process is water.

This work presents attempts to lay the background for fabrication of photocatalytically active nanowires and heterostructures (axially-segmented nanowires), which can then be utilized in the process of water splitting and hydrogen production. In this study, CdSe was used as a model semiconductor-solar-energy absorber for several reasons. CdSe is a highly absorbing, direct bandgap semiconductor which is expected to show strong photoconductivity. The bandgap of CdSe is 1.7 eV, which is well-matched to the visible part of the solar spectrum, hence visible light has sufficient energy to excite electrons from the valence band to the conduction band. This is particularly important in solar energy harvesting as the visible spectrum accounts for $\sim$ 44% of the total solar energy irradiation.

1.2 Outline

The main purpose of this thesis is to describe the electrochemical deposition of photocatalytically active nanowires and their applications. To this end, the chapters reported here are divided into two main domains. The first part of the work deals with the fabrication and characterization of the nanowires, while the second part covers the utilization of these wires in electrical measurements and photocatalytic applications.

In more detail, the thesis is organized as follows: Chapter 2 introduces the templated electrodeposition technique used throughout this work to fabricate the nanowires, followed by an overview of CdSe nanostructures electrodeposition. Chapter 3 includes all the detailed experimental procedures that are necessary for templated electrodeposition and provides a know-how for preparing the required materials. Chapter 4 explores the electrical transport characteristics in the synthesized nanowire arrays, together with the fabrication and investigation of single CdSe nanowire based devices. Chapter 5 presents an introduction to the aspects of photocatalysis and examines the applications of CdSe nanowires in photocatalytic production of hydrogen gas. Finally, chapter 6 provides a summary of the work with a discussion of future studies.

2. Templated Electrodeposition Technique

Templated electrodeposition is an extensively used technique to fabricate functional nanowires with different dimensions. This chapter provides an introduction to this procedure, which will be employed throughout the work of this thesis.

The chapter is divided into four main sections. After a brief presentation on one-dimensional structures synthesis methods and growth mechanisms in section 2.1, section 2.2 introduces the different templates utilized in templated electrodeposition. Section 2.3 addresses the theoretical aspects of electrochemical deposition process. Finally, section 2.4 explores the various mechanisms used in synthesizing CdSe which is the main focus of the coming work.

2.1 One Dimensional Structures Preparation Methods

Many techniques have been developed for the fabrication of nanostructures. In this section, we briefly discuss the different approaches for one-dimensional structures growth followed by the various chemistries used in preparing template-synthesized nanostructures and the advantages associated with the templated electrodeposition process.

There are basically two main approaches in creating very small structures or devices. The first approach is the so called *top-down*, where the macro-scale materials are transformed into nano-scale dimensions by a series of sequential reduction procedures. The most common top-down mechanism is lithography. In this technique, the base material is shielded by a mask (photoresist) and then exposed to a high energy light beam (photolithography) or an electron beam (e-beam lithography), which develop a pattern in the photoresist. The resist can then be etched away, using proper solvents, leaving behind the desired structure. The second approach is known as the *bottom-up* construction method, which is most widely used and a more controllable procedure. It involves the direct growth of one-dimensional nanostructures onto a substrate, using various chemical methods.

According to the synthesis environment, one-dimensional nanostrucutres can be divided into two main categories*; vapour phase growth and liquid phase growth. Chemical Vapour Deposition (CVD) (Shan et al., 2007) and Vapour-Liquid-Solid (VLS) (Ma and Wang, 2005) are examples of the former, while Solution-Liquid-Solid (SLS) (Grebinski et al., 2004) and hydrothermal method are examples of the latter (Peng et al., 2002; Vayssieres, 2003).

2.1.1 Template Synthesized Nanostructures

When a deposition process that does not induce one-dimensional growth is applied, a template is then required to produce an array of nano-wires, rods or tubes. The template synthesis method, which makes use of nano- or micro- porous membranes, is one of the most popular bottom-up techniques to fabricate nanomaterials.

Typically, this mechanism includes fabricating a desired material within the pores of the membrane, which have cylindrical channels of a certain diameter. A nano-cylinder of the desired material is then formed replicating the dimensions of the pores, which can be either solid (nanowire) or a hollow structure

*The articles referenced here are those associated with CdSe nanostructures fabrication.

(nanotube). This depends strongly on the synthesizing conditions and on the structure of the pore walls.

The main advantage of this template-based technique is the fine control over the dimensions of the produced materials. Using AAO templates in particular (discussed in the following section), where various sets of the manufacturing parameters can be altered resulting in different pore sizes, allows generating of highly controlled aspect ratio structures which is not easy with the other solution-based methods.

There are various types of chemistries that can be used to prepare template-synthesized nanostructures. The major chemical strategies that are suitable for filling the pores will be reviewed below (Hulteen and Martin, 1997, and references therein). First is the *chemical polymerization* technique, where the fabrication of many polymers can be done by immersing the porous template into a solution of the desired monomers and a suitable polymerization reagent. Second is combining the *chemical vapour deposition* method with template synthesis. Next is the *sol-gel* chemistry, which involves hydrolysis of a solution of a precursor molecule to obtain first a suspension of colloidal particles (the sol) and then a gel composed of aggregated sol particles. This gel is thermally treated afterwards to yield the desired product. Another chemical route to fill the templates is the *electroless deposition* process, which involves the reduction of metal ions in solution using a chemical reducing agent. The final process is the *electrochemical deposition* or *electrodeposition*, which will be discussed in detail in section 2.3.

Electrodeposition offers many advantages over other chemical routes for the synthesis of one-dimensional nanostructures. Electrodeposition operates at temperatures less than 100°C, at ambient pressure, and does not require any expensive instrumentation. This makes it a simple, efficient, and cost-effective technique. Also, using electrodeposition, a wide range of metals, semiconductors and conductive polymers can be deposited. Moreover, the synthesized material can be easily controlled by the electrodeposition parameters such as the applied potential, temperature and composition of the electrolyte.

2.1.2 Template-Based Electrodeposition

Combining templates with the electrochemical deposition process resulted in an up-to-date widely used templated electrodeposition technique.

One of the very first attempts to fabricate nanowires using this method was achieved by Possin et al. who managed to synthesize single metal wires (Sn, In and Zn with diameters of 40 nm) in the holes of mica formed through etching of the damage tracks produced by high energy charged particles (Possin, 1970). The next big step was in the late 1980s when Penner and Martin published their results on fabricating an ultramicroelectrode made of platinum ensembles by templated electrodeposition in the pores of polycarbonate membranes (Penner and Martin, 1987).

Since these influential set of experiments pioneered by Martin (Martin, 1994, 1995, 1996), Moskovits (Almawlawi et al., 1991; Preston and Moskovits, 1993), and Searson (Whitney et al., 1993), tremendous amount of work has been done on fabricating different materials using templated electrodeposition. Various structures have been synthesized into the pores of AAO and PCTE templates such as metals, semiconductors, and conducting polymers (Hurst et al., 2006).

Other approaches using alternative templates, which are not associated with the commonly used AAO or PCTE templates, have been developed as well. One example is the electrochemical step edge decoration (ESED) technique (Roder et al., 1993), which utilizes step edges on single crystalline substrates as templates for the formation of nanowires. This technique results in a horizontally oriented nanowires, unlike the ones formed in the pores of membranes in a vertical orientation (i.e. perpendicular to the

plane of the electrode). Using this method, Penner et al. have managed to electrodeposit stoichiometric compound semiconductor nanowires, such as CdSe (Li et al., 2006) and Bi_2Te_3 (Menke et al., 2004, 2006a), on the step edges of highly oriented pyrolytic graphite (HOPG) surfaces.

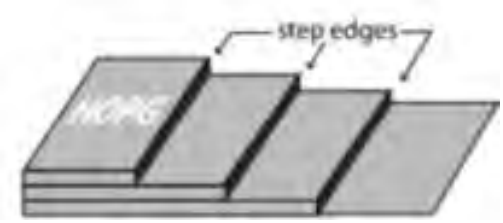

Figure 2.1: Schematic diagram showing the step edges of HOPG where nanowires can be formed (Li et al., 2006).

Another example is the lithography patterened nanowire electrodeposition (LPNE) technique developed by Penner and co-workers (Menke et al., 2006b), which combines lithography and electrodeposition. In this method, photolithography is used to define the nano-gaps or nano-bands which then act as a template for the nanostructures to be deposited. For instance, Kung et al. (Kung et al., 2010, 2011) and Talin et el. (Ayvazian et al., 2013) used this mechanism to prepare nanocrystalline CdSe nanowires.

2.1.3 Advantages of Templated Electrodeposition Technique

In addition to the separate advantages of both the template-synthesis method and the electrochemical deposition route mentioned above, templated electrodeposition has a number of interesting and useful features. One feature is the relative ease of formation of multi-segmented nanowires, which can be easily produced by varying the electrodeposition solution during the nanowires formation process. This presents an efficient way that allows for the direct coupling between segments with different functions in the same nanowire. For instance, in photocatalytic applications which will be discussed in chapter 5, the light absorber (semiconducting material) is easily incorporated with the required metal electro-catalysts to facilitate fast conversion and absorption of solar light into a usable chemical or electrical energy. Another important feature is the final product of templated electrodeposition; the arrays of parallel nanowires which offer several advantages for both studying the properties of the materials and investigating practical applications.

2.2 Templates

Since the introduction of the templated electrodeposition technique, various types of templates have been created and used as a mould for nanowires fabrication.

The template selected for electrodeposition should be electrically insulating to prevent materials from depositing directly onto it. It also has to withstand the deposition solution and conditions of the deposition process and to avoid blockage of the pores at any point. In other words, it has to be stable both chemically and thermally during the deposition. Additional concerns about the ability of the precursor solutions used to prepare desired materials, to wet (i.e. hydrophilic/hydrophobic conditions) the template pores should be taken into account as well. Other considerations include the ease of handling during the experiments and the ease of releasing the nanowires/tubes from the template afterwards.

Hard templates, which are mainly used in the fabrication of one dimensional structures, are membranes with well-confined nano or micro spaces in the form of channels or interconnected networks. These templates are generally fabricated by either ion-track etching (Young, 1958; Silk and Barnes, 1959) or electrochemical etching techniques. AAO (Masuda, 2005) and porous silicon (Aravamudhan et al., 2007) are examples of the latter. Commercial track-etched membranes are usually prepared from polycarbonate or polyester thin films (Fleischer et al., 1975), however other materials can be used in this technique such as polyimide and mica sheets (Possin, 1970).

Apart from ion-track and electrochemically etched membranes, other nanoporous materials could be employed as templates such as glass (Tonucci et al., 1992), self-organized block copolymer films (Kim et al., 2009a), zeolites (Senthilkumar et al., 2008), mesoporous silica (Wang et al., 2003), and a variety of nanoporous solids (Ozin, 1992).

While the template-assisted electrochemical fabrication of nanowires makes use of many of these porous membranes, AAO and PCTE templates which will be discussed below, are the two commonly used among many researchers including this work.

2.2.1 Anodic Aluminium Oxide Templates

AAO membranes are ceramic materials with a dense hexagonally-shaped pore structure. The pore channels are normal to the surface, and the pores can have sizes ranging from few nanometers up to a couple of hundred and with densities as high as 10^{11} per cm^2.

Figure 2.2 shows SEM images of the top and cross section of Whatman anodic alumina membrane. The diameter of the pores and the membrane thickness were measured to be around 200 nm and 60 $\mu\mathrm{m}$ respectively.

These templates are formed by anodic oxidation of aluminium foil in acidic electrolytes (Keller et al., 1953; Booker et al., 1957; Hoar and Mott, 1959; O'sullivan and Wood, 1970). First, a piece of cleaned and polished high purity aluminium foil is placed as an anode in an anodization acidic bath. A voltage is then applied between the two electrodes leading the formed alumina surface to arrange in a honeycomb structure.

Well-organized hexagonal AAO pore arrays were first reported by Masuda et al. after their work on refining anodization mechanisms via long-period anodization times and utilizing a two-step anodization process (Masuda and Fukuda, 1995; Masuda and Satoh, 1996; Masuda et al., 1997, 1998).

In the two-step anodizing process, which is typically used in lab-synthesized templates, a second anodization step is done after the aluminium foil surface is converted into porous alumina. Formed pores are then selectively etched away, leaving indentations which are then exposed to another anodization step as shown in figure 2.3. This technique enables the formation of a more ordered array of pores with a high aspect ratio.

Anodizing parameters such as voltage, temperature and composition of the bath may be varied to engineer the target pore size. Anodization time controls the thickness of the aluminum oxide layer.

An additional step is then required, where the original aluminium supporting layer and alumina interface between it and the bottom of the pores (barrier layer) are both etched resulting in the through-holes structure. This step is essential when the produced membrane is used in the electrochemical deposition process.

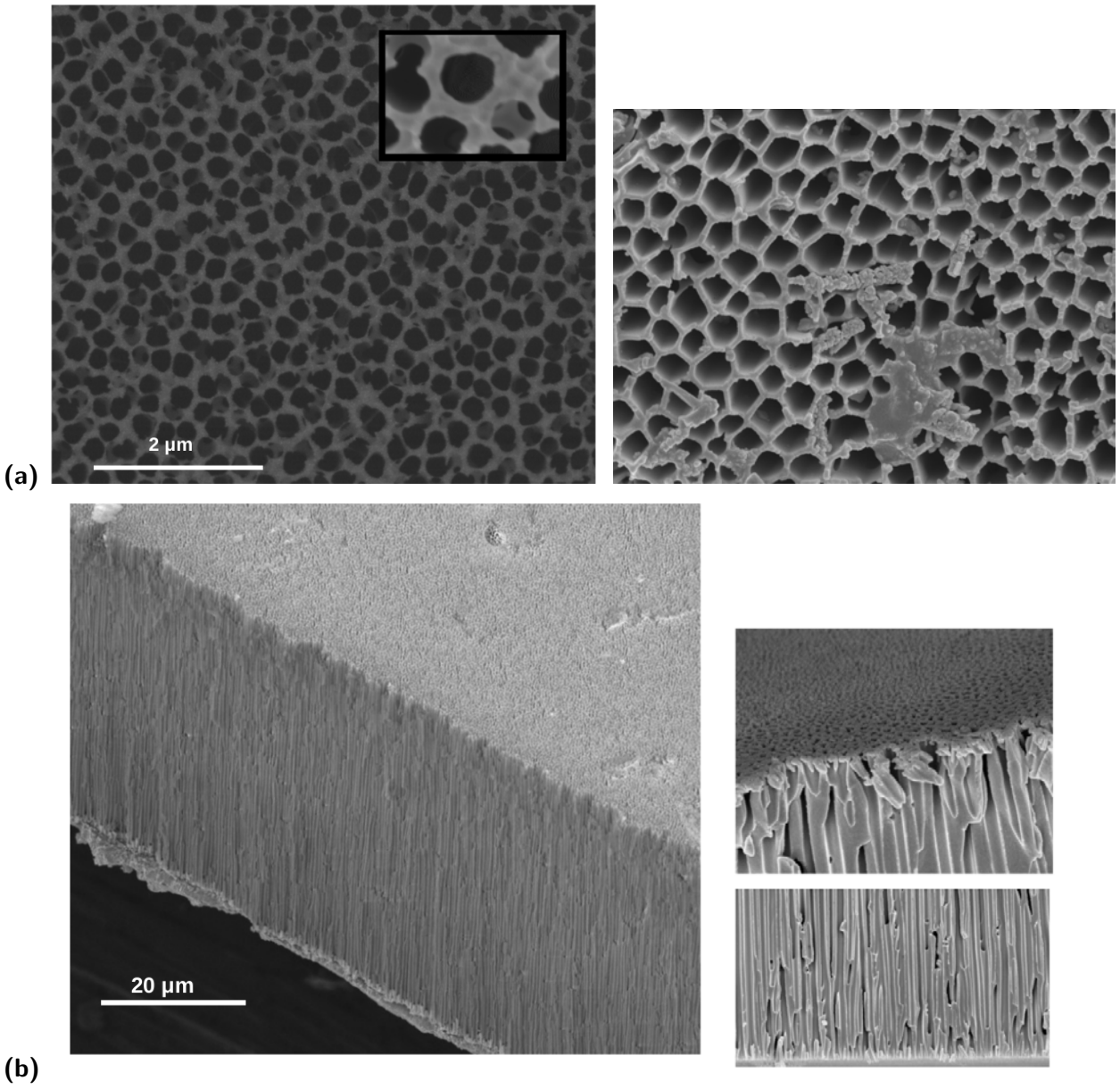

Figure 2.2: AAO templates:(a) top and (b) cross sectional views. The inset is a closer look at a single pore structure. Top right picture shows the honeycomb's structure of the pores after dissolving the surface of the template. Zoomed in (bottom right) cross sections appear rough as the template was simply broken by hand.

The AAO membranes, used in nanostructures fabrication, can be either purchased or produced in house by the two-step anodization method described above. Researchers tend to fabricate their own templates as they are more robust, easier to handle and much better in quality than the commercially available ones. For example, actual pore sizes of the commercially Whatman 0.2 μm template used in this work can sometimes go up to 350 nm as found during SEM inspections. This variation, which occurs within one template and/or across templates in the same box, is not ideal if precise dimensions are needed for the manufactured structures. Usually, purchased templates are used when dimensions are not critical to the performed experiments. Moreover, when used in further experiments, home-made templates provide

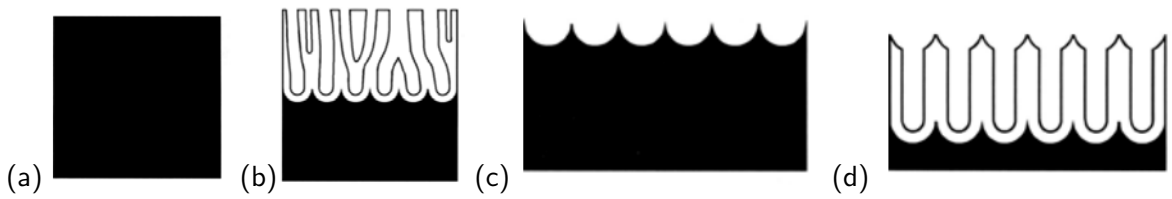

Figure 2.3: Schematic diagram of the two-step anodization process. (a) aluminium sheet, (b) after first anodization, (c) after etching alumina, and (d) ordered pore channels after second anodization (Masuda, 2005).

a set of diverse and easily controllable options such as the substrate choice. For instance, Schierhorn et al. (Schierhorn et al., 2009) have used porous aluminium oxide (PAO) grown on ITO-coated glass as a hard template to synthesize CdSe nanowire arrays and perform photoelectric measurements on them.

2.2.2 Polycarbonate Track Etched Templates

PCTE templates are flexible, nano or micro-porous membranes made from a thin polycarbonate film material. The pores are formed through bombardment of the film with high energy charged particles, causing randomly spaced, cylindrical damage tracks in the membrane. These tracks are then chemically etched to form uniform pores with densities as high as 10^9 per cm^2.

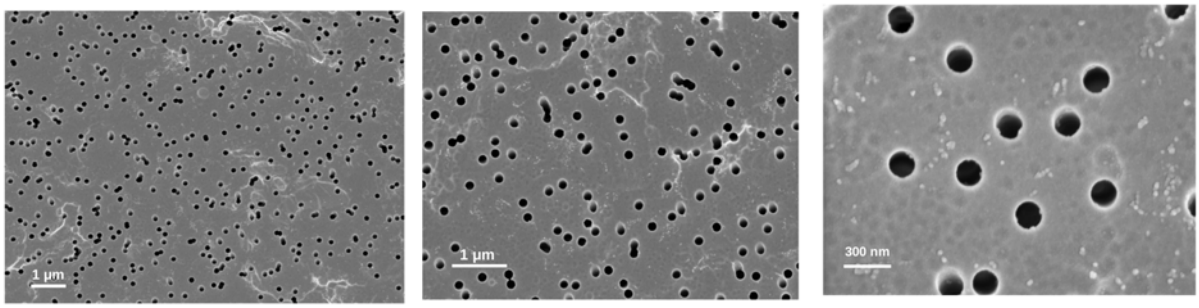

Figure 2.4: PCTE template with ~ 200 nm pores. Different magnification surface views.

The random nature of pores created by this technique can result in a large number of tilted non-parallel pores crossing with others, which affects the shape and dimensions of the synthesized nanowires, unlike AAO which has nearly parallel, uniform and ordered pore structure. Also, compared to self-ordered AAO formed by the anodization mechanism, which produce dense and closely-packed pores, ion-track etching process usually results in lower pore density leading to limited yield of wires.

Another drawback of PCTE membranes, is the chemical instability to some of the organic electrolytes which might be used in the electrodeposition process of some materials. Furthermore, PCTE templates cannot withstand high temperatures so it is not suitable for any annealing processes. However, the main advantage of PCTE over AAO templates is their flexibility, which facilitates handling.

In summary, the choice for using either AAO or PCTE templates in the electrodeposition of nanowires usually depends on the conditions and purpose of the experiments. In this research, AAO templates are used when an annealing step is required to form an ohmic contact between two segments of a multi-segmented nanowire. However, PCTE templates were used in preparing nanowire ensembles for electrical measurements. They were preferred over AAO as they are much thinner (6 μm in contrast to 60 μm),

and therefore it is faster to fill the template and contact the wires from the top for measurements as discussed in detail in chapter 4.

2.3 Electrochemical Deposition

Understanding the growth mechanism of one-dimensional structures is essential in controlling the characteristics of the produced materials. For that, the aspects of electrochemical deposition (method used to fabricate nanowires in this thesis) will be introduced below.

Electrochemical deposition is the process where ions of metals or semiconductors are reduced from a solution onto a conducting substrate. Typically, the solution contains dissolved salts of the materials which are going to be deposited.

The basic electrochemical setup is the two-electrode arrangement, with a cathode and an anode placed in an electrolyte containing the ions of interest. However, in research, the most common used setup for electrodeposition experiments is the three-electrode electrochemical cell shown in figure 2.5. This configuration comprises a working electrode (WE) corresponding to the cathode, a counter electrode (CE) corresponding to the anode and an additional reference electrode (RE).

Unlike the two-electrode setup, the voltage applied to the working electrode in the three-electrode setup will be measured versus a known, stable reference potential (i.e. RE potential). This ensures that the voltages applied to the working electrode will be reproducible in all performed experiments. Different reference electrodes have different fixed potentials with respect to the normal hydrogen electrode (NHE) being defined as zero. The most common reference electrodes are saturated silver/silver chloride (Ag/AgCl/sat. KCl) and saturated calomel electrode (SCE). For example, Ag/AgCl/ sat. KCl and saturated calomel reference electrodes have potentials of $+0.197$ V and $+0.242$ V with respect to NHE at $25°$C respectively (Paunovic and Schlesinger, 2006).

The working electrode is the conductive surface where the desired reaction should take place. In the case of templated electrodeposition, which will be presented in detail in section 3.1, it is a porous membrane with a conductive layer on one end. Generally, the counter electrode is made of electrochemically inert materials such as platinum or carbon. In electrochemical cells, it is advisable to minimize the distance between the working and the reference electrodes to avoid large potential drops between the working and the references electrodes, which could be responsible for inaccurate measurements.

When a potential more negative than the open circuit potential (OCP) is applied to the working electrode, a current will start to flow between the counter and the working electrodes to compensate for the potential difference. This current passing through the electrochemical cell allows the ions to migrate through the bath and deposit onto the working electrode according to the reduction reaction 2.3.1, where M represents some metal of z valency.

$$\mathrm{M^{z+}} + \mathrm{ze} \rightarrow \mathrm{M(s)} \tag{2.3.1}$$

Initially, this reaction occurs at the solution-substrate interface at nucleation sites, and then proceeds to the interface of the electrolyte and the deposited material where transfer of charge takes place. This limits the electrodeposition process to electrically conductive materials such as metals, semiconductors, and conductive polymers. During electrochemical growth of nanowires, two mechanisms occur simultaneously inside the template channels; nucleation of new grains and growth of existing nuclei.

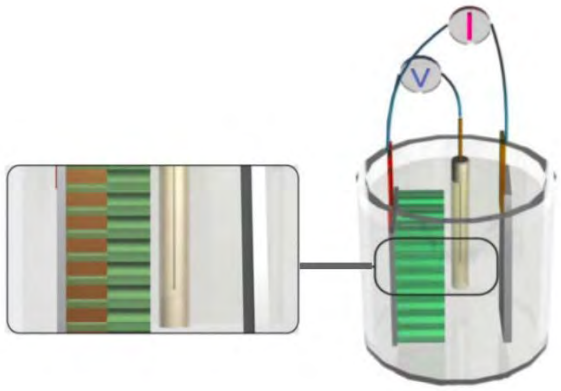

Figure 2.5: Schematic representation of a three-electrode electrochemical cell (Liu, 2009). A voltage is applied between the WE and RE, while current is measured between WE and CE. The closer view is of templated electrodeposition process, showing that the growth of nanowires initiates at the pore tips and proceeds in the direction towards the pore openings.

An alternative to direct electrodeposition in which a metal is deposited from its respective ions, is an indirect approach in which the pH is locally increased at the working electrode by nitrate reduction. This approach is often used for electrodeposition of metal oxides such as ZnO at $60 - 90°\mathrm{C}$ according to the following reactions.

$$\begin{aligned} \mathrm{Zn(NO_3)_2} &\rightarrow \mathrm{Zn^{2+} + 2NO_3^-} \\ \mathrm{NO_3^- + H_2O + 2e^-} &\rightarrow \mathrm{NO_2^- + 2(OH)^-} \\ \mathrm{Zn^{2+} + 2(OH)^-} &\rightarrow \mathrm{ZnO + H_2O} \end{aligned} \tag{2.3.2}$$

In general, the electrochemical methods require a precise definition of experimental conditions such as solution composition (concentration of reagents, solvents, pH, supporting electrolytes, etc.), applied potential, temperature, and deposition time.

Theoretically, the potential of the $\mathrm{M^{z+}/M}$ electrode (i.e. the potential required for an electrochemical reaction to take place) can be written using the Nernst equation as follows.

$$\mathrm{E} = \mathrm{E^0} + \frac{\mathrm{RT}}{\mathrm{zF}} \ln \mathrm{a(M^{z+})} \tag{2.3.3}$$

where E is the electrode potential, $\mathrm{E^0}$ is the standard redox potential for the desired reaction, R is the gas constant, F is Faraday's constant, T is the temperature, z is the number of electrons involved in the reaction, and a is the activity of the metal ions in the solution. The activity of the ions, $\mathrm{a(M^{z+})}$, is defined by (Schlesinger and Paunovic, 2011)

$$\mathrm{a(M^{z+})} = \gamma\, \mathrm{c(M^{z+})} \tag{2.3.4}$$

where c is the concentration (in moles per litre) of $\mathrm{M^{z+}}$, and γ is the activity coefficient of $\mathrm{M^{z+}}$.

Equations (2.3.3) and (2.3.4) demonstrate that the actual value of the deposition potential at which a specific metal is deposited will be strongly related to the concentration of its respective ions in the

deposition bath. This becomes of great importance when attempting to deposit compound semiconductors, such as CdSe, in which the electrodeposition potentials of the compound semiconductor elements are widely different (Pandey et al., 1996).

Optimization of all the above-mentioned experimental conditions demands a cyclic voltammogram to be performed for each deposition bath of interest, as this presents a more detailed view and understanding of the kinetics of the system during electrodeposition.

Various electrochemical methods, either potentiodynamic or potentiostatic, could be employed to electrodeposit different materials. All of them are applied using a potentiostat equipped with an appropriate physical electrochemistry software, which supplies a chosen voltage to the three-electrode cell, and monitors the output current. We will address below the ones used in synthesizing the single and multi-segmented nanowires during our research.

2.3.1 Cyclic Voltammetry

Cyclic voltammetry is a potentiodynamic electrochemical technique, where the current is measured at the working electrode while the potential between the working and reference electrodes is cycled from an intial to a final value at a constant scan rate (usually mV per second depending on the nature of the experiment). Cyclic voltammetry analysis of the electrochemical cell is a very helpful tool that provides information about the different processes occurring at the electrode during electrodeposition. It is usually used to optimize the conditions, such as the potential window, required for each deposition bath.

Figure 2.6 is the potential wave form for the cyclic voltammetry (left) and a typical cyclic voltammogram (right). As the sign of the potential is changed, oxidative and reductive processes can be distinguished. Scanning the potential from V_1 to V_2 shows a cathodic peak while scanning from V_2 to V_1 features an anodic peak. Typically, the cyclic voltammogram recorded shows the rates of chemical deposition and stripping of electrochemical species at the supplied voltages.

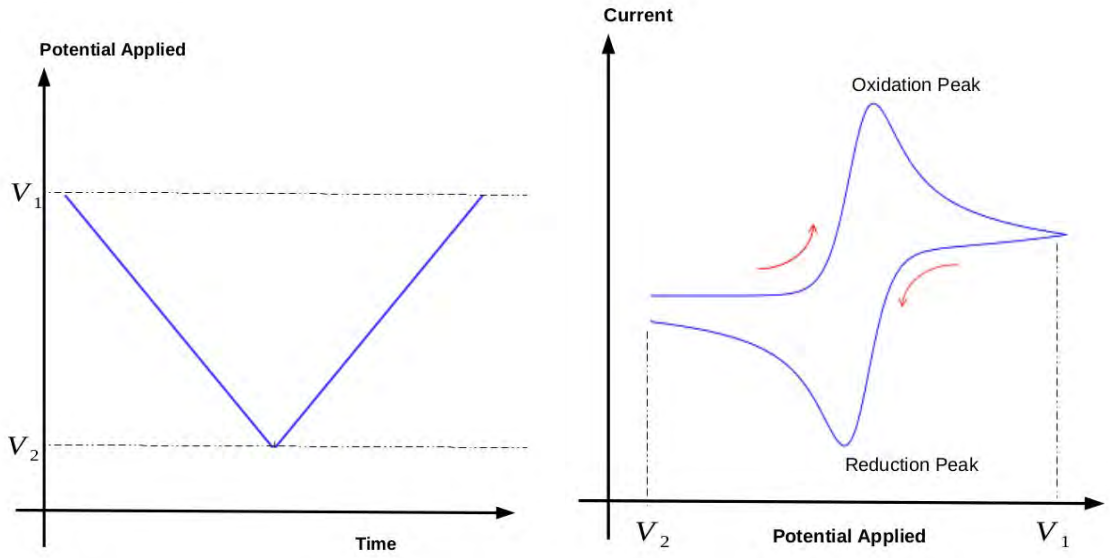

Figure 2.6: Schematics of an applied potential scan and the resulting current response at the WE.

This voltammetric technique takes into account several parameters without having to determine their influences separately. For example, the potential drop between working and reference electrodes, reversibility of the reaction, and the temperature dependence of both the reaction and the reference electrode potentials. Any possible side reactions can also be identified.

In our experiments of electrodepositing CdSe nanowires using a cyclic voltammetric technique (Kressin et al., 1991), the potential range and scan rates used were found to greatly affect the morphology and composition of the produced structures.

2.3.2 Linear Sweep Voltammetry

Linear sweep voltammetry (LSV) is another potentiodynamic technique, where the current is measured at the working electrode while the potential between the working and reference electrodes is swept from an initial to a final point. Unlike cyclic voltammetry, here the potential is not scanned back again after reaching the end value. In other words, a linear sweep voltammogram is one-half of a cyclic voltammogram. Generally, it is used to determine the standard reduction or oxidation potentials of the species in the electrolyte when the desired reaction is not reversible, or when there is no interest in the reverse direction scan. The reduction or oxidation of the species appears as a peak (in the recorded current signal) at the potential where they begin to be reduced or oxidized.

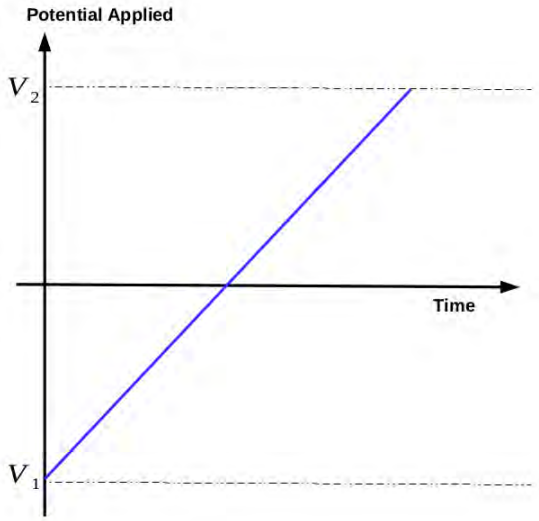

Figure 2.7: A schematic of a typical linear voltage sweep.

In our research, LSV studies were done before depositing the metallic nanowires to determine the proper reduction potentials of the used setup for each metal.

2.3.3 Chronoamperometry

Chronoamperometry is a potentiostatic technique where a certain potential is applied to the working electrode and the current signal is monitored as a function of time.

The chronoamperometry method is used to electrodeposit a specific material. During the electrodeposition process, the chronoamperogram (I-t curve), is directly related to the amount of material deposited

at the electrode. In the case of nanowires electrodeposition, the I-t curve is connected to the length of the wires in the pores as shown in figure 2.8.

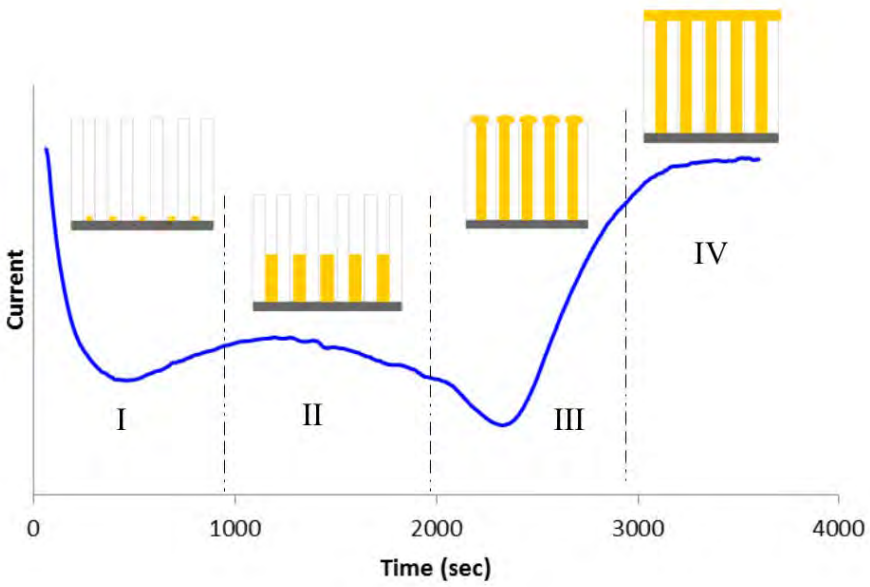

Figure 2.8: Potentiostatic electrodeposition of Ni nanowires in PCTE membrane pores. Different phases of current response[†] with schematic diagrams show the stages of nanowires growth.

The current response during electrodeposition in the membrane pores is usually divided into four main regions as follows. Region I includes the immediate nucleation of the material at the WE surface, which is recorded as an initial large current value that slowly depletes afterwards. As the surface area of deposition increases, leading to deposition of more material at the same time, the current slightly increases again indicating the start of filling process at the bottom of the nanopores. Region II represents resuming the growth of the material in the pores. During this stage, the current is almost constant as the change in the surface area is minimal. By reaching region III, the surface area available for deposition decreases slightly as the pores are now almost full causing a short decrease in current. This is rapidly followed by a sharp current rise, induced by a fast increase in electrode surface area, when the material start to emerge from the pores forming the mushroom-shaped hemispherical caps on top of the template. Finally, in region IV the hemispherical caps coalescence and eventually form a continuous film with a steady-state current.

Monitoring these chronoamperograms permits us to end the deposition process at the proper time for obtaining nanowires with specific lengths. In our work, chronoamperometry is used in the electrodeposition of metallic nanowires.

2.4 Overview of CdSe Electrodeposition

The single-material nanowires studied in this work are CdSe nanowires, so this section will present an overview of CdSe preparation methods focusing on the templated electrodeposition technique.

[†] Current always has a negative sign during electrodeposition as electrons move from CE to WE.

At present, micro- and nano- CdSe structures have been successfully synthesized by several methods, including electrochemical deposition (Klein et al., 1993), SLS (Grebinski et al., 2004), hydrothermal (Peng et al., 2002), CVD (Shan et al., 2007), and VLS (Ma and Wang, 2005). Among these different synthetic routes, electrodeposition offers a simple and cheap approach.

There have been various papers in the literature that discuss the electrochemical deposition of CdSe on different substrates and in the pores of templates. The conclusions of which will be summarized here.

Much research has been done on the electrodeposition of CdSe from aqueous acidic (Kazacos and Miller, 1980) or alkaline baths (Hodes et al., 1982; Peng et al., 2001), and non-aqueous baths (Sanders and Cocivera, 1987). The majority of the work reviewed here describes the cathodic electrodeposition from an acidic bath as it is the most common method and the one used in fabricating structures in this thesis.

An early report on the cathodic deposition of CdSe from an acidic aqueous solution containing Cd^{2+} and SeO_2 was that of Hodes et al. (Hodes et al., 1976). The mechanism of CdSe electrodeposition was then reported by Kazacos and Miller (Kazacos and Miller, 1980), after studying the reaction sequence for H_2SeO_3 reduction in a H_2SO_4 medium with Cd ions present. Tomikiewicz et al. (Tomkiewicz et al., 1982) proposed an alternative mechanism to explain the cauliflower-like morphology observed in the electrodeposited CdSe films, and then examined their performance in liquid junction solar cells. Later, Mishra and Rajeshwar (Mishra and Rajeshwar, 1989) also studied the electrodeposition of CdSe by cyclic voltammetry and proposed a mechanism similar to that of Kazacos and Miller. Despite all these trials, the preferential deposition of one component over the other in the as-deposited films (usually Se-rich deposits) remained a major obstacle to form high quality CdSe films via cathodic deposition. Moreover, the morphology of the electrodeposited CdSe films was highly variable and condition sensitive as pointed out by Boudreau and Rauh (Boudreau and Rauh, 1982). They stated that the concentration of Cd^{2+}, H_2SeO_3, and the applied current density are critical parameters in obtaining stoichiometric CdSe films using cathodic deposition.

One of the convenient attempts to create stoichiometric CdSe films was done by Kressin et al. (Kressin et al., 1991) via a sequential monolayer electrodeposition technique. Their method employs a cyclic voltammetry scheme (will be referred to as cyclic electrodeposition/stripping technique) to produce homogeneous films of CdSe that are close to 1:1 atomic ratio of Cd to Se.

2.4.1 Electrodeposition of CdSe Nanostructures

Following Kressin's work, many researchers utilized this cyclic electrodeposition/stripping technique to fabricate either stoichiometric CdSe films or wires/rods.

Klein et al. (Klein et al., 1993) were the first to deposit cadmium chalogenide microdiode arrays into Anopore membranes. Later, Pena et al. (Pena et al., 2000, 2002) also employed the same technique to grow metal-CdSe-metal nanowires, inside both AAO and PCTE membranes, and studied their photo-conductive properties. Their experiments have opened the door to develop other heterojunction devices incorporating CdSe as a functional material.

Following on, several groups made use of the same cyclic electrodeposition/stripping technique to fabricate and study CdSe nanowires alone or as part of a heterostructure. For instance, Schierhorn et al. (Schierhorn et al., 2008, 2009, 2010) and Lee et al. (Lee et al., 2013) fabricated various configurations of CdSe nanorod arrays and reported their electrochemical photovoltaic performance. Li et al. (Li et al., 2006) coupled this cyclic electrodeposition/stripping technique with step edge decoration on HOPG surfaces to produce CdSe nanowires with lengths exceeding 100 μm.

In the last decade, many researchers have further studied the different aspects of CdSe electrodeposition such as the electroplating solution compositions, potentials used, and different scan rates. Among them is Bienkowski et al. (Bieńkowski et al., 2010) who pointed out how the concentration and ratios of reagents in the deposition bath crucially affected the stoichiometry of CdSe structures, while Shpasiman et al. (Shpaisman et al., 2010) concentrated on the effects of varying scan rates on the morphology of electrodeposited CdSe wires.

In general, a wide range of experimental conditions were examined in order to determine the optimum way of synthesizing CdSe structures with the proper elemental stoichiometric ratio and the desired dimensions as seen in table 2.1. For instance, in the work surveyed here, the Cd:Se ratio varied from 1000:1 to 5:1 while scan rates ranged from 10 V/sec to 20 mV/sec. The main studies followed in this thesis are those which either employ the 500:1 ratio with high scan rates of $\sim$ 750 mV/sec (Klein et al., 1993; Pena et al., 2000, 2002; Schierhorn et al., 2008, 2009) or those that employ low scan rates of about 50 mV/sec with 5:1 Cd:Se ratio (Bieńkowski et al., 2010; Bocchetta et al., 2013).

Deposited Structure	Deposition Solution		Applied Voltage	Reference
	Cd:Se ratio	H_2SO_4 or pH		
Thin Films	100:1	1 M	-0.6 V	Kazacos and Miller (1980)
Thin Films	1000:1	0.25 M	-0.4 $\rightleftharpoons$ -0.8 V at 10 V/s	Kressin et al. (1991)
Nanowires	500:1	0.25 M	-0.4 $\rightleftharpoons$ -0.8 V at 10 V/s	Klein et al. (1993)
Nanowires	500:1	0.25 M	-0.35 $\rightleftharpoons$ -0.8 V at 750 mV/s	Pena et al. (2000)
Thin Films	1000:1	pH = 2.5*	-0.7 V	Shen et al. (2001)
Nanowires	1000:1	0.5 M	-0.35 $\rightleftharpoons$ -0.5 V at 500 mV/s	Pena et al. (2002)
Thin Films	1000:1	pH = 2.5	-0.7 V*	Shen et al. (2005)
Nanowires	100:1	pH = 2.5-3.5	+1 $\rightleftharpoons$ -1 V at 20 mV/s	Li et al. (2006)
Nanowires	500:1	0.25 M	-0.357 $\rightleftharpoons$ -0.757 V† at 750 mV/s	Schierhorn et al. (2008) Schierhorn et al. (2009)
Nanowires	500:1	0.25 M	-0.4 $\rightleftharpoons$ -0.8 V at 50 mV/s	Kung et al. (2010)
Nanowires	20:1	0.25 M	-0.4 $\rightleftharpoons$ -0.8 V ‡	Shpaisman et al. (2010)
Thin Films	5:1	pH = 3	0.4 $\rightleftharpoons$ -0.9 V at 50 mV/s	Bieńkowski et al. (2010)
Nanowires	100:1	pH = 0.6-1	-0.6 V	Kim et al. (2010)
Nano Particles	500:1	0.25 M	-0.6 V†	Xing et al. (2012)
Nanotubes	5:1	pH = 3	0 $\rightleftharpoons$ -1.2 V† at 50 mV/s	Bocchetta et al. (2013)
Nanowires	100:1	pH = 2.5	-0.55 V	Kalhori et al. (2015)

Table 2.1: Survey of the conditions used to deposit CdSe structures. All voltages are with respect to the SCE unless otherwise stated. Duration of deposition process varied according to the purpose of the study.

Although there are many different conditions reported for electrodeposition of CdSe thin films and nanowires, as seen in table 2.1, precise detailed comparison between them is lacking. Attempts to examine results from different deposition conditions will be presented in section 3.5.

*Varies across the study.
†Voltage is applied with respect to Ag/AgCl.
‡Voltage is applied with respect to Ag/AgCl. Scan rate is varied across the study.

3. Fabrication and Characterization of the Nanowires

In this chapter, we will be addressing how the templated electrodeposition method introduced in chapter 2 is applied to fabricate the functional one dimensional nanostructures in detail.

The experimental procedure consists of four parts: the arrangement of the working electrode discussed in section 3.1, the preparation of the deposition solution, the electrochemical deposition, which are both illustrated in section 3.2, and the harvesting of the nanowires for characterization shown in sections 3.3 and 3.4 respectively. Finally, the general results and conclusions are presented in section 3.5.

3.1 Experimental Set Up

This section presents the scheme and instrumentation used in the electrodeposition of the nanowires. The nanowires synthesis was performed using a standard three-electrode arrangement as discussed in section 2.3.

Preparation of the Working Electrode

In order to be used for synthesizing the nanowires, the AAO and PCTE membranes are prepared as follows.* Initially, a thin film of silver (thickness ranging from hundreds of nanometers to couple of microns) is thermally evaporated in vacuum ($\sim 10^{-6}$ mbar) onto one side of the template to cover the pores completely and to serve as the working electrode during electrochemical deposition.

A metal sheet, with three holes for AAO membranes and one hole for PCTE membranes (13 & 25 mm respectively), is designed to hold the templates in the thermal evaporation chamber. This holder is placed on a small table to expose the bottom face, decided arbitrarily, of the templates to the evaporation site. All was fabricated in house in the Department of Physics mechanical workshop.

Performing the silver evaporation at a slower rate did not appear to have any noticeable benefits, as this film is only meant to act as a conducting layer for initiating the electrodeposition of desired materials from the bottom of the template channels. However, evaporating onto PCTE templates at high rates damaged the membranes. The thermally evaporated silver layer was not homogeneous throughout the template area. Also, the thickness of the deposited layer varied slightly from one template to the other, which can be seen sometimes from the colour of the template (thicker layers appear darker from the front surface). This was confirmed by measuring the thickness of different areas/templates using SEM. Further inspections of the evaporated silver layer under SEM showed that the film consisted of about 90 nm diameter spheres at the bottom of the pores. As the pores had high aspect ratios, no significant amount of metal penetrated through the pores.

The prepared silvered templates were stored in a container at atmospheric conditions until further use.

*Extra care was taken to avoid cracking or breaking the AAO templates (commercially available Anodisc 13 membranes used here are extremely fragile and they are not supported with a polypropylene ring for ease of handling like Anodisc 25 or 47). Cracked templates can not be used as depositions will preferentially happen at the crack/defect rather than into the pores.

Figure 3.1: Pictures of the template holders for thermal evaporation of silver.

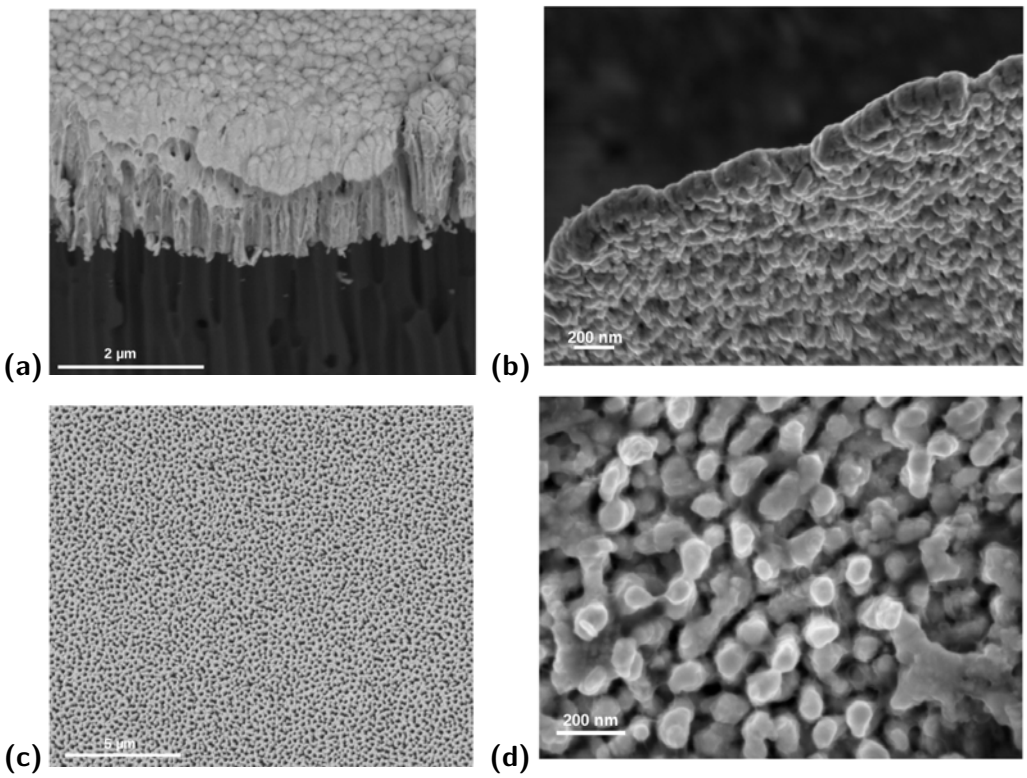

Figure 3.2: Various SEM pictures of the thermally evaporated silver backing layer. (a) Side view showing the thickness of silver layer on the AAO membrane, (b) cross section after dissolving the template, (c) top view of the outer side, and (d) inner side of silver layer after dissolving the template.

The silver-coated AAO membrane is then placed (coated side down) onto a glass slide, with a strip of copper tape connected to the silver film as shown in figure 3.3. A sheet of silicone rubber (or any other non-conducting structure), with a hole of diameter slightly less than AAO area, is then put on top of the glass slide to isolate the silver layer from the electrolyte. This served as an insulating mask to prevent desired material from depositing on any exposed conductive surface, as the diffusion of ions onto a flat electrode is much faster than into the pores. In this configuration, only the non-coated face of template is in contact with the electrolyte, which ensures that deposition occurs exclusively into the pores of the membrane. Prior to electrodeposition, the template was soaked in either distilled water or the desired plating solution to completely wet the membrane pores so that the deposition process

occurs simultaneously in all pores. In some cases, the electrolyte is bubbled with Argon or Nitrogen to remove any oxygen traces in the liquid that might affect the results.

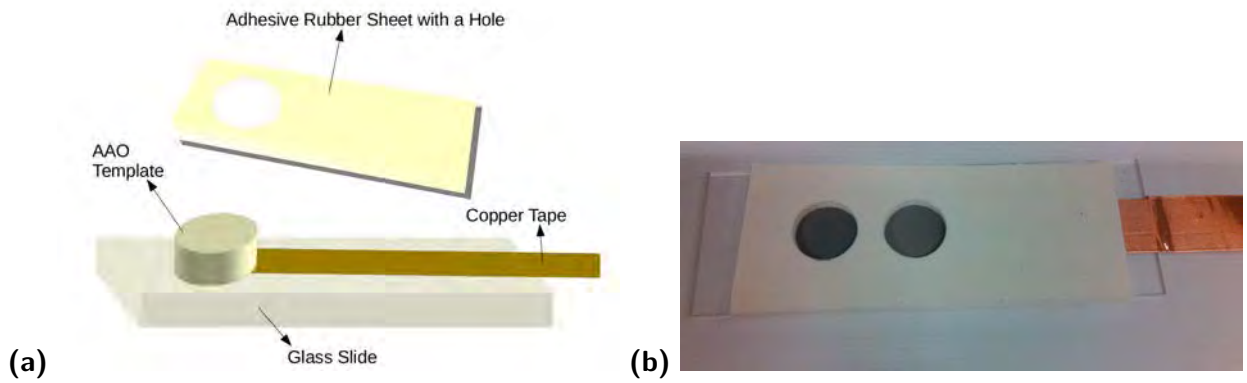

Figure 3.3: (a) Schematic representation of the working electrode area and (b) picture showing the working electrode assembly where two templates can be used at the same time. Copper tape which sticks out from the glass slide is then connected to the potentiostat working electrode crocodile clip. This arrangement provides mechanical stability to the membrane during the deposition process. For longer electrodepositions, masking tape could be added to the edges for more secured isolation.

For performing the electrochemical deposition of all materials in the next section, we used a typical three- electrode electrochemical cell with an Ag/AgCl reference electrode, a platinum mesh counter electrode (anodic surface area $\sim$ 25 x 25 mm), and a silver backed AAO or PCTE membrane which served as the working electrode. The electrochemical cell, containing the desired plating solution, is a conical glass beaker with a Teflon lid that has holes to hold the three electrodes, which are then connected to a potentiostat to carry out the electrodeposition process. This configuration ensures an equal distance between the electrodes for all depositions. Additional lid holes are also available for a gas inlet such as Argon which can be bubbled through the solution to remove any traces of dissolved oxygen.

3.2 Nanowires Synthesis

In this section, the experimental procedures and conditions[†] used in the preparation of single and multi segmented nanowires via templated electrodeposition are explained.

3.2.1 Metallic Nanowires

Electrochemical deposition into the nanoporous templates such as AAO or PCTE permits the fabrication of various high aspect ratio metal nanowires with different functions (Kline et al., 2006). For instance, nanowires made of Ag (Sun et al., 2005), Au (Wu et al., 2013; Zhang et al., 2009), Co (Strijkers et al., 1999), Cu (Riveros et al., 2005), Fe (Haehnel et al., 2010), Ni (Lin et al., 2004; Napolskii et al., 2007; Li et al., 2009), Pt (Zhao et al., 2007; Maijenburg et al., 2012), and Zn (Wang et al., 2005,

[†]All electrodeposition experiments in this section were performed at room temperature and the voltages applied during deposition are versus an Ag/AgCl reference electrode unless stated otherwise.

2007) were successfully manufactured. Due to the unique geometries and physical properties of metal nanowires, a wide range of applications incorporating them has emerged in the past few decades such as employing the metal nanowire arrays as nanoelectrodes for many electrochemical purposes (Mai et al., 2014). Metal nanowires are also attractive for applications in optics and magnetism (Sellmyer et al., 2001; Piraux et al., 2005) and/or chemical and biological sensing devices (García et al., 2014).

In our research, we have attempted to electrodeposit various metals either to provide electrical contacts or for supporting the photocatalytic process of hydrogen production acting as electrocatalysts.

3.2.1.1 Nickel Nanowires

Nickel nanowires were successfully grown, in both PCTE and AAO membranes, from an aqueous solution containing 0.23 M $NiSO_4.6H_2O$ and 0.15 M H_3BO_3. The deposition occurred at a potential of -1 V vs. Ag/AgCl. The duration of the deposition varied according to the desired length. In AAO templates, 1.5 hours yielded about 6 μm, while in PCTE membranes 40 minutes are almost enough to fill the template ($\sim$ 6 μm). PCTE membranes are filled faster than AAO membranes as they have lower pore density.

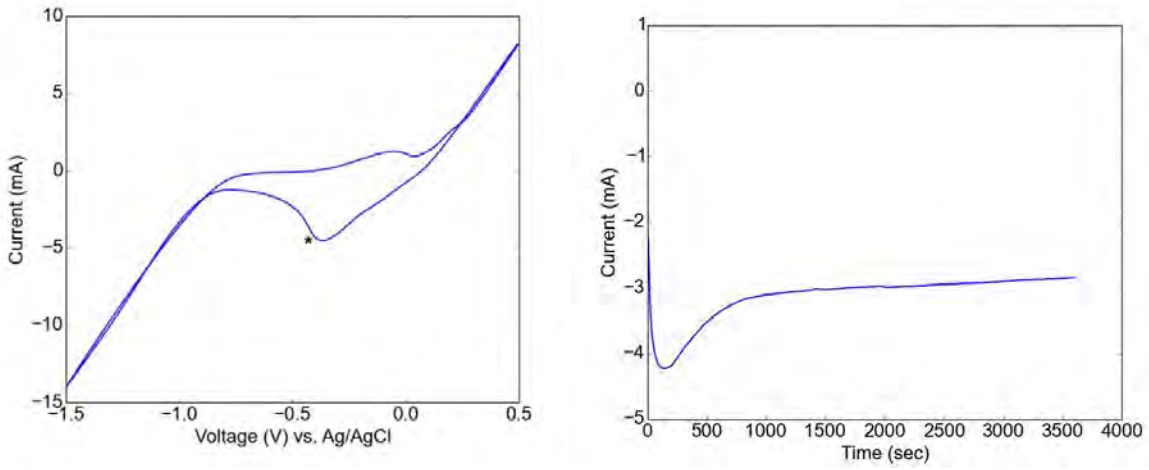

Figure 3.4: Left plot is a cyclic voltammogram of nickel deposited into a 10 mm diameter silver-backed AAO template with 50 mV/sec scan rate (* denotes the reduction peak). Right plot is a chronoamperogram showing nickel nanowires growth in an AAO template at -1 V vs. Ag/AgCl for 1.5 hours.

3.2.1.2 Gold Nanowires

Gold nanowires were fabricated in AAO templates from an aqueous electrolyte solution of 5 mM $HAuCl_4.aq$ and 0.5 M H_3BO_3. Prior to the deposition of gold, cyclic and linear sweep voltammetries were performed on silver-backed AAO templates to determine the deposition potential range as shown in the top plots of figure 3.6. The duration of the deposition varied according to the desired length of the gold segment.

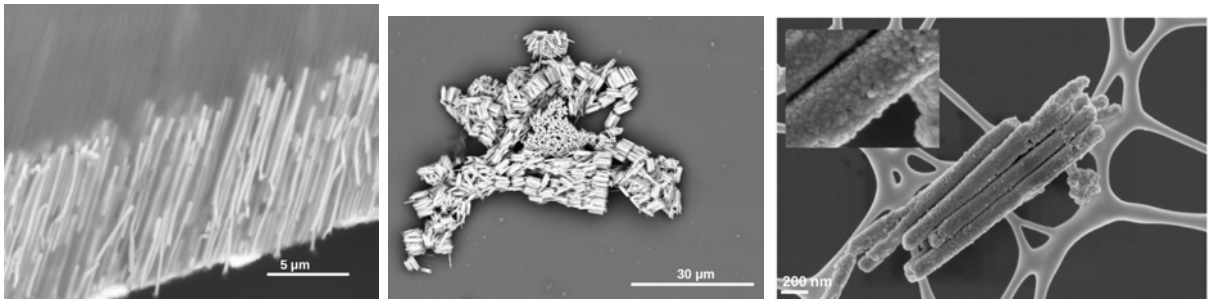

Figure 3.5: SEM pictures of nickel nanowires of different lengths, configurations, and magnifications. In the first image (left) nanowires are still embedded in the AAO template. Middle image shows clustered wires due to the usage of a strong magnet on the colloidal solutions of wires. Right image is a closer view of the wires (inset is a highly magnified image showing that average grain size of the as-prepared nickel nanowires is roughly 30 nm).

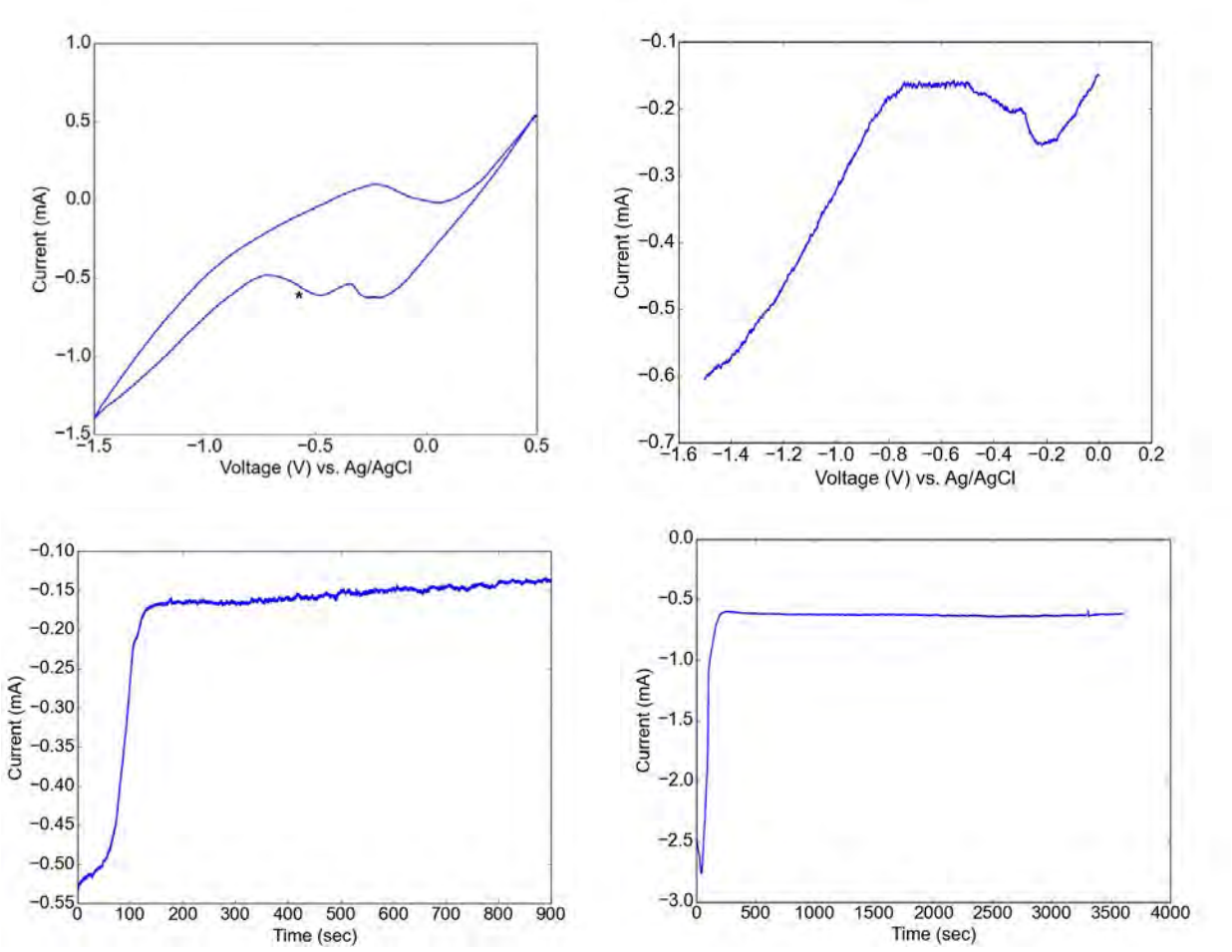

Figure 3.6: Top plots: a cyclic voltammogram with 50 mV/sec scan rate (left) and a linear sweep voltammogram (right) of gold deposited into a 10 mm silver-backed AAO template. The * denotes the gold reduction peak. Bottom plots are the chronoamperograms showing gold nanowires growth in an AAO template at -0.35 V for 15 minutes (left) and at -1 V for 1 hour (right).

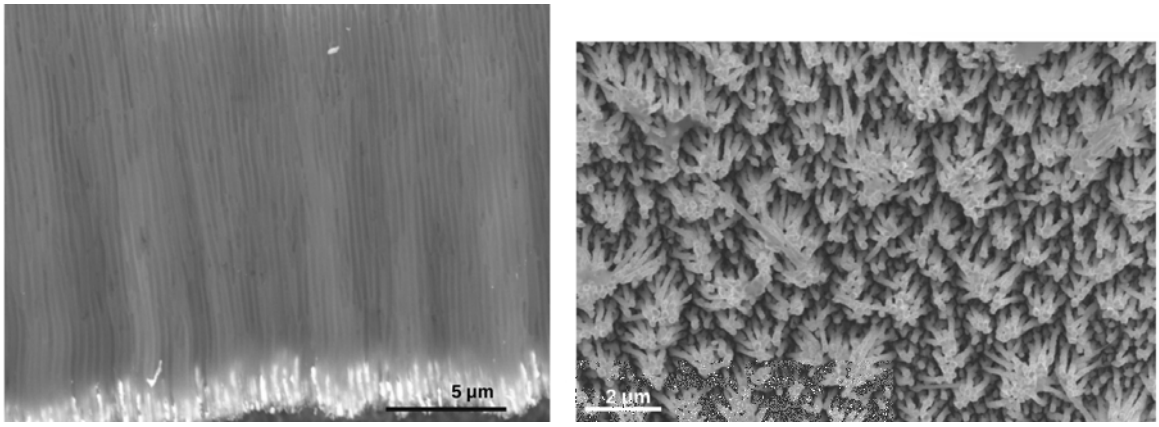

Figure 3.7: SEM pictures of gold nanowires. Left image is a cross-sectional view of nanowires embedded in the AAO template. Right image is an array of free-standing wires after dissolving the AAO template.

3.2.1.3 Platinum Nanowires

Platinum is a noble metal with interesting catalytic applications. In this work, platinum nanowires were electrodeposited into the pores of AAO templates from 0.01 M $H_2PtCl_6.6H_2O$. The potential range for the deposition of platinum was determined from the voltammograms in figure 3.8.The duration of deposition was chosen according to the required length, for example 30 minutes results in about 1 μm long wires.

In all the presented voltammograms (figures 3.4, 3.6, and 3.8), the reduction peak denoted by * marks the start of the deposition of ions in the solution. Hence, any value at this peak or lower (more negative potential) can be chosen for the electrodeposition of the required metal. However, it should be taken into account that in aqueous solutions, hydrogen evolution is a byproduct of increased negative potentials. As more negative potentials are applied, the electrodeposition current increases as shown in the chronoamperograms of gold deposition at two different potentials. At sufficiently large currents, the deposition reaction becomes rate-limited by diffusion of the ions in the electrolyte. Typically, an optimum deposition voltage is in the range of the desired reaction without any other side reactions, and with a measurable current.

3.2.2 Semiconducting Nanowires

Semiconducting materials such as metal oxides and metal chalcogenides (Lincot, 2005) were also electrodeposited inside the pores of AAO and PCTE templates forming one-dimensional structures (Şişman, 2011). The work done here focuses on photocatalytically active semiconducting materials (Hochbaum and Yang, 2009; Qu and Duan, 2012; Dasgupta and Yang, 2014).

3.2.2.1 Cadmium Selenide Nanowires

CdSe nanowires, the main focus of this work, were successfully grown inside the pores of PCTE and AAO templates from an acidic aqueous bath with cadmium sulfate and selenium dioxide as sources of cadmium and selenium ions respectively. A cyclic electrodeposition/stripping technique (Kressin et al., 1991) was used to deposit the wires with potentials ranging from -0.35 V to -0.8 V vs. Ag/AgCl at

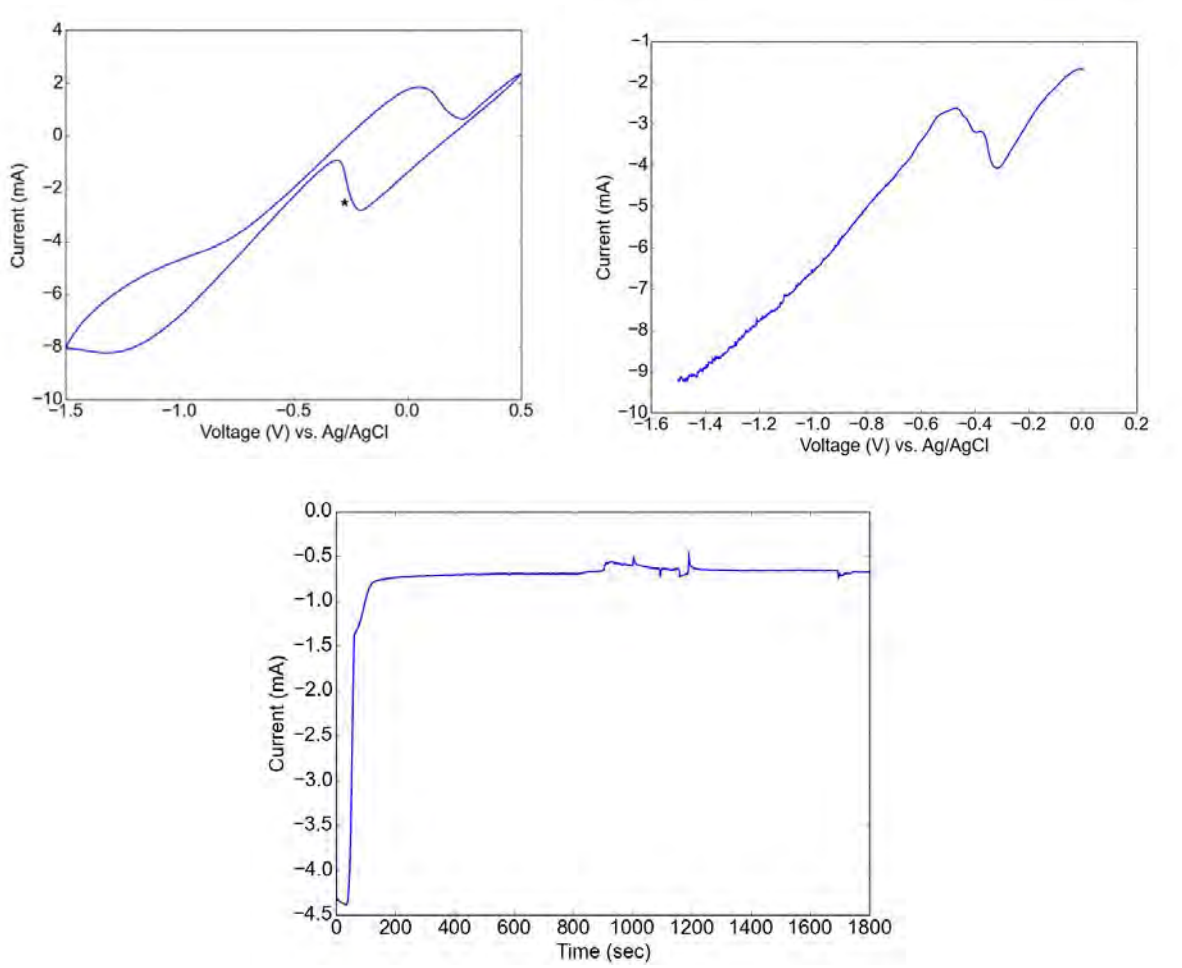

Figure 3.8: Top plots: a cyclic voltammogram with 50 mV/sec scan rate (left) and a linear sweep voltammogram (right) of platinum deposited into a 10 mm diameter silver-backed AAO template. The * denotes the platinum reduction peak. Bottom plot is the chronoamperogram of platinum nanowires growth in an AAO template at -0.3 V for 30 minutes.

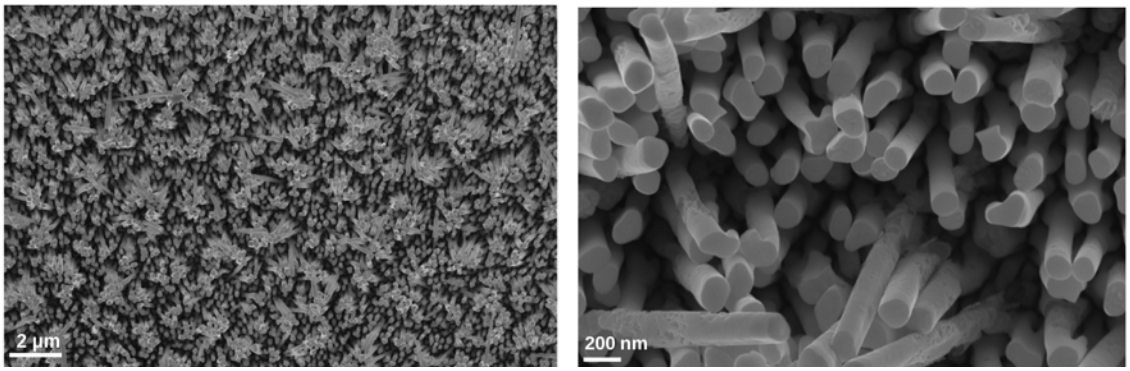

Figure 3.9: SEM pictures of platinum nanowires. Left image is an array of free-standing wires after dissolving the AAO template. Right image is a closer view of the nanowires.

scan rates of (10 - 50) mV/sec. The optimum solution [‡] for depositing stoichiometric CdSe wires was found to be 5 mM $CdSO_4.^8/_3H_2O$, 1 mM SeO_2, and 0.25 M H_2SO_4. Addition of H_2SO_4 increases the conductivity of the solution and lowers the cathode over-potential. However, higher concentrations of H_2SO_4 (strong acid pH values) were found to be accompanied with an intense hydrogen release. The deposition times varied according to the desired length of wires. It should be noted that the growth rate for semiconducting materials is much lower than the corresponding metal rate due to lower conductivity of the semiconductor as seen in figure 3.11. The detailed mechanism of CdSe electrodeposition is discussed in 3.4.

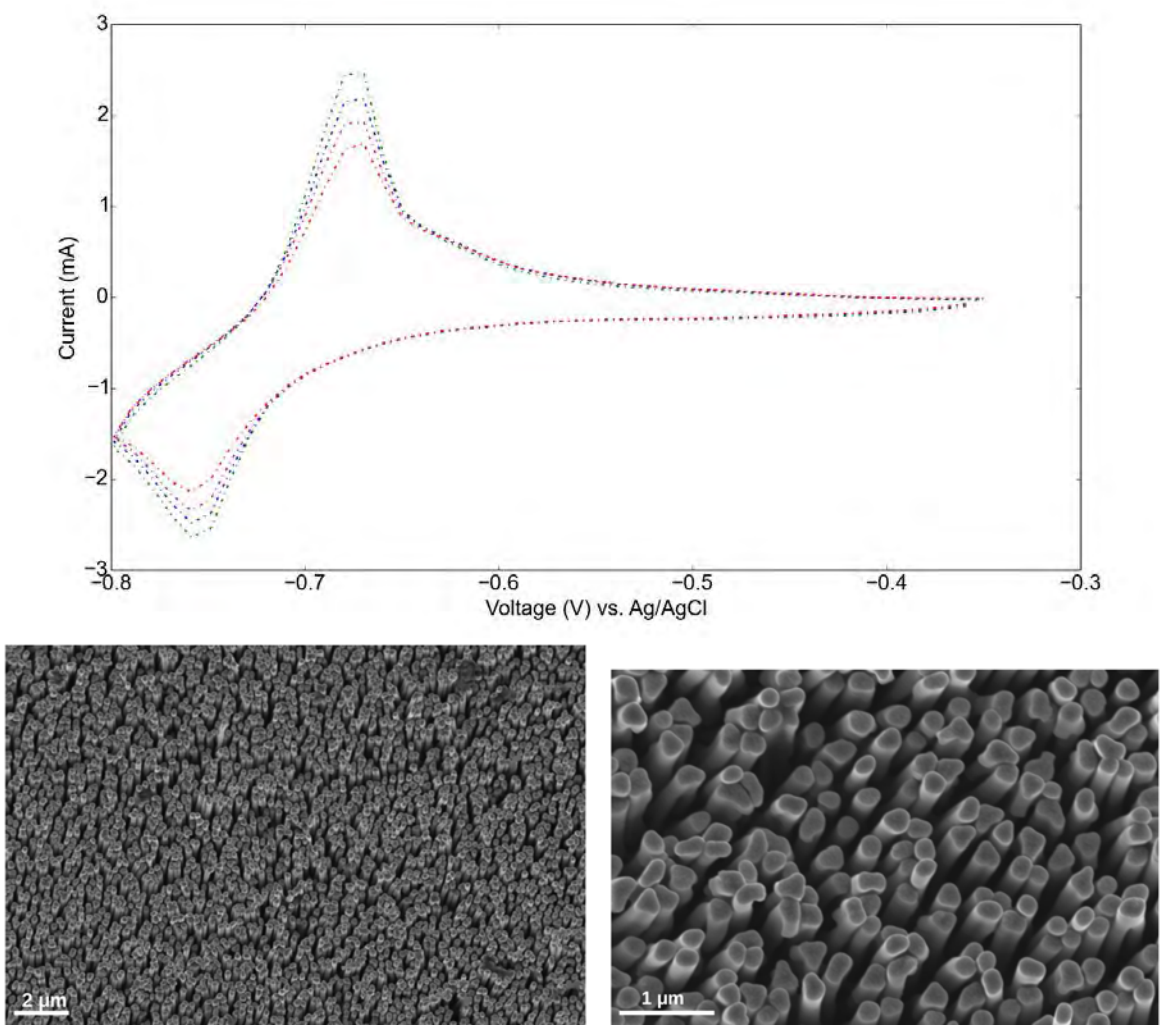

Figure 3.10: Top plot is some of the steady-state cycles of CdSe deposition into a 10 mm diameter silver-backed AAO template with a scan rate of 10 mV/sec (deposition cycles were 160). During the deposition, the current peaks decreases as a consequence of the high resistance of the semiconductor layer formed. Bottom images are SEM pictures of an array of free-standing CdSe nanowires after dissolving the AAO template. Right picture is enlarged view of the wires.

[‡]The CdSe nanowires mentioned throughout the thesis are fabricated using this solution unless stated otherwise.

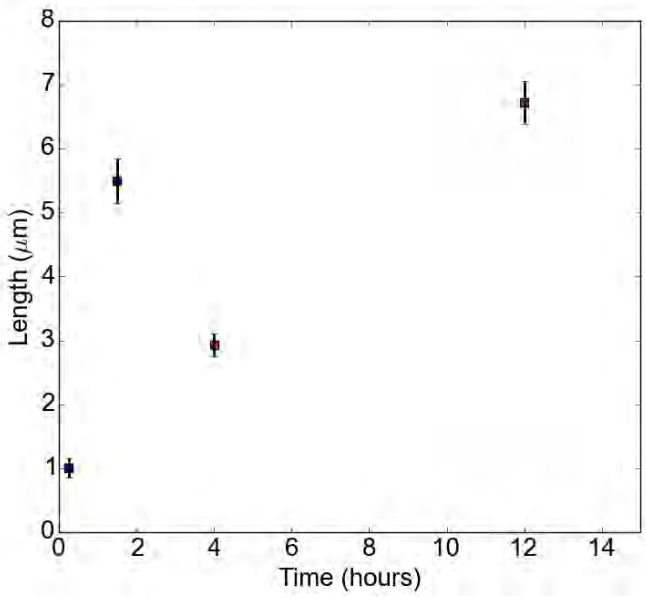

Figure 3.11: CdSe (red) and Ni (blue) nanowires length versus electrodeposition time. Error bars show the standard uncertainty in the measured length. It can be seen that growth rate of the Ni is much larger compared to the CdSe.

3.2.2.2 Zinc Oxide Nanowires

ZnO is another n-type semiconducting material which can be used in photocatalytic water splitting experiments (Gupta et al., 2009; Maijenburg et al., 2011b). ZnO films and nanowires (not shown here) have been electrochemically grown on FTO glass slides and in the pores of PCTE membranes respectively using zinc nitrate and the mechanism (2.3.2) mentioned in chapter 2. The deposition bath contained 0.1 M $\mathrm{Zn(NO)_2.6H_2O}$, as a source of zinc ions, which was heated to 70 $^{o}\mathrm{C}$ in a stirred water bath during the deposition period.

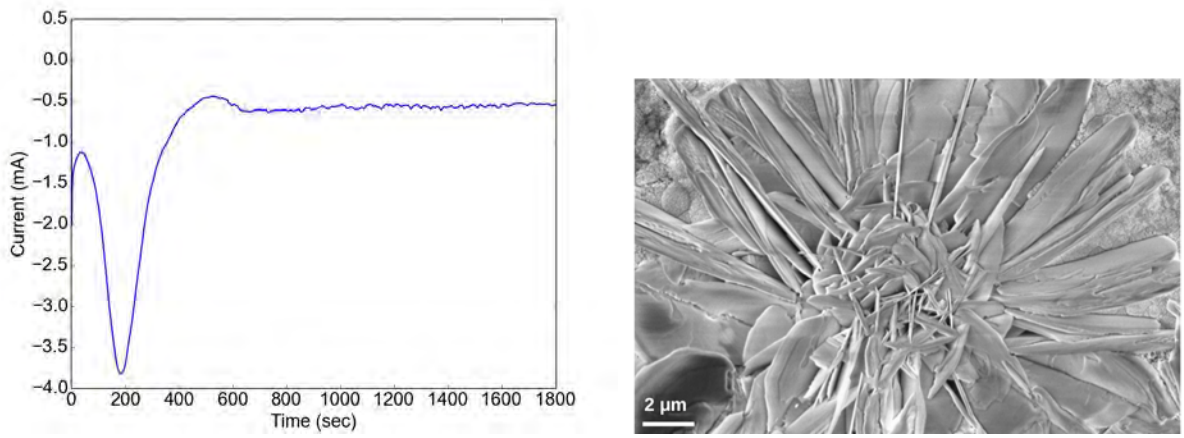

Figure 3.12: Left plot is the chronoamperogram of ZnO deposition into silver-backed PCTE membrane pores at -1 V for 30 minutes. Right is a SEM image showing the nano-flower structure of ZnO films.

3.2.3 Heterostructured Nanowires

In addition to synthesizing single metal and semiconductor nanowires, templated electrodeposition also provides an easy path to grow multi-material segmented nanowires. The variation along the length of these wires is often used to combine catalytic, electrical, and optical activities. Incorporating various materials into one segmented heterostructure either allows the production of multi-functional nanowires (consisting of different segments with different activities) or offers functionalities that are not available in the individual segments. For instance, Au-Pt nanowires were reported to move autonomously when placed in a hydrogen peroxide solution (Paxton et al., 2004).

In this research, metal segments were incorporated with a semiconducting segment, as shown in figure 3.13, in attempts towards a more stable photocatalytically active heterostructure. These axially segmented nanowires were formed by sequential electrodeposition of materials inside the AAO pores. After the first segment deposition, the electrochemical cell and electrodes are thoroughly rinsed three times with DI water, and the cell is then filled with the next segment plating solution. This electrodeposition and rinsing process is then repeated until all desired segments are grown inside the pores. As part of experimenting the different conditions, the following combinations were tried; Ni-CdSe, CdSe-Ni, Ni-CdSe-Ni, Au-CdSe, Au-Pt, and Ni-CdSe-Au-Pt.

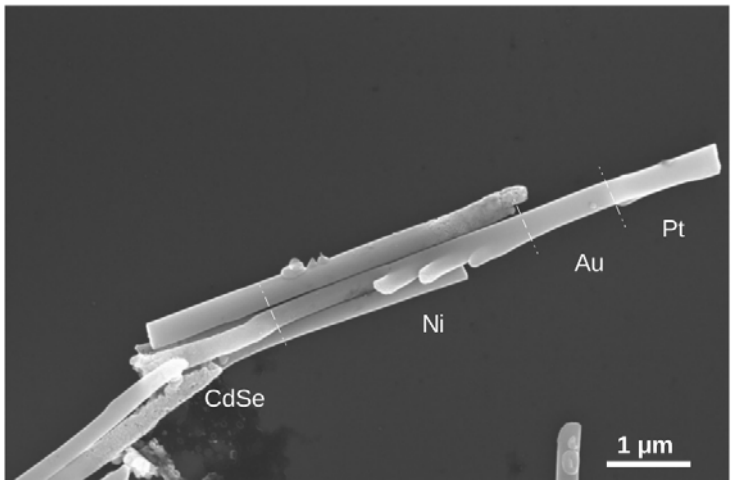

Figure 3.13: SEM image of a multi-segmented functional nanowire containing 4 different materials (CdSe-Ni-Au-Pt). CdSe is the photocatalytically active segment, Pt is a metallic electrocatalyst, and Ni-Au segment provides an ohmic contact between CdSe and Pt. Various segments were visually identified from the contrast in SEM images and confirmed via EDS analysis. CdSe and Pt ends could also be distinguished from each other through surface appearance. CdSe end tends to be more rough and branched resembling the AAO templates bottom surface.

3.3 Nanowires Collection

After filling the templates with the desired single/multi-segmented nanowires, harvesting of these wires is then essential to fabricate the devices for transport measurements reported in Chapter 4.

While deposition can be crudely confirmed by visual inspection (templates turn black when filled with the CdSe), the wires must be separated from the template for characterization. After deposition, the template was removed from the solution and rinsed with distilled water. Initially, the working electrode assembly was cleaned with acetone to separate the silicone rubber sheet from the glass slide and smoothly release the filled template, which was subsequently washed several times by distilled water.

For the collection of nanowires, the filled templates were treated as follows. The filled membrane is placed in a Petri dish with silver shiny film facing upwards (pores facing downwards). Using a micro pipette, a very small droplet of concentrated nitric acid was dropped to selectively dissolve the silver. The silver film was etched away instantaneously and DI water was flushed onto the template immediately to prevent further etching of the semiconducting wires. It should be noted that using diluted nitric acid to etch away the silver film as suggested in some literature took a very long time and did not etch it completely. Also, using an ultrasonic bath to get the wires to fall off the silver film (after dissolving the template) resulted in splitting it into small pieces with wires still attached to them (no significant number of free wires were seen under the SEM) as shown in figure 3.14.

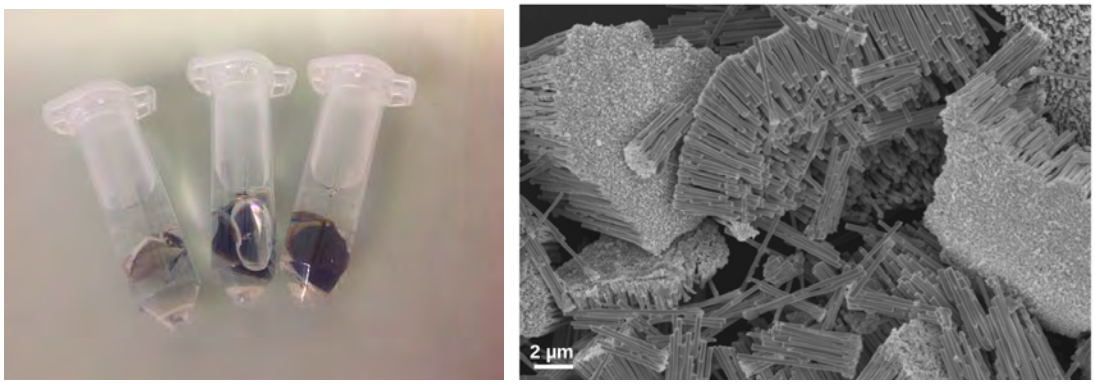

Figure 3.14: Left is an image of 3 AAO templates with nanowires during the dissolving process. Right is a SEM picture showing few silver pieces with CdSe nanowires arrays still attached to them.

After dissolving the silver, the template was transferred to a new dish, rinsed with fresh DI water several times, dried, and placed into a 2 mL centrifuge tube. The tube was then filled with 3 M NaOH, left for almost 30 minutes with little shaking, to dissolve the AAO template completely and release the wires. The free nanowires were then sedimented into a pellet by centrifuging the suspension at 10,000 RPM (7378 g) for about 3 minutes, then NaOH was removed and replaced with DI water. This was repeated two or three times to make sure that all NaOH is replaced by DI water. Finally, this centrifugation process was repeated again using ethanol instead of water to store the suspension of nanowires for further investigations.

Figure 3.15 summarizes the steps taken to synthesize nanowires via templated-electrodeposition and the various end configurations for different characterizations and/or applications.

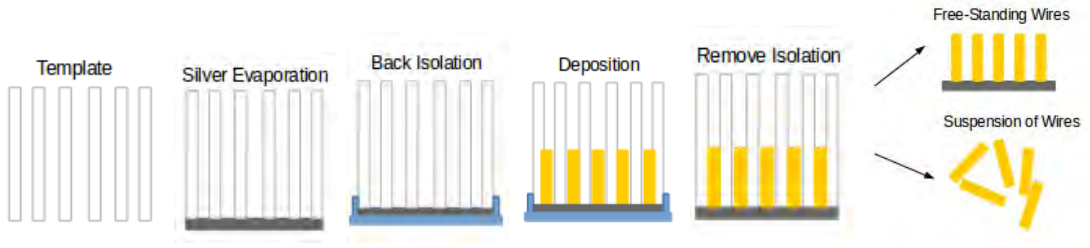

Figure 3.15: Schematic representation of the steps taken to synthesize and collect the nanowires. After the deposition, either template is dissolved leaving an array of free-standing wires onto silver backing-film or both the template and the film are etched leaving a suspension of wires.

3.4 Nanowires Characterization

The investigations performed on the grown nanostructures were carried out using a range of techniques and special characterization equipment that can focus on such small dimensions. Techniques such as SEM, TEM, EDX, XRD, UV-VIS absorption spectra, and photoluminescence will be presented in this section.

3.4.1 Structural Characterizations

The morphology, composition, and crystallinity of the electrodeposited nanowires were observed and verified via electron microscopy and x-ray diffraction studies.

3.4.1.1 Scanning and Transmission Electron Microscopies

For SEM and TEM analysis, nanowires can be studied either in the pores of the template or free after the dissolution of the membrane. Specimens of template cross-sections or wires embedded in template were obtained by simply snapping the templates in half. This method was not always successful as the configuration of wires might be damaged through the process resulting in poor quality images. Alternatively, if the template containing the wires is attached to a surface and then the template is dissolved, an array of free-standing wires protruding from that surface can be obtained (nanowires forest). For these specimens, the silver coated side of the AAO template was mounted on a small piece of copper tape for mechanical stability and easy handling, then immersed in 3M NaOH for 30 minutes to dissolve the template and expose the wires. The silver film with the protruding wires (still connected to the copper piece), was then rinsed carefully[§] with DI water several times, to remove any excess NaOH, and stored in ethanol solution until the SEM session. To view in a SEM, the copper piece is attached to the carbon tape on the SEM stub. TEM specimens and some SEM samples are prepared by dropcasting few droplets of the desired nanowires suspension onto either a copper grid (200 mesh) or a silicone wafer respectively. The ethanol is then allowed to evaporate, with the aid of a drying lamp, leaving wires adsorbed to the substrate via the Van der Waals interaction. Before dropcasting, the wires dispersed in ethanol are sonicated for a few minutes to make sure that the wires are well separated from each other. Coating of samples was not required as all the nanowires were either conducting or semi-

[§]Evaporated silver film is thin and can easily flip over or split during rinsing which might result in some damaging to the wires structure.

conducting. However when viewing the templates a very thin film (few nanometers) of gold-palladium was sputtered before analysis.

In addition to the images of different nanowires presented throughout the previous section, the different observations acquired during SEM analysis (figure 3.16) provided insight into the growing techniques and conditions.

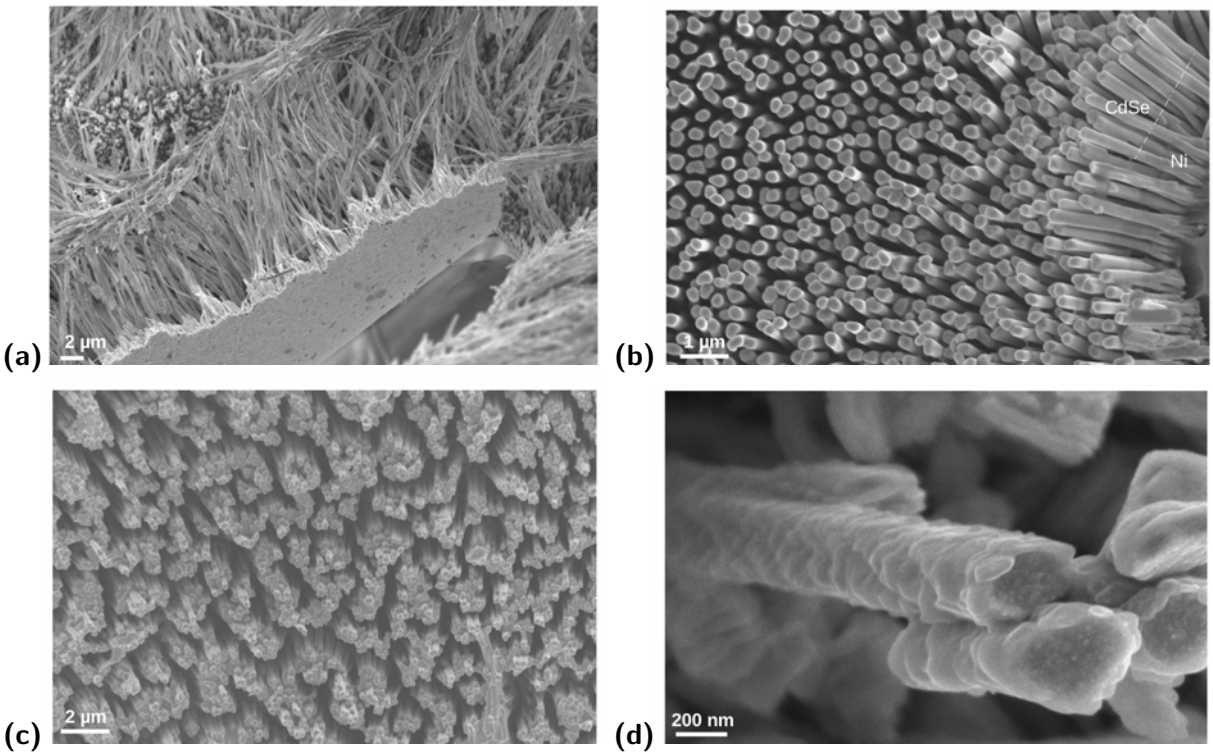

Figure 3.16: SEM micrographs of various electrodeposited nanowires. (a) overgrowth of silver nanowires at high deposition bias (very high growth speed filling the template within a few minutes), (b) contrast between Ni and CdSe segments in a free-standing array of Ni-CdSe wires, (c) agglomeration of the nanowires into bundles after dissolving the host template, and (d) close look at one nanowire showing the amount of surface roughness.

Beside the wires analysis, the dimensions and structure of the AAO templates were also examined by SEM as shown in figures 2.2 and 3.17. For instance, figure 3.17 highlights the imperfections in the commercial AAO templates used in this work.

Atomic composition of the different wires and segments within one wire, particularly CdSe, was checked using the energy dispersive x-ray spectroscopy (EDS) system attached to the SEM and TEM. CdSe stoichiometry was examined under different deposition conditions (section 3.5) until optimum conditions were decided. Figures 3.18 and 3.19 show CdSe nanowires SEM and TEM images with the corresponding EDS spectra confirming the desired stoichiometry of the deposits. The ratio of Cd:Se atomic percentages in the nanowires was found to be ~ 0.92 from SEM measurements. TEM EDS was not quantified here, but the peak heights presented in figure 3.19 (bottom) confirm the SEM results (close ratio of Cd and Se in the nanowires). All SEM EDS spectra included traces of silver and copper due to the template backing layer and copper supporting tape, whereas TEM EDS spectra had signals of carbon and copper from the TEM grids. The EDS spectra are usually taken at several positions through the sample to account for any variations across the wires, and the average atomic composition is reported.

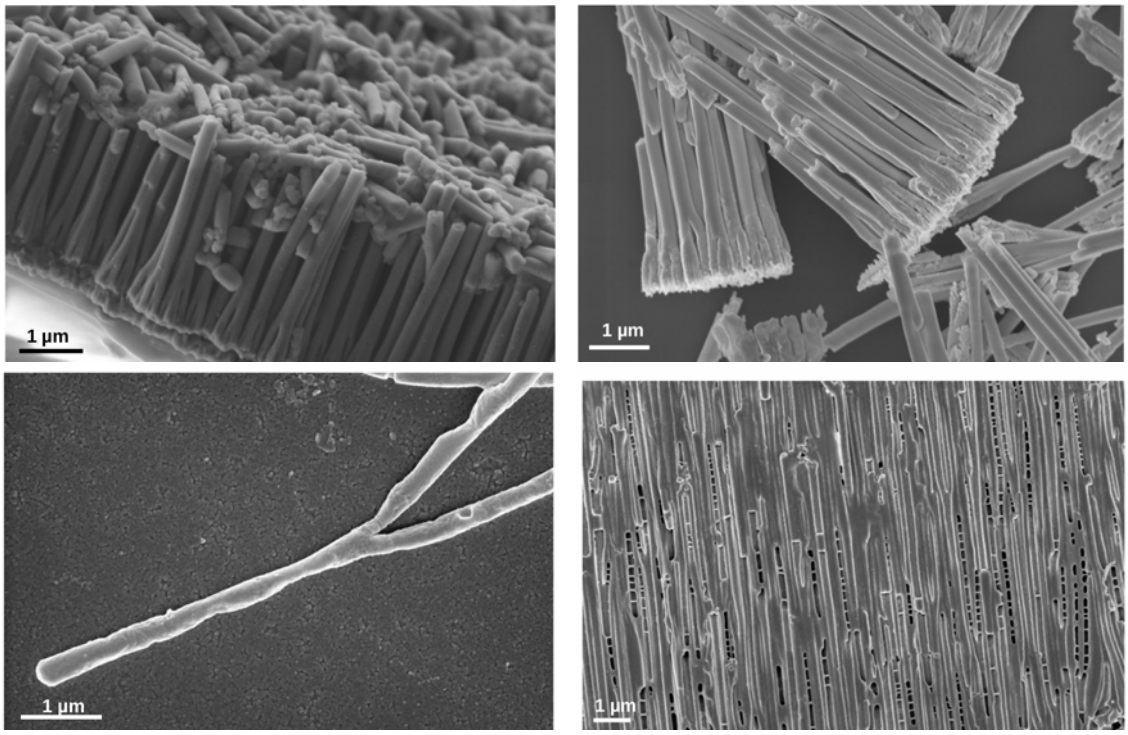

Figure 3.17: SEM images showing imperfections in the AAO templates. Top images are views of CdSe nanowires resembling the branched structure at the bottom of the template. Bottom left image is one of the Y-shaped nanowires. This branching could be avoided by growing a sacrificial conducting layer at the bottom. Bottom right image is a template cross-section view showing defects in the channels.

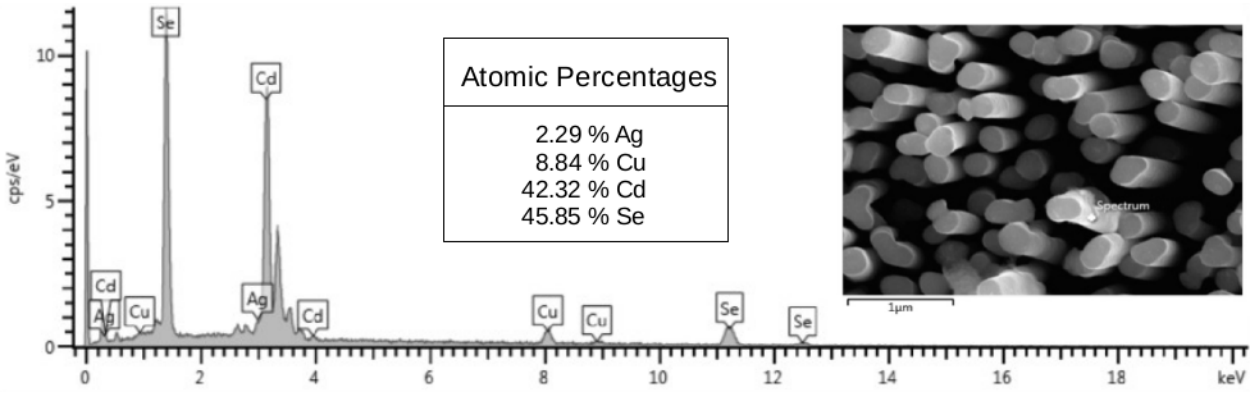

Figure 3.18: An array of CdSe nanowires is presented together with the corresponding EDS showing the stoichiometric composition of the wires. Ag and Cu peaks are from silver-backing layer and Cu tape respectively.

Although segments could be differentiated by contrast due to atomic weight differences (higher atomic weights appear brighter due to less dispersing capabilities), further confirmation was made by analysing the elemental composition of each segment through EDS. Figure 3.20 shows EDS taken at dark and bright segments in a Ni-CdSe nanowire. The bright spots/segments showed larger Cd and Se signals whereas the darker spots demonstrated a larger Ni peak as expected.

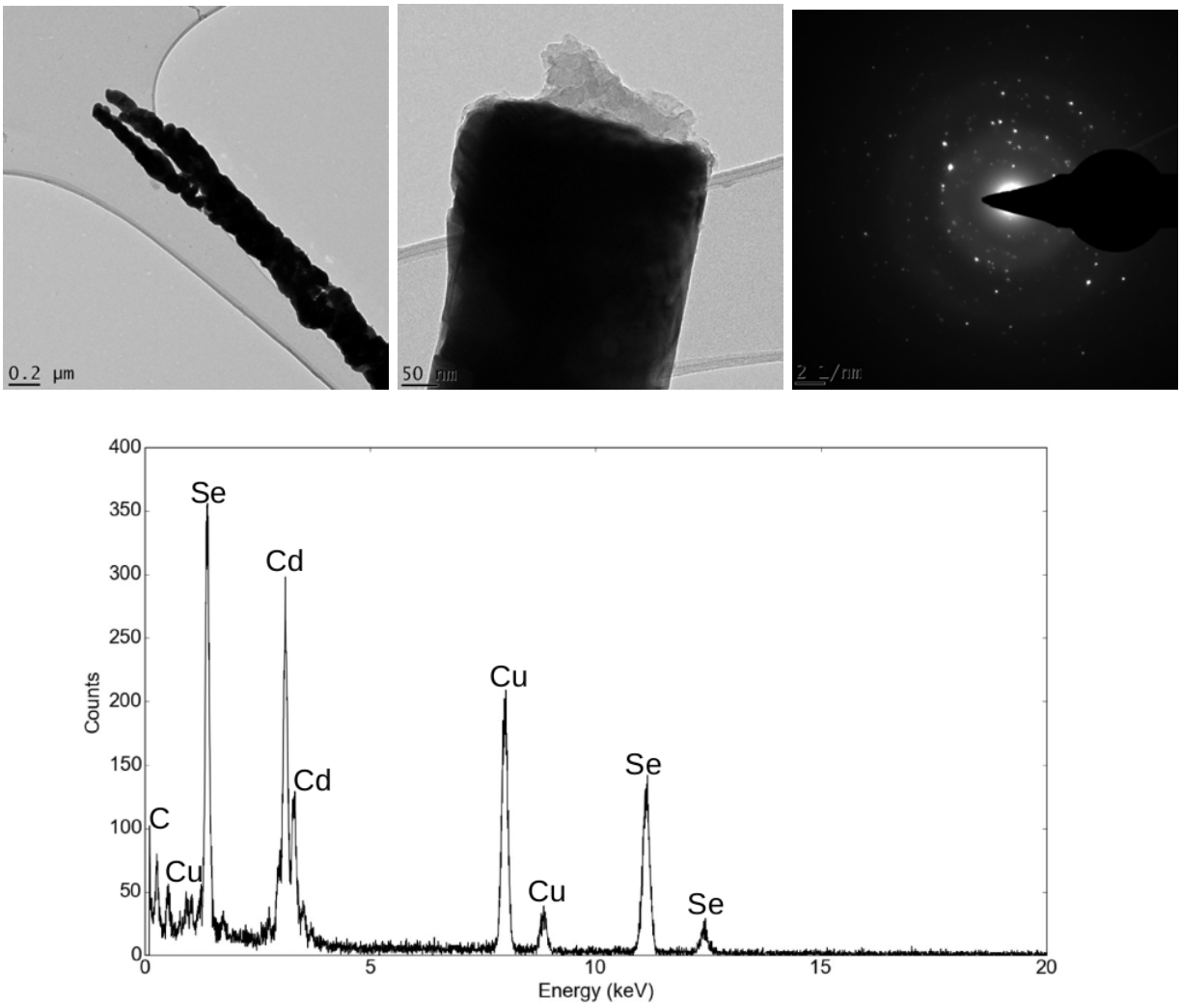

Figure 3.19: TEM analysis of CdSe nanowires. Top pictures are HRTEM images of an as-prepared (left) and an annealed (middle) dense continuous CdSe nanowire at 500 °C in an argon atmosphere for 1 hour. Top right image is the SAED pattern of the polycrystalline as-prepared nanowire. Bottom plot is the EDS spectra of the annealed CdSe nanowires.

3.4.1.2 X-Ray Diffraction

X-ray diffractometry was employed to examine the phase structure and the crystal orientation of the CdSe nanowires. Samples were prepared by dropcasting the nanowires onto a standard amorphous glass slide. This was chosen to avoid strong signals, masking the CdSe peaks, from the silver film (acting as substrate for wires) or copper tape (mechanical support), if a free-standing array of wires was used instead. Figure 3.21 presents the XRD patterns of electrodeposited CdSe nanowires, as-prepared and annealed in an argon atmosphere[¶] at 500 °C. The electrodeposited CdSe wires were polycrystalline as investigated by XRD and confirmed by SAED. The main diffraction peaks recorded in the as-prepared diffractogram can be indexed as face-centered-cubic (fcc) zinc-blende CdSe with peak positions that matches those

[¶]If annealed in air, the oxygen from the air could react with CdSe forming a thin layer of cadmium oxide on the CdSe surface.

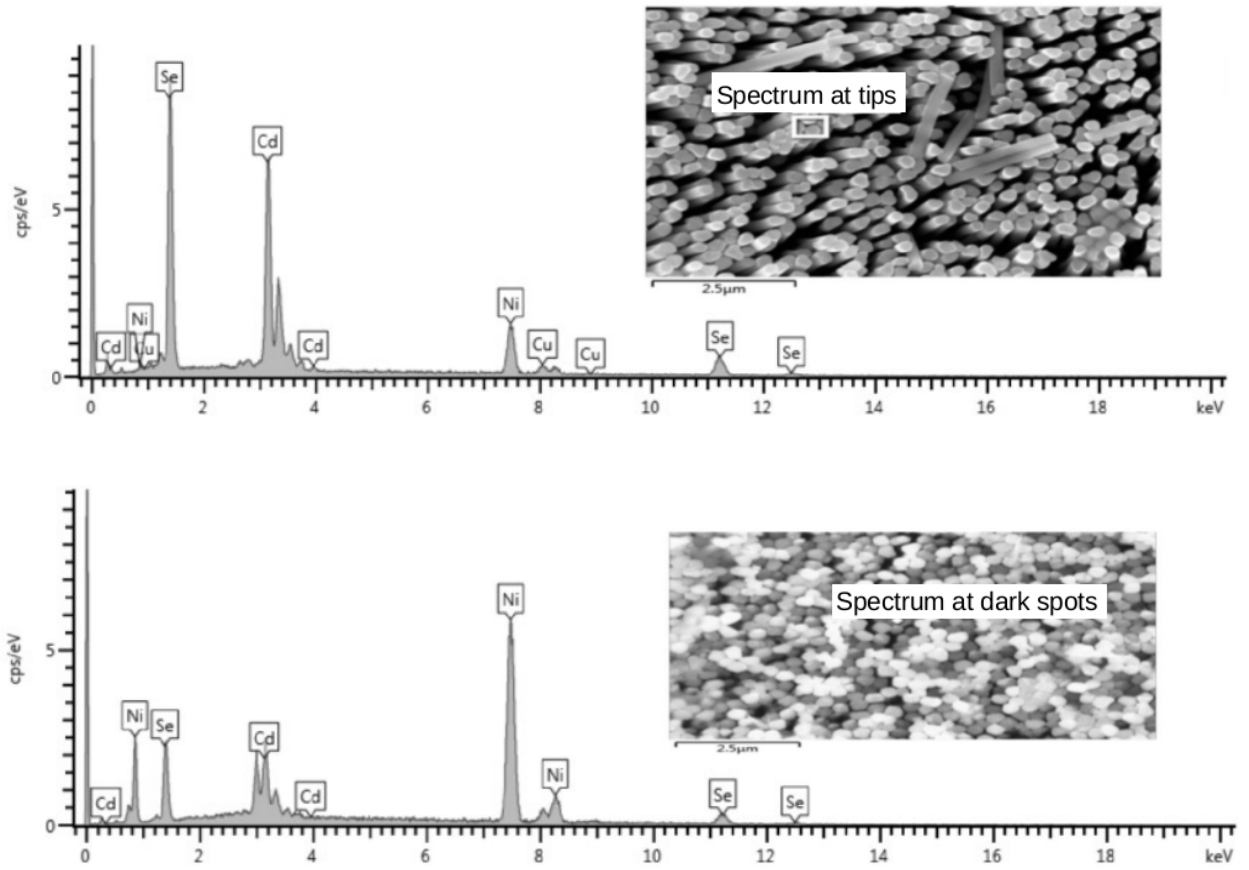

Figure 3.20: EDS spectra of Ni-CdSe array of wires with corresponding SEM images. Spectrum taken at tips of wires have larger Cd and Se peaks as expected (top). Spectrum from darker spots (bottom) indicates places with Ni nanowires (larger Ni signal). Spectra were taken from different parts of sample.

of CdSe JCPDS card 19-0191. This result is in agreement with those previously reported for the electrodeposition of CdSe, in which the as-grown structures exhibited a zinc-blende phase (Bocchetta et al., 2013; Kung et al., 2010). However, some researchers (Riveros et al., 2008) have reported that electrodeposited CdSe nanowires from aqueous electrolytes are amorphous, and the fcc diffraction peaks are only observed as the deposition temperature is progressively increased (temperatures remain below the limit where cubic structure transforms into hexagonal). This could explain the broad and rather noisy cubic peaks obtained in the top plot of figure 3.21. After annealing in an argon atmosphere at 500 $^{\circ}\mathrm{C}$ for 1 hour, CdSe nanowires displayed sharp diffraction patterns corresponding to the hexagonal wurtzite structure matching those of JCPDS card 8-0459. This annealing process apparently results in a complete conversion of the wires structure into the wurtzite form, which is consistent with the well-known phase transition of CdSe from cubic to hexagonal in the 350-400 $^{\circ}\mathrm{C}$ range (Bandaranayake et al., 1995). We observed also that annealing changes the surface of CdSe nanowires; annealed wires (bottom inset of figure 3.21) had some small surface holes which were not noticed in any of the as-prepared samples. In our work, the composition of the electrodeposited wires remained the same before and after the annealing process as confirmed via EDS, whereas many researchers have used this heat treatment to remove excess Se in the deposits (Li et al., 2006).

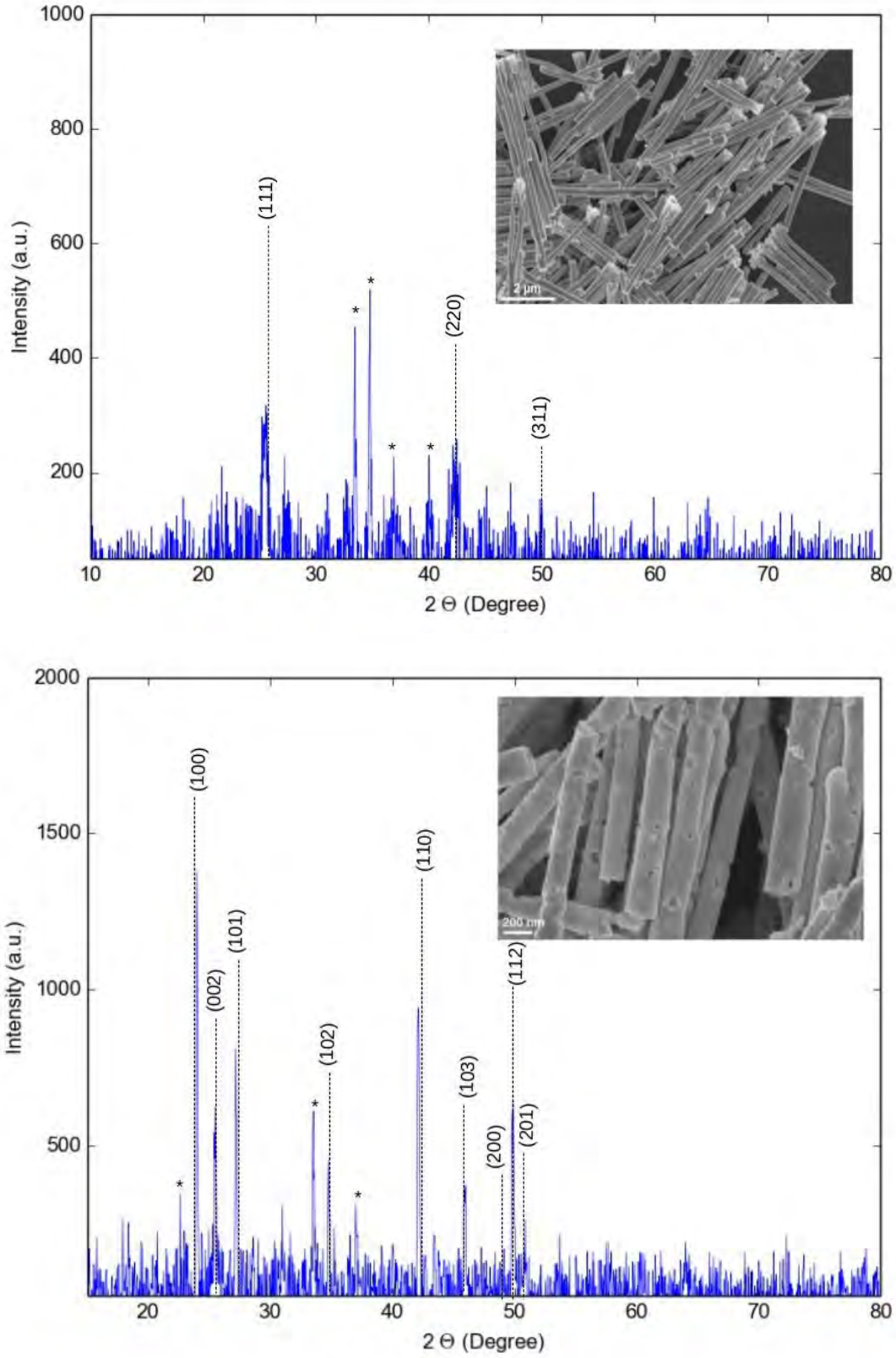

Figure 3.21: X-ray diffraction patterns of as-prepared (top) and annealed (bottom) CdSe nanowires with corresponding SEM pictures. The minor peaks denoted by * are Ag_2Se phases, which is possibly formed as a byproduct of the silver backing-layer and Se ions in the deposition solution. The lines are JCPDS references for cubic (top) and hexagonal (bottom) CdSe structures.

3.4.2 Optical Characterizations

The optical characteristics of the CdSe nanowires were examined using UV-Vis spectroscopy and photoluminescence (PL) as displayed in the figure below. The samples were prepared by simply placing the wires, suspended in ethanol, in a quartz cuvette and then loading them to the spectrophotometer or spectrofluorometer. Prior to inspection of the samples, the suspension of wires should be lightly shaken or sonicated for a few seconds as the wires tend to cluster near the tip of the vial during storage.

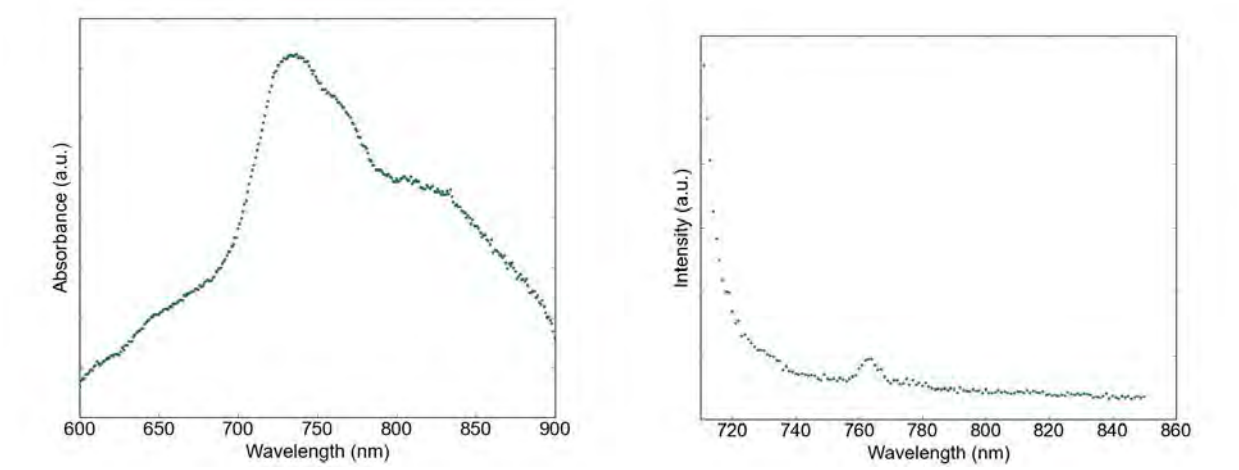

Figure 3.22: CdSe nanowires absorption spectrum (left) focusing on the strong signal around 750 nm and photoluminescence spectrum (right) for this same sample acquired with excitation at 696 nm. In the PL spectrum, the huge signal to the left (~ 710 nm) is expected to be the laser excitation peak.

From the analysis done in Appendix A, the average PL peak of CdSe nanowires is found to be at 763 nm, which corresponds to a bandgap of 1.63 eV. The standard bandgap of CdSe is known to be 1.74 eV at 300K (Pandey et al., 1996). One reason for this shift in our value could be the atomic compositions of Cd and Se within the nanowires. However, more experiments should be done including samples of nanowires with varying Cd:Se ratios to confirm this. Similar shifts to lower bandgaps were reported by Riveros et al. in their study on electrodeposited polycrystalline CdSe microwire arrays (Riveros et al., 2008). They obtained values of 1.46 eV for direct bandgap energy and 1.33 eV for indirect edge. They attributed this behaviour to be generated by an amorphous or disordered phase in the material.

3.5 Results and Discussions

Electrochemical deposition process of nanostructures in the pores of templates is influenced by several parameters. In this section, the factors affecting the growth of the previously mentioned nanowires, together with the mechanism of CdSe formation will be discussed in detail.

3.5.1 Mechanism of CdSe Electrodeposition

Electrodeposition of compound semiconductors is more challenging than metals. The major difficulty in preparing these materials is due to the fact that one of the constituents tends to be formed excessively

resulting in non-stoichiometric deposits. Moreover, when this deposition is performed into micro- or nano- porous membranes, additional complications emerge from the diffusion and migration of ions through the pores. CdSe is not an exception; the reduction potential[‖] of Cd is much more negative than Se, which means it oxidises easier than Se but reduces more difficultly (i.e. Se is more noble than Cd) (Pandey et al., 1996). Given this, we expect that the voltage of deposition solution relative to the working electrode (containing Cd and Se ions) will have values where Se is reduced/deposited but Cd is not. However, at potentials where Cd is easily deposited, Se is also deposited from the solution onto the cathode, which often results in non-stoichiometric CdSe deposits. To address this, we attempted two approaches; using a significantly smaller amount of selenium salt in the solution and applying the cyclic electrodeposition/stripping technique suggested by (Kressin et al., 1991).

This mechanism, represented schematically in figure 3.23, involves three stages. In I, CdSe along with Se are deposited into the substrate. Region II includes excessive deposition of Cd due to the high concentration of Cd ions in the solution, and since the CdSe phase has a large negative free energy of formation (ΔG_f^0 = -100.4 kJ mol^{-1}), it is believed that any free Se will react with that excess Cd forming CdSe (Lincot, 2005). Finally, in region III (the anodic half of the scan), the excess Cd that has not reacted with Se is stripped back, leaving behind stoichiometric CdSe. This sequence is then repeated, building layers of CdSe on the electrode surface, i.e. increasing the length of the nanowires produced.

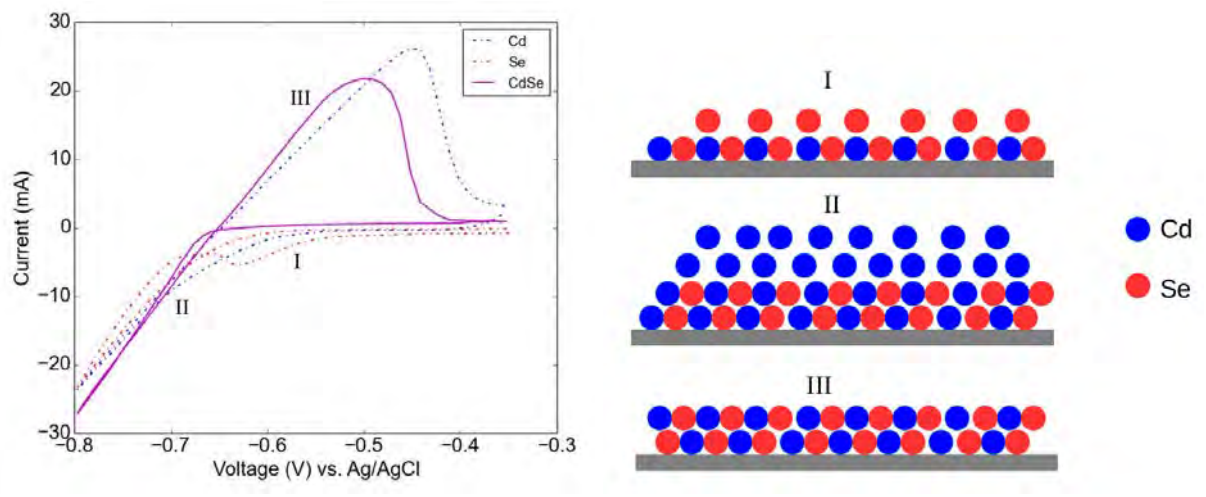

Figure 3.23: Left plot is a cyclic voltammetry analysis of solutions containing Cd ions only, Se ions only and both (stages I, II, and III apply to the voltammogram of Cd and Se ions solution). Right picture is a set of schematic diagrams of the formation mechanism of CdSe through this applied potential scan.

In an acidic solution where $CdSO_4$ and SeO_2 salts are hydrolysed to $Cd^{2+} + SO_4^{2-}$ and H_2SeO_3 respectively, the following reactions can occur at the cathode. According to Kazacos and Miller (Kazacos and Miller, 1980), the electrodeposition of CdSe starts by the formation of H_2Se which then combines with Cd^{2+} in the solution to produce CdSe

$$H_2SeO_3 + 6H^+ + 6e^- \rightarrow H_2Se + 3H_2O \tag{3.5.1}$$

[‖] The standard reduction potentials tell us which reduction reaction will be more favorable. A reduction reaction with a higher positive potential is more favourable thermodynamically than a reduction reaction with a low reduction potential. Standard reduction potentials of Cd and Se are -0.4029 V and +0.74 V versus NHE respectively.

$$H_2Se + Cd^{2+} \rightarrow CdSe + 2H^+ \tag{3.5.2}$$

During this, formation of Se can occur according to reaction 3.5.3, which competes with reaction 3.5.2. However, at low concentrations of H_2SeO_3 (i.e. low quantities of SeO_2 salt), reaction 3.5.3 can be suppressed limiting the excess Se in the deposits.

$$2H_2Se + H_2SeO_3 \rightarrow 3Se + 3H_2O \tag{3.5.3}$$

But Mishra and Rajeshwar (Mishra and Rajeshwar, 1989) have argued that the formation of CdSe is a direct $6e^-$ reduction through the following equation

$$H_2SeO_3 + Cd^{2+} + 6e^- + 4H^+ \rightarrow CdSe + 3H_2O \tag{3.5.4}$$

In either methods, the net reaction can be expressed via equation 3.5.4.

3.5.2 Electrodeposition Conditions

The experiments identified four parameters that affect the electrodeposited structures. These are applied potential range, concentration of the ions in the deposition bath, pH of the electrolyte, and scan rate values for the cyclic voltammetry deposits. In the CdSe case discussed below, these parameters are crucial for the stoichiometry of the produced deposits. Starting with the applied potential range, a wide CV scan was performed on the required working electrode in the presence of the Cd and Se ions. The voltammogram presented in figure 3.24 shows various peaks and plateaus associated with CdSe plating solution and silver-backed AAO template. In the forward negative-going scan, selenium begins to deposit at -0.5 V, while cadmium deposition onsets at ca. -0.65 V. One can notice here that Cd deposition took place at the more negative potential compared to Se deposition, which is consistent with Se being the noble element. During the reverse positive scan, cadmium stripping usually occurs at ca. -0.6 V, but if the voltage is scanned toward more positive values (not shown here), Se and CdSe oxidation will start to occur around $+0.8$ V and $+1.3$ V respectively resulting in additional two current peaks (Li et al., 2006). This assignment of the peaks is supported by the voltammograms of solutions containing either Cd^{2+} or SeO_3^{2-} ions in figure 3.23. Moreover, the peaks in figure 3.24 are consistent with the extensive study done by Benkowski et al. (Bieńkowski et al., 2010) listing the deposition and dissolution of CdSe, and the possible redox processes of Cd^{2+} and SeO_3^{2-} ions at different electrode conditions. In general, fabricating nanostructures could possibly leave parts of the working electrode exposed to the solution which results in other behaviours (represented in the electroactivity of the working electrode) appearing during the applied potential sweep. Based on the above analysis, the potentials were swept between -0.35 and -0.8 V for all the other depositions of CdSe nanowires. The chosen electrodeposition window was kept as narrow as possible to minimize the roughness due to diffusion-limited growth caused by large overpotential (Gu et al., 2012). This potential window also matches the ranges suggested in literature for CdSe deposition from acidic baths (Kressin et al., 1991; Pena et al., 2002).

As mentioned earlier, it is more favourable for Se to be reduced when a negative potential is applied (compared to Cd) leading to Se-excess deposits. Therefore, adjusting the concentrations of Cd^{2+} and SeO_3^{2-} ions in the aqueous plating solutions is necessary for achieving stoichiometric CdSe structures. Most of the acidic baths employed for CdSe deposition used a Cd salt and millimolar concentrations of H_2SeO_3 or SeO_2 (Klein et al., 1993; Pena et al., 2002; Li et al., 2006; Schierhorn et al., 2008; Shpaisman

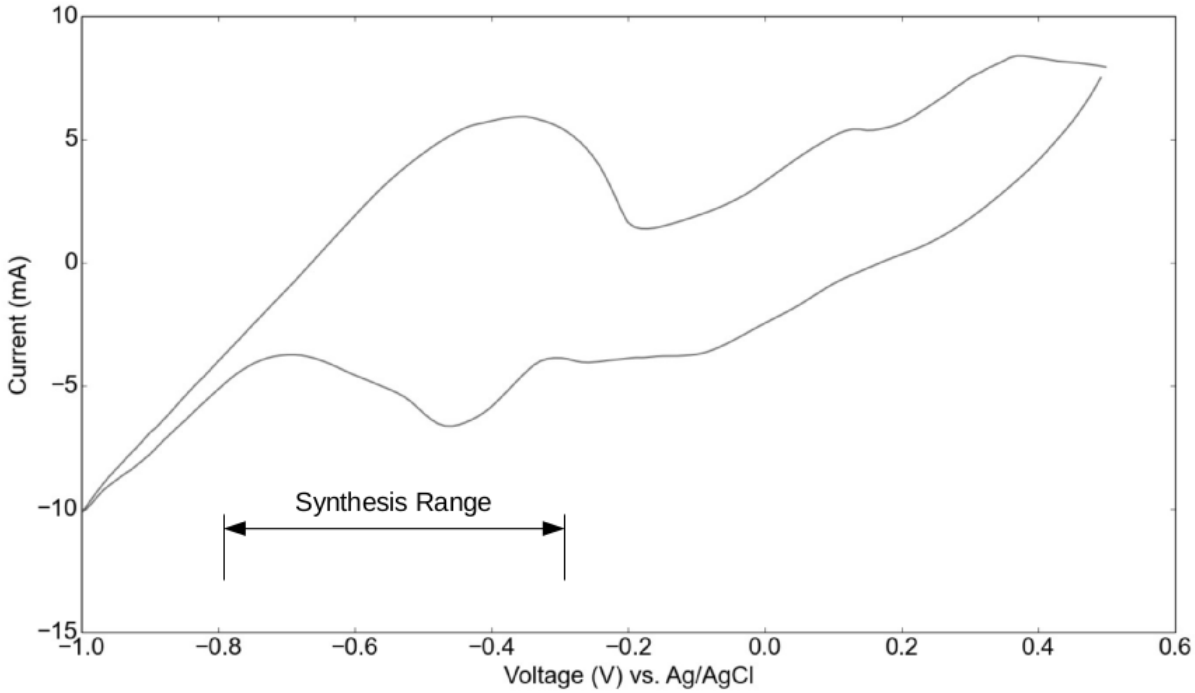

Figure 3.24: A survey cyclic voltammogram of 0.3 M $CdSO_4$ + 0.7 mM SeO_2 + 0.25 M H_2SO_4 solution. Scan rate is 30 mV/sec. Marked synthesis range is chosen for further depositions.

et al., 2010). In the electrodeposition/stripping technique pioneered by Kressin et al. (Kressin et al., 1991) and followed later by many researchers to produce CdSe nanowires (Klein et al., 1993; Pena et al., 2000; Schierhorn et al., 2008, 2009), an acidic solution containing 0.3 M $CdSO_4$ and 0.7 mM SeO_2 was reported to produce stoichiometric CdSe deposits. Interestingly in our work, cathodic deposition into the pores of silver-backed AAO templates from this solution always produced Se-rich structures. A similar problem was also described by Kung et al. while preparing arrays of lithographically patterned electrodeposited CdSe nanowires (Kung et al., 2011). To overcome this, a modified Cd:Se ratio of 5:1 was used (instead of the 500:1 ratio solution mentioned above). By employing this solution, the amount of excess Se is minimized producing near-stoichiometric CdSe one-dimensional structures. Furthermore, in a detailed study performed by Bienkowski et al. investigating the influence of deposition solution composition on the stoichiometeries of electrochemically grown CdSe films, the ratio $Cd^{2+} : SeO_3^{2-} =$ 5:1 was found to be the most satisfactory in obtaining stoichiometric CdSe deposits (Bieńkowski et al., 2010). This solution also produced high-quality wires (in terms of morphology) when compared to the 500:1 ratio deposition solution as seen in figure 3.25.

The elemental stoichiometry of the CdSe nanowires is affected not only by the Cd:Se ratio in the deposition solution, but also by the potential scan rates. For instance, earlier attempts on the 500:1 deposition solution produced Se-rich nanowires at higher scan rates (>250 mV/sec) while lower scan rates resulted in Cd deposits. Moreover, the morphology of nanowires were affected by varying scan rates as seen in figure 3.26.

It should be also noted that the scan rates and the deposition solutions together with the nature of the substrate affect greatly the recorded cyclic voltammogram of CdSe deposition as shown in figure 3.27.

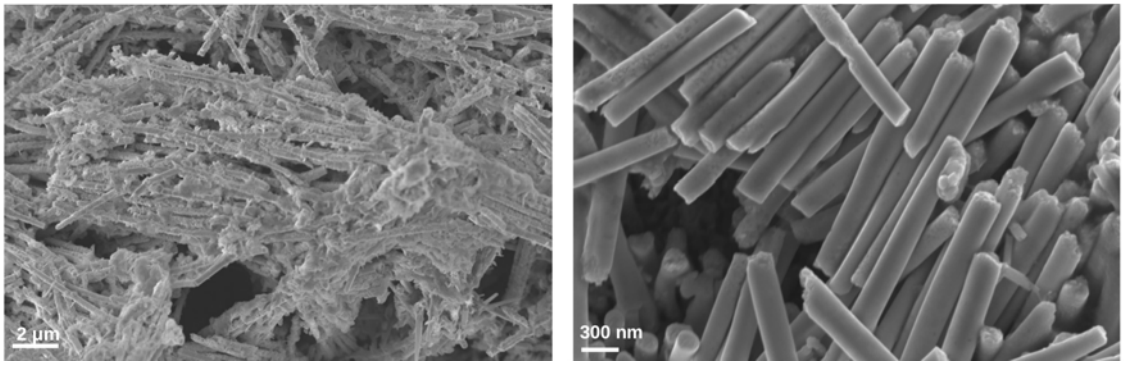

Figure 3.25: SEM pictures of Ni-CdSe nanowires prepared in AAO templates with different CdSe deposition solutions. Ratio of Cd:Se is 500:1 (left) and 5:1 (right) in the first and the second solutions. Potential range was (-0.35 → -0.8) V at a scan rate of 50 mV/sec.

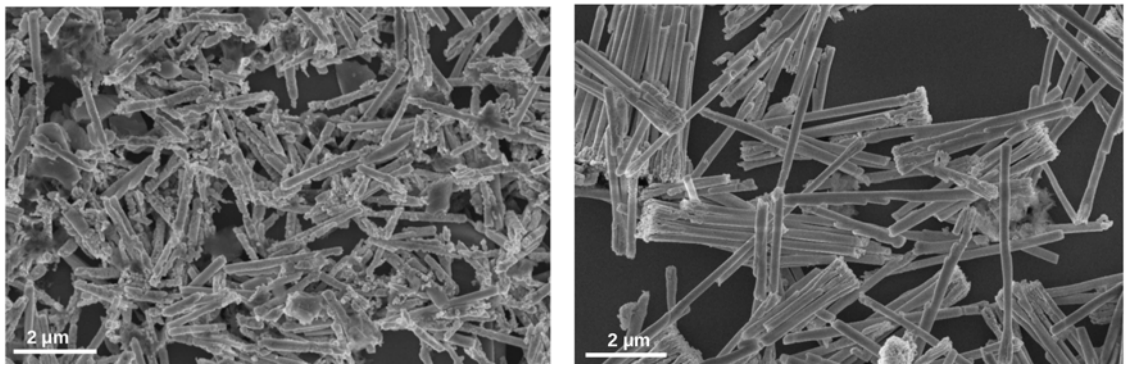

Figure 3.26: SEM pictures of CdSe nanowires prepared in AAO templates from the 5:1 Cd:Se solution and applied potential of (-0.35 → -0.8) V at different scan rates: 50 mV/sec (left) and 10 mV/sec (right). Duration of electrodepsition of both nanowires was 600 cycles.

For further investigations, the two previously mentioned deposition solutions were prepared (500:1 and 5:1 in Cd:Se ratio) and the applied voltages were swept at two extreme scan rates (very low=10 mV/sec and very high=750 mV/sec). Samples using the different combinations of these conditions were synthesized and the morphology of the produced nanowires was observed. Compositional analysis (EDS) was also performed on them.

Using the 500:1 solution with the high scan rates produced rough Se-rich structures, while low scan rates produced rough thin Cd deposits as shown in figure 3.28 (a-c). In the first case, this could be attributed to a diffusion problem through the template pores as, interestingly, CdSe films prepared under the same conditions were stoichiometric. In the second case, some of these wires are believed to be growing too fast, protruding from the pores, and blocking them forming large Cd crystals on the surface of the template as confirmed by SEM investigations. This behaviour was repeated, most of the times a solution with very high quantities of Cd was used in a low scan rate regime. The deposition of Cd only in this environment was confirmed when a CdSe film sample was prepared under the same conditions and was found to be composed of Cd only with very tiny amounts of Se. The deposited film appeared silver-greyish not dark brown as expected for CdSe, which was confirmed via EDS measurements to be Cd. When the 5:1 solution was used with a high scan rate, stoichiometric wires were formed but with Cd chunks on the top (after the template was dissolved) as seen in figure 3.28 (d). The final combination

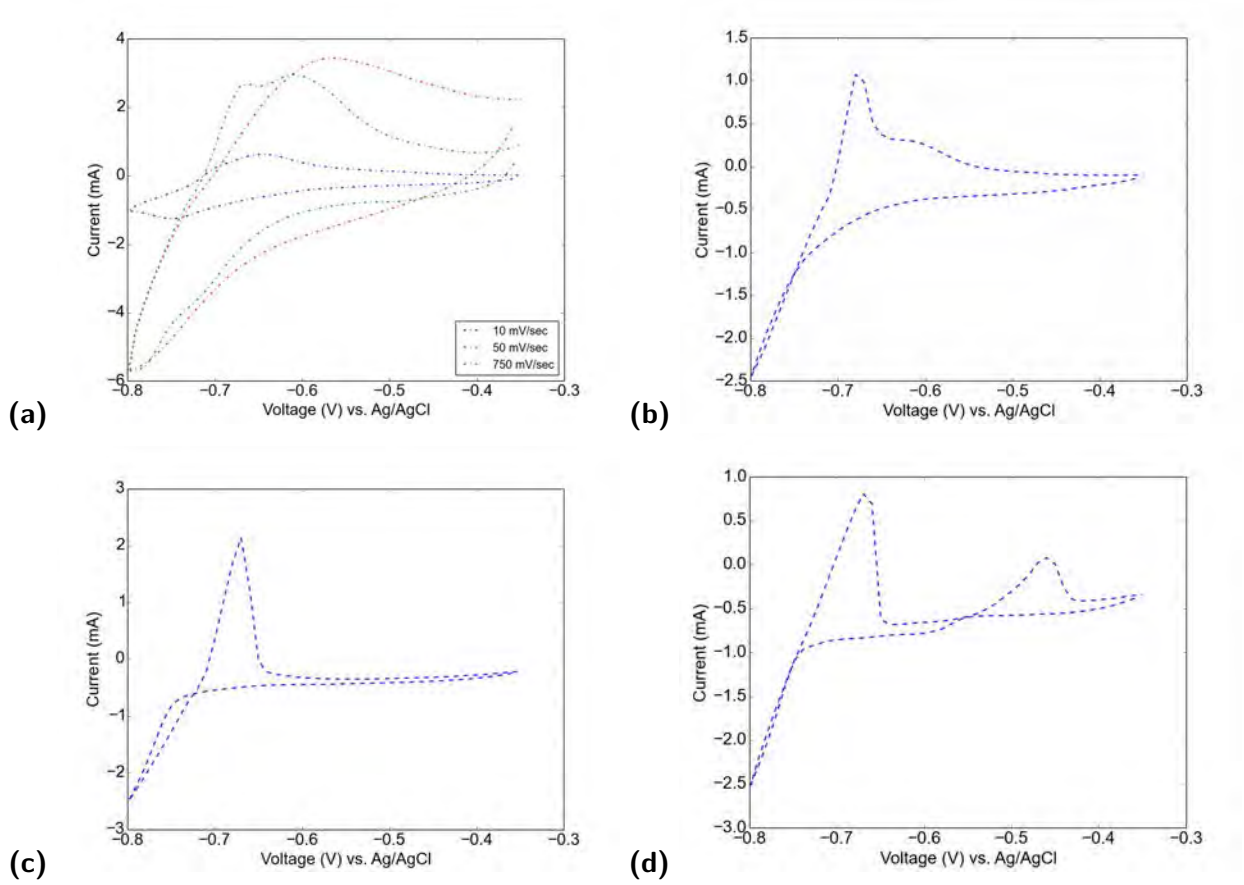

Figure 3.27: Cyclic voltammograms of CdSe deposition from 5 mM $CdSO_4$ + 1 mM SeO_2 + 0.25 M H_2SO_4 solution using (-0.35 → -0.8) V at a scan rate of 10 mV/sec onto various substrates. (a) AAO templates, (b) PCTE templates, (c) Cu film, and (d) FTO glass. In (a) different scan rates are plotted under the same conditions, increasing the scan rate resulted in higher current values which is typical for a diffusion-control process.

of the 5:1 solution and a low scan rate was found to produce the best yield. Nanowires synthesized under these conditions were of high-quality, smooth, and with stoichiometry near 1:1 ratios. Therefore, based on these inspections, the 5:1 Cd:Se ratio solution is used with low scan rate at the previously chosen potential range for further experiments in chapters 4 and 5.

For metal nanowires, the process was simpler, once the proper deposition potentials were decided as presented in section 3.2 growth was straightforward. For the scope of this research, successful growth of a required metallic segment inside the pores was sufficient.

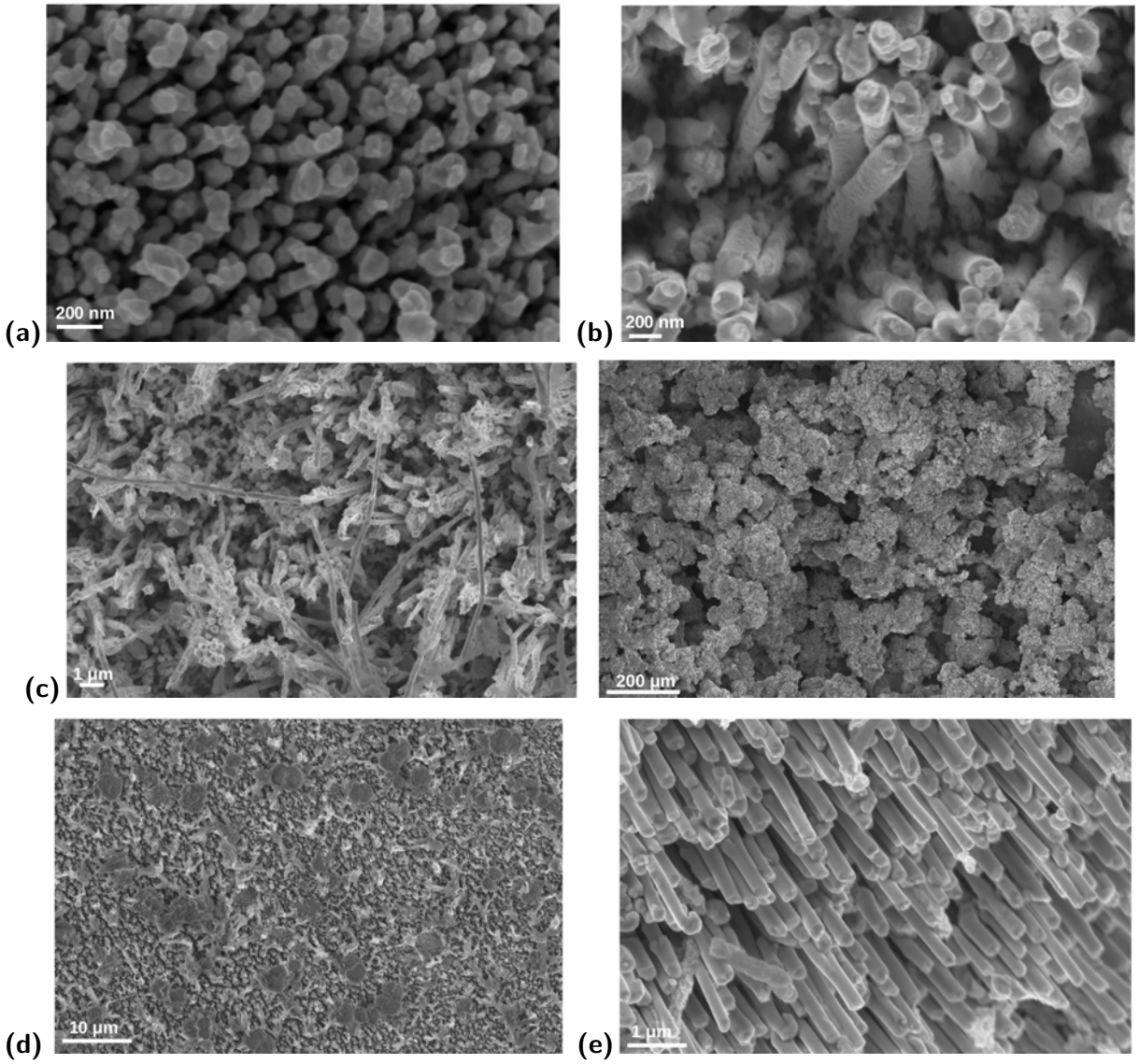

Figure 3.28: SEM images of CdSe deposition trials under different solutions and scan rates into the pores of silver-backed AAO templates. Applied voltage was (-0.35 $\rightarrow$ -0.8) V. (a) 500:1 solution at 750 mV/sec for 80 minutes, (b) 500:1 solution at 750 mV/sec for 4 hours, (c) 500:1 solution at 10 mV/sec and Cd deposits on the surface of template (right), (d) 5:1 solution at 750 mV/sec, and (e) 5:1 solution at 10 mV/sec.

4. Electrical Properties and Photoconductivity Measurements

In this chapter, the electrical characteristics of the grown structures are explored. A review of the current methods used to establish electrical contacts to the electrodeposited nanowires, either individually or in arrays, is presented. The first section deals with the measurements on an array of nanowires, while the second section introduces the fabrication of single-nanowire devices, and their transport measurements.

4.1 Array of Nanowires

The templated electrodeposition technique produces an array of nanowires, embedded in an insulating structurally-stable template (usually AAO or PCTE), to which macroscopic contacts can be easily made resulting in a simple qualitative two-point measurement setup.

4.1.1 Array Structure and Fabrication

Electrical contacts to the top surface of the template can be made in several ways such as thermal evaporation, sputtering, conducting paste, pressure contacts, or using a microscopic plunger tip. Post-electrodeposition chemical etching or mechanical polishing of the template could be effective in facilitating contacts to nanowires grown in AAO membranes. Although the conducting paste method is the simplest, microscopic plunger tips allow to perform a number of measurements at different locations on the same sample (Tang et al., 2007).

In our work, the array of the desired nanowires were fabricated via electrodeposition, as discussed in section 3.3, inside the pores of silver-backed PCTE membranes. The only difference is that the deposition is continued here until the nanowires start to emerge from the pores forming the caps (mushroom structures usually micron-size), so that macroscopic contacts can be made. Monitoring the growth of the wires* in the template channels can be done through the chronoamperogram as shown in figure 2.8. After the templates have been washed and dried, two macroscopic silver wires were attached to both sides of the membrane using silver epoxy (cured overnight). These two wires were then soldered to a BNC connector, attached to a small sample holder box as shown in figure 4.1, which is connected to a computer-controlled Keithly source measuring unit (SMU) via a preamplifier.

Beside providing a simple setup for checking IV characteristics of nanowires, this measurement technique has the advantage of protecting the wires from oxidation effects (nanowires remain isolated during the whole process). On the other hand, in these measurements the number of contacted nanowires is usually unknown, and therefore it is difficult to preform any quantitative analysis.

4.1.2 Array Measurements

Klein was one of the first to fabricate and examine the I-V characteristics of cadmium chalcogenide arrays in alumina templates (Klein et al., 1993). He also preformed point-contact I-V measurements

*It is important here to ensure complete isolation of the backing conductive layer in order to relate the recorded chronoamperogram to the wires growing into the template channels.

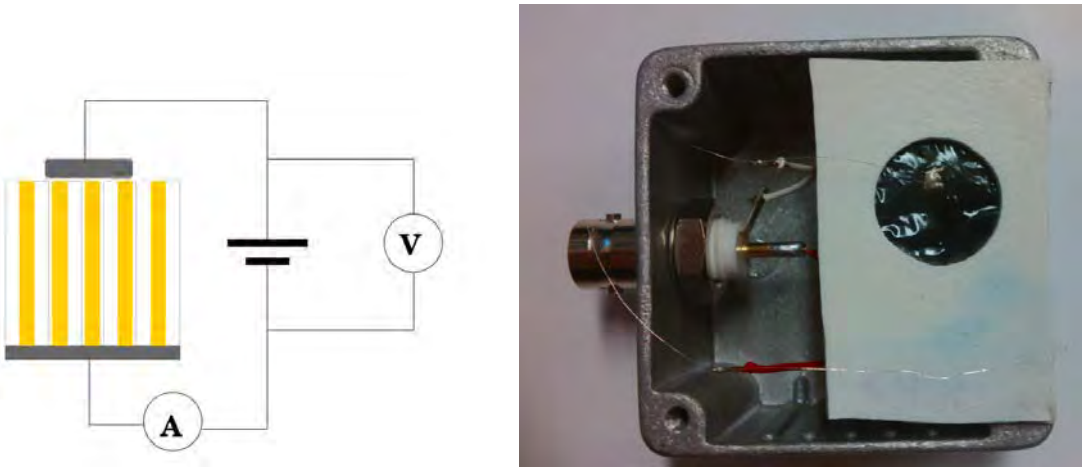

Figure 4.1: Left is a schematic diagram of nanowires array in a template with conductive paste on top. Right is a picture of the box used in our measurements. A hole is drilled for the BNC connector which can be soldered to any template that needs to be measured. The template is supported by the same insulating rubber sheet used in the electrodeposition process.

on CdSe-Ni samples and indicated that the CdSe-Ni interface is rectifying. Pena et al. (Pena et al., 2000) have also produced arrays of metal-CdSe-metal and metal-CdTe-metal nanowires in both PCTE and AAO templates and reported their electrical characteristics. Later, Shpaisman (Shpaisman et al., 2010) et al. synthesized arrays of morphology-based segmented and non-segmented CdSe nanowires in PCTE membranes and investigated the effect of this segmentation on the electrical transport and photoresponse of the ensemble of nanowires. Kalhori et al. (Kalhori et al., 2015) also explored the photoresponse of CdSe nanowires array electrodeposited in PCTE membranes.

Here, we report the two-point measurements performed on arrays of nanowires embedded in PCTE templates. Figure 4.2 presents the current response of a voltage sweep on Ni and CdSe nanowires ensembles. As seen, Ni and CdSe are showing ohmic and semiconductor-like (near-ohmic) behaviours respectively. Both responses were symmetrical and did not show a rectifying behaviour, suggesting ohmic contacts with the silver top and bottom electrodes.

The I-V measurements of the nanowires were also carried out at liquid nitrogen temperatures. Both arrays of Ni and CdSe nanowires behave as expected for metals and semiconductors respectively. As seen in figure 4.3 plots, the resistance of Ni nanowires decreases by almost a factor of two when the sample holder is inserted in liquid nitrogen. On the contrary, CdSe nanowires resistance is nearly infinite at liquid nitrogen temperatures. This is a typical behaviour of an intrinsic (undoped) semiconductor as all of the available charge carriers are expected to be thermally-generated.

Measurements were also preformed on Ni-CdSe nanowires as demonstrated in figure 4.4, where the junction between Ni and CdSe segments is showing a rectifying behaviour as expected between a metal with a work function (ϕ_{m}) higher than that of the semiconductor (ϕ_{s}). The schematic band diagrams of Ni (metal) and CdSe (n-type semiconductor) before contact, after the junction is formed, and upon applying a bias are also shown in figure 4.4. When a forward bias is applied to the nanowires, i.e. Ni is connected to the positive terminal while CdSe is connected to the negative terminal, the potential barrier is lowered so that electrons can easily move from the semiconductor into the metal creating a net current flow.

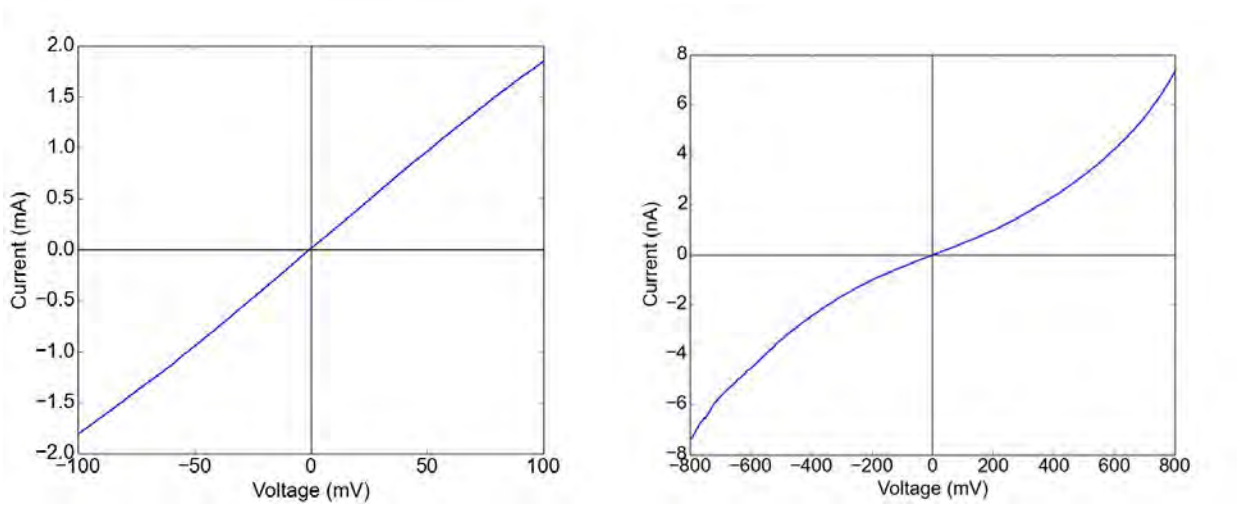

Figure 4.2: I-V plots of Ni (left) and CdSe (right) nanowires array.

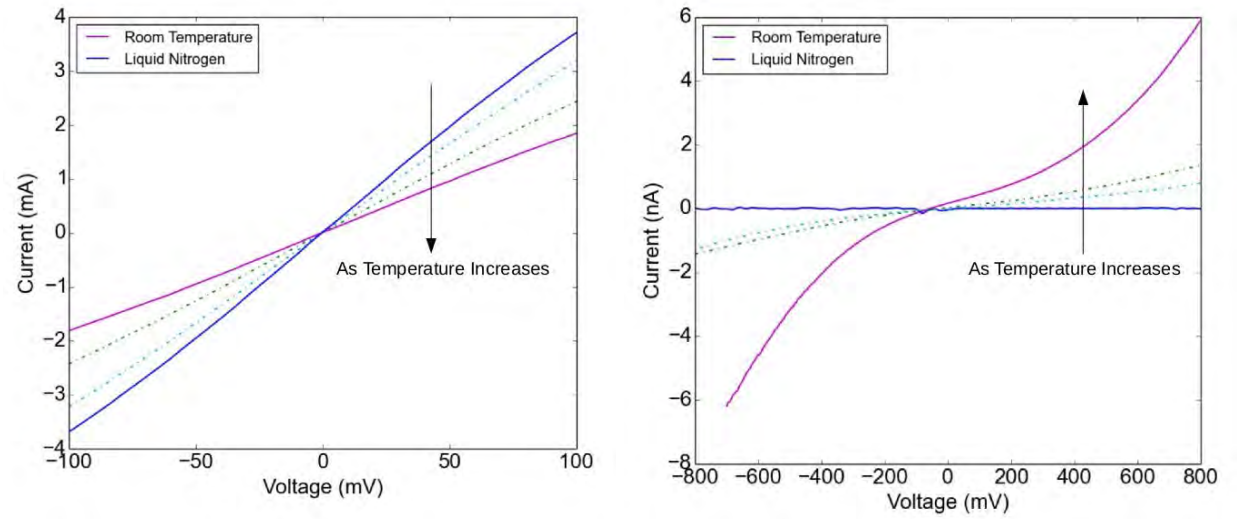

Figure 4.3: Ni (left) and CdSe (right) nanowires I-V characteristics as a function of temperature. The dotted lines represent I-V data recorded as the temperature increases from liquid nitrogen to room temperature.

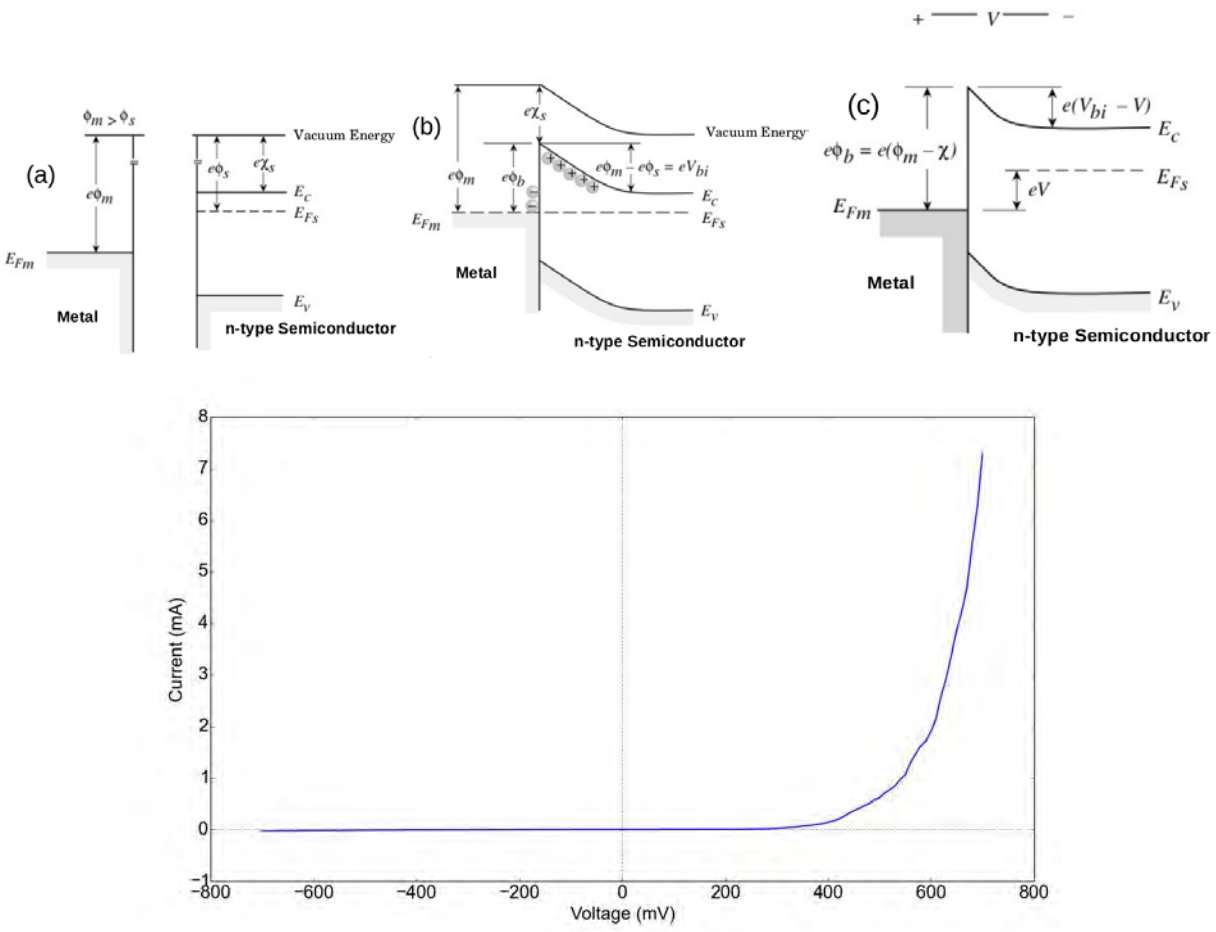

Figure 4.4: Top pictures are schematic energy diagrams of a metal-semiconductor junction. (a) Band profiles of the metal and semiconductor before contact, (b) formation of the Schottky junction after contact (at equilibrium), and (c) after applying a forward bias. Bottom left plot is the I-V characteristics of the Ni-CdSe nanowires array. From the responses of CdSe and Ni shown in figure 4.2, we may assume that Ni-CdSe nanowires have ohmic contacts with the external silver electrodes and the rectifying behaviour is solely due to the Ni-CdSe interface.

Since CdSe is a photo-active semiconductor, measurements on CdSe nanowires were preformed in dark and under illumination as shown in figure 4.5. As seen, there is a significant enhancement in current when wires are illuminated by low-intensity white illumination from a magnifying lamp and blue laser source. When the wires are under illumination, the incident photons with energy higher than the bandgap of CdSe will excite electron-hole pairs (excess free carriers) generating a photo-current, i.e. an enhancement to the current through nanowires at a certain bias, which relies on the illumination intensity[†]. As shown in figure 4.5, the increase in current at the same bias for a low intensity light source is about 5 times lower than upon using an focused laser beam. For our device, the resistance[‡] is found to be 125 ± 8 MΩ from the dark currents at -1 V. Under white-light lamp and blue laser illumination, the resistances of the device were found to be 25 ± 1 MΩ and 5.00 ± 0.25 MΩ respectively. These

[†]Given the low intensity of the used laser beam (few mW per cm^2) and the relatively wide bandgap of CdSe, it is unlikely that thermally generated carriers contribute to the enhancement of current.

[‡]The uncertainty in resistance calculations associated with measurements is presented in Appendix A.

values correspond to a decrease in the device resistivity by values of ca. 5 and 25. Other researchers reported the decrease in resistivities of electrodeposited CdSe nanowires arrays upon illumination to be ca. 15 (Azulai et al., 2012) and 110 (Kalhori et al., 2015).

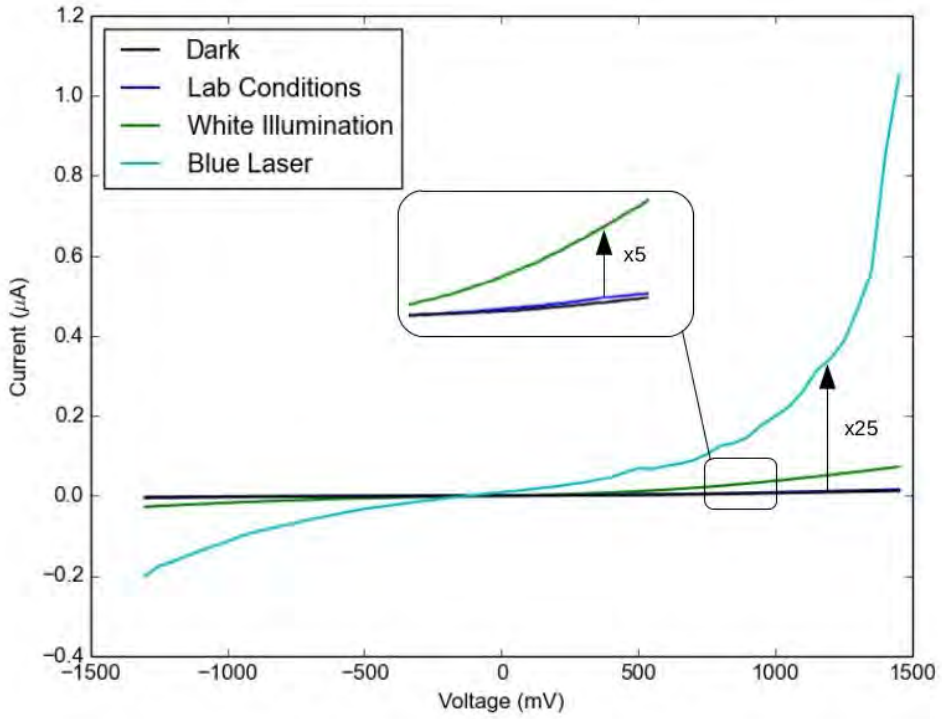

Figure 4.5: I-V characteristics of CdSe nanowires array in dark and different illuminations. Inset: zoomed-in view on the current enhancement due to low intensity white illumination.

4.2 Single Nanowire Device

Although nanowires array measurements provide an easy tool to investigate the electrical characteristics of the grown structures and the nature of junctions between different segments of nanowires, quantitative analysis (such as absolute conductivity) is not possible on these setups as the exact number of nanowires remains unknown. One method to achieve that is fabricating a device with a single nanowire (of known dimensions) and preform measurements on it (Pena et al., 2002). In this section, we attempt to fabricate a single CdSe nanowire device and examine its transport properties.

4.2.1 Device Fabrication

The fabrication of low-resistance macroscopic contacts to nanostructures is a very challenging task. In the case of single-nanowire device, several methods have already been reported to isolate and measure a single nanowire. The most common technique involves depositing the already grown nanowires onto a silicon/silicon oxide substrate and then forming contacts to individual wires via optical and ebeam lithography, or nano-manipulating probes (Talin et al., 2010).

Some of the other used approaches are shown in figure 4.6. The first method involves positioning of the dropcasted wires between prepared electrodes using the dielectrophoretic alignment technique (Maijenburg et al., 2011a). Another interesting procedure for contacting single nanowires is based on single-ion irradiation of polymer membranes (Toimil-Molares, 2012). The single-wire fabrication and contacting process is demonstrated in figure 4.6. The steps include (a) fabricating a single-pore membrane by ion irradiation and etching, (b) depositing the conducting back-layer, (c) electrodepositing the single nanowire, (d) contacting the embedded nanowire via a conductive layer on the top surface of the template, and (e) attaching macroscopic wires to both ends for measurements. This approach avoids the delicate handling of the nanowires and thus minimizes the risk of mechanical damage.

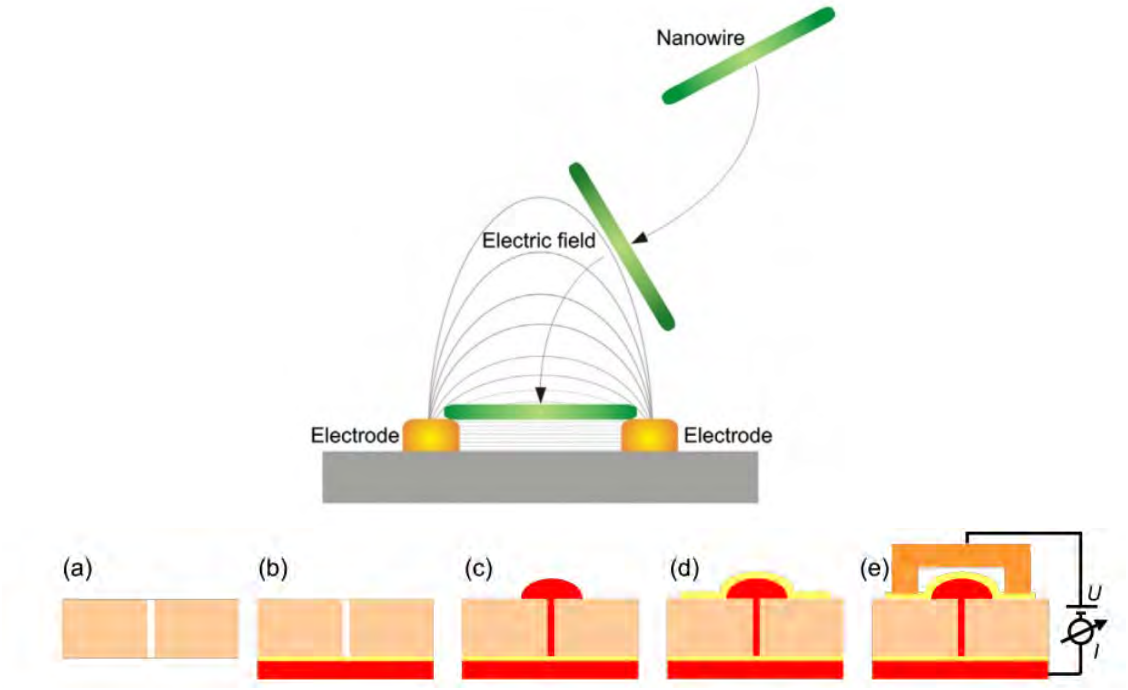

Figure 4.6: Schematic representations of other methods used to contact a single nanowire. Dielectrophoretic alignment technique (top) (Maijenburg et al., 2011a) and utilizing a single-pore membrane (bottom) (Toimil-Molares, 2012).

In our work, we fabricated single-wire devices via electron beam lithography as follows.

First: Dropcasting of the nanowires. The CdSe nanowires electrodeposited into AAO templates are released and suspended in ethanol solution as discussed in section 3.3. After lightly shaking the vial to spread the wires uniformly throughout the solution, a single drop was drawn by a pipette and dropcasted onto patterned silicon wafers[§] with a silicon oxide coating (cleaved to dimensions according to desire). To remove bigger clusters of the wires and drying stains, the wafer is then cleaned by submerging and lightly shaking in acetone and isopropanol, and dried off on a hot plate at $100^{\circ}\mathrm{C}$ until liquid has evaporated. After inspection by optical microscope, the cleaning process is repeated if needed. It should be noted that the number of wires on the substrate is controlled by varying the concentration of wires in the solution and/or the number of drops deposited on the wafer as seen in figure 4.8. Next, suitable candidates are identified under the optical microscope, with 1500 magnification (in both bright and dark field). The criteria of suitability are: the wires are single, of adequate length, as homogenous in

[§]Electron beam patterned silicon wafers were fabricated in the Cavendish Laboratory, UK.

structure as possible to determine, and relatively far (at least a few μm) from any other wires/clusters or alignment marks. The candidate wires are then further inspected by electron microscope to confirm the above criteria.

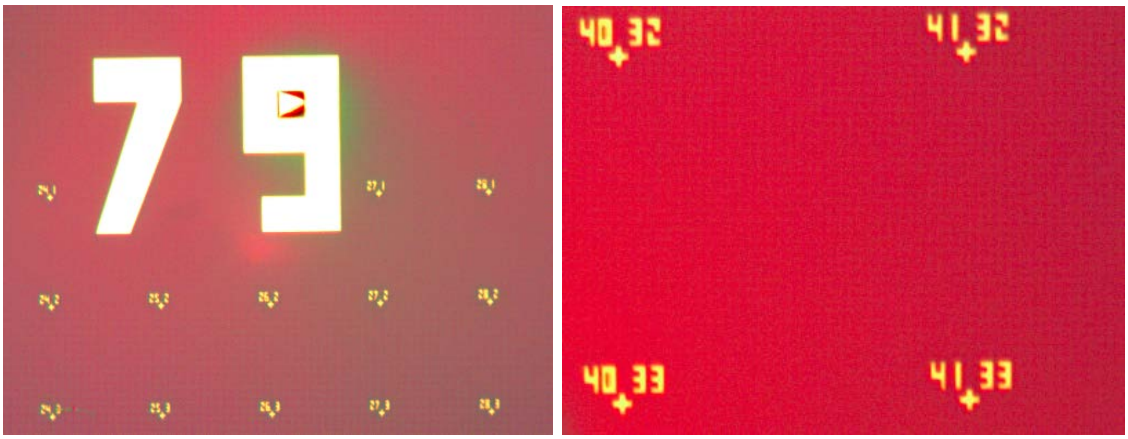

Figure 4.7: Optical microscope images (taken at different magnifications) of the patterned silicon substrates with Ti/Au alignment marks used in making the devices. The distance between two adjacent alignment marks is about 50 μm.

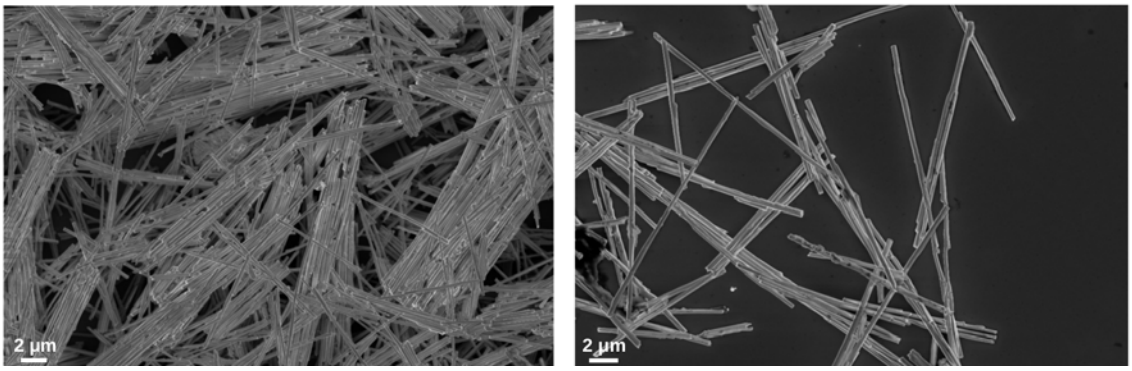

Figure 4.8: Nanowires networks formed on a silicon wafer upon dropcasting from a dense solution (left) and dilute solution (right) of nanowires.

Second: Designing contacts and pads. In this research, two softwares for designing the contacts using electron beam lithography were utilized, namely: (A) AutoCAD and (B) Nanomaker software and the Nanomaker beam control apparatus integrated into the electron microscope. In (A), the SEM images of the dropcasted wires are imported to AutoCAD and aligned to the dropcast mask using the grids as shown in figure 4.9 (left), followed by designing the metal contacts and pads to the desired nanowires as shown in figure 4.9 (right). In (B), Nanomaker software was used to draw the contacts and the larger pads, followed by positioning the required nanowires with respect to the alignment marks. The wafer was then taken out of the SEM for the next step.

Third: Electron beam lithography. After the design file for the nanowires had been finished, the wafers were coated with a layer/layers of the electron beam resist, poly methyl methacrylate (PMMA), ensuring a good coverage of the wires. Wafers are then returned to the electron microscope for defining the electrical contacts by exposing the electron resist. The exposure time depends on the surface area that needs to be exposed, resist type and thickness, and total beam current, all of which parameters were

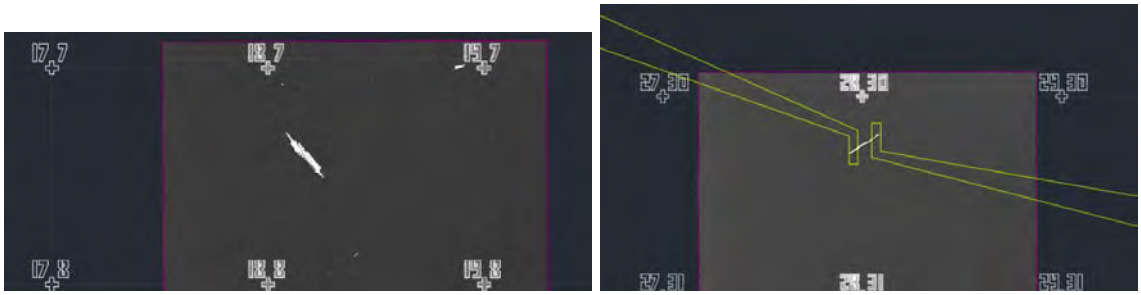

Figure 4.9: Pictures from AutoCAD file used in designing contacts to the wires. Left image is aligning the SEM pictures to the dropcast mask. Right image is defining the electrical contacts over one of the chosen nanowires.

set as appropriate. The wafers are then taken out of the microscope, dipped in a developer solution (such as MIBK) for a few seconds, and submerged into a stopper solution (isopropanol). The sample was finally inspected under the microscope, and developed for a few seconds further, if required.

Fourth: Evaporating metal contacts and pads. Titanium/Gold thin films were evaporated onto the wafers. Wafers are then placed in acetone to remove the unwanted PMMA layer (with Ti/Au on top), leaving the metal contacts and pads. A 10 μm of titanium 400 μm of gold were used in these as contact pads in these devices. The wafers are then inspected under optical microscope and placed in acetone for longer to remove any stubborn resist. This process is called lift-off.

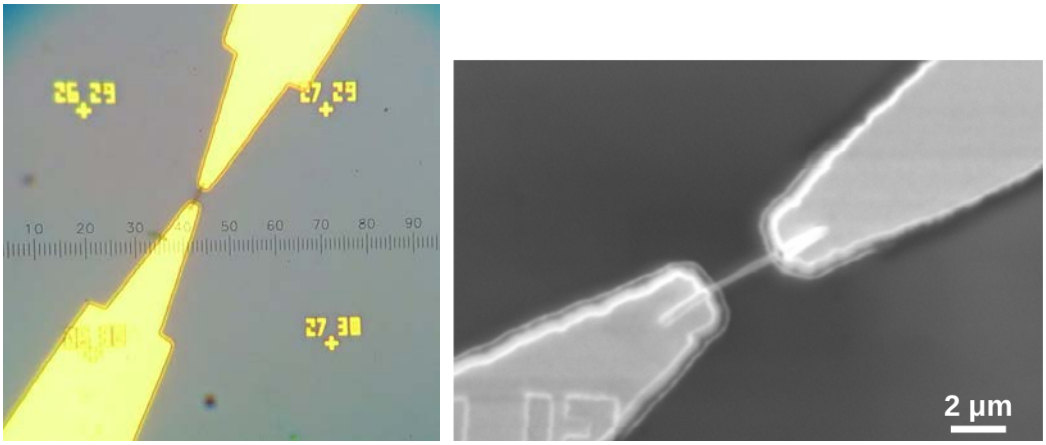

Figure 4.10: Single CdSe nanowire device. Left is an optical microscope image (ruler scale is in μm) and right is a SEM picture. The spacing between the contacts varied among devices ranging from 2 μm to 3 μm.

Fifth: Bonding the wafers for measurements. Wafers are then attached to a sample holder, and electrical connections are made from the Ti/Au pads to the macroscopic contacts using a ball and/or wedge bonder. Lastly, the sample holder is soldered into the measurement apparatus (depending on the available setup). Figure 4.11 shows the wafers after being bonded, and the box made for connecting them to the measurement station.

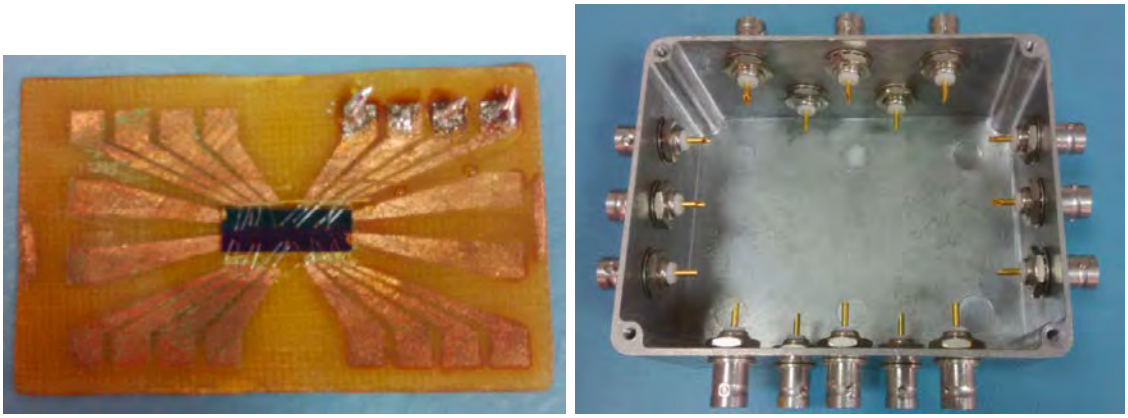

Figure 4.11: Pictures of a substrate containing the wafers bonded to copper contacts (left). The macroscopic copper contacts were soldered to the BNC connectors in the box (right) prior to the measurements.

Difficulties in Devices Fabrication

During the preparation and fabrication of the single nanowire devices, a number of problems can often arise resulting in damaged samples. Among these issues are; movement of the nanowires during processing, misalignment of the contacts, breaking of the nanowires, and nanowires lifting-off the contacts. Some of these are shown below in figure 4.12. One of the attempts to limit the movement and breaking of the nanowires is to apply a small pad of crosslinked PMMA (negative resist) on the center of the nanowire (i.e. tips of the nanowire should remain exposed for the electric contacts). This helps to fix the wires in place and protect them from breaking.

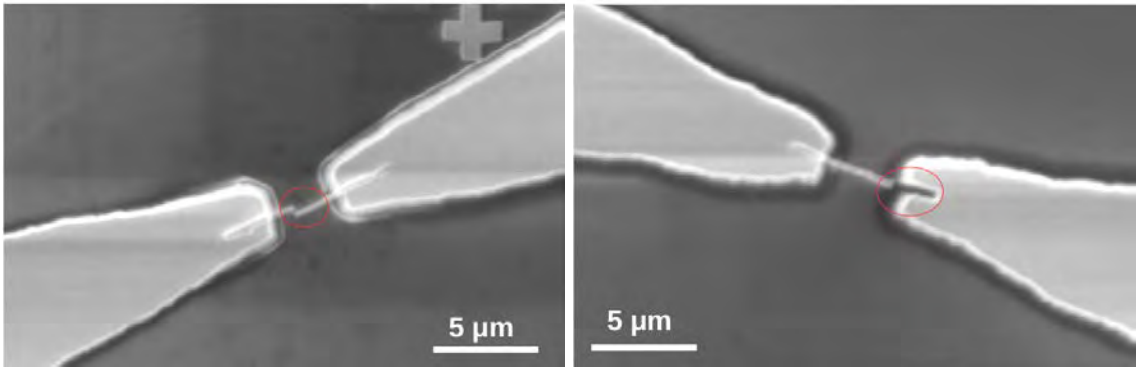

Figure 4.12: SEM images of CdSe single nanowire devices showing difficulties in the preparation: a broken nanowire (left) and a tip lifting-off the electrical contact (right).

4.2.2 Device Measurements

After bonding the samples, transport measurements can be preformed, using a computer-controlled Keithly source measuring unit via a preamplifier. A voltage sweep is applied between source-drain contacts and the current is measured between the same. Current conduction is observed between only those contact pads that are connected by nanowires. (i.e. not connected pads showed currents in

the fA range). Figure 4.13 presents the I-V characteristics of a single CdSe nanowire device. In the second device, the data are for two voltage sweeps (up and down). The two devices showed the same behaviour, but with approximately two orders of magnitude difference in current values at the same voltages. This could be attributed to the fabrication of the Ti/Au contacts to the semiconductor, and how the resistance between the nanowire and contacts vary from one experimental device to the other. In fabrication of electrical contacts to a single nanowire device, proper ohmic connections are often desired between the metals and the semiconductor. For instance, evaporating In/Au contacts to CdSe wires was reported to result in an ohmic behaviour (Gao et al., 2013). In the case of the electrodeposited CdSe nanowires used here, the Ti/Au contacts produce Schottky barriers. The electrodeposition of in-situ metal contacts to the semiconductor segment was also thought to minimize the resistive nature between the semiconductor nanowire and metal contacts. Using this approach could reduce any effects from an insulating layer between the material interfaces (Skinner et al., 2008). Investigations will be done on Au-CdSe-Au and Ni-CdSe-Ni devices to further explore this.

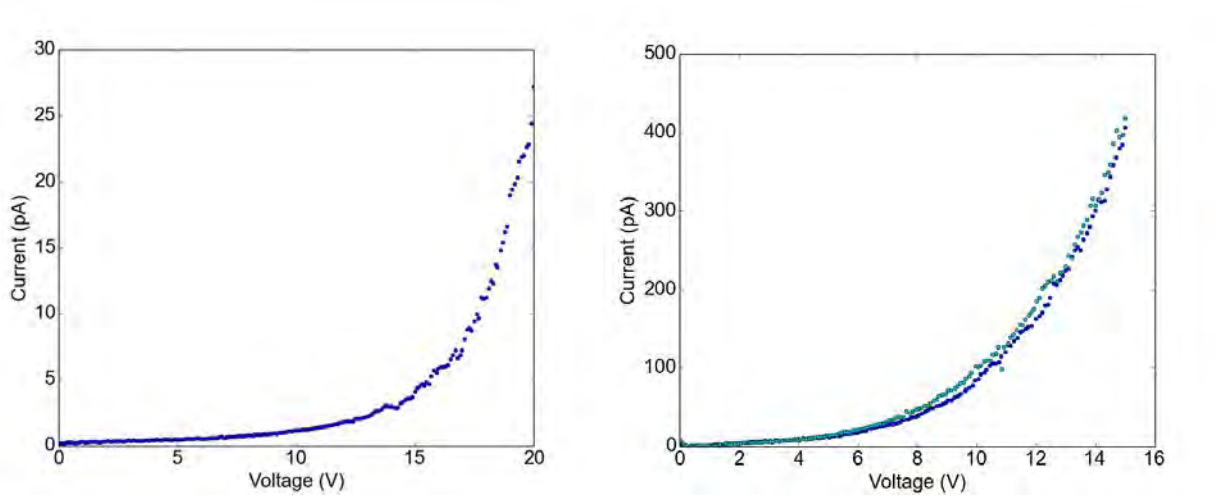

Figure 4.13: I-V plots of two single CdSe nanowire devices. The mean diameters of the nanowires are 200 nm. The length of the first device (left) and the second device (right) was 3 μm and 2 μm respectively. Only few pA of current flow through a single nanowire compared to 1000s of pA through the nanowires array for the same voltages.

The pronounced curvature of these I-V curves, compared to CdSe nanowires array previously measured, is a characteristic of a metal-semiconductor device that incorporate Schottky barriers at the contacts (Ayvazian et al., 2013; Kim et al., 2009b). In our device, CdSe nanowire and the two gold contacts (Au/CdSe/Au) can be considered as two back-to-back Schottky barriers. The height of the Schottky barrier has a direct effect on the non-linearity of the I-V curve, and as this height increases, the nature of the curve changes from linear to non-linear to rectifying. The ohmic resistance of a single CdSe nanowire cannot be precisely determined from these I-V curves, however a minimum value of the wire resistance can be acquired from $\mathrm{dV/dI}$ calculated at the high applied voltages regime (Zhang et al., 2007). According to Zhang et al. model, the majority of the voltage drop is across the nanowire at high applied bias, whereas at low bias the current flowing through the device is tiny and the total voltage is distributed mainly on the two Schottky barriers. Thus, the measurement of the resistance at low bias regime (where the voltage drop across the nanowire itself is insignificant) can greatly affect the accuracy.

Using the above-mentioned approach, the electrical resistance of the CdSe nanowire is evaluated. From

this, and the measured diameter and length of the nanowire from SEM images, the conductivity of the CdSe nanowire was estimated to be in the order of 10^{-5} S/cm. Similar conductivities were also reported for single undoped CdSe nanowires (He et al., 2009; Khandelwal et al., 2006) and for electrodeposited CdTe nanowire device (Kum et al., 2008). The high resistivity of the electrodeposited CdSe nanowire could be explained by the lack of any dopants during the growth technique. Hence, any carriers in the nanowires are either due to the presence of lattice defects and impurities or thermally generated. However, because of the large CdSe bandgap, the number of thermal carriers at room temperature is low ($\sim 10^3 \mathrm{cm}^{-3}$). He et al. have demonstrated that doping CdSe nanowires with indium greatly enhanced the conductivities. The conductivity of CdSe nanowires was raised by almost five orders of magnitude from 10^{-5} (undoped set) to tens of S/cm via a simple indium doping process, and carrier concentration as high as $\sim 10^{19} \mathrm{cm}^{-3}$ for the heaviest doped set (He et al., 2009).

5. Towards the Photocatalytic Production of Hydrogen Gas

One of the promising applications of photocatalytic nanowires is the production of hydrogen gas from water splitting. The nanowires grown by the templated electrodeposition technique are particularly appealing for photocatalytic water splitting because a simple electrochemical method is used to produce multisegmented nanowires in which the photocatalytically active semiconductors can be easily incorporated with metal electrocatalysts.

In this chapter, we will briefly introduce the photocatalytic production of hydrogen gas using one-dimensional structures, together with some of our preliminary results of utilizing CdSe nanowires in that process.

5.1 The Photocatalytic Process

Photocatalytic processes can imitate the natural photosynthesis in harnessing and conversion of solar energy into chemical energy. In photocatalysis, solar photons are used to drive various redox reactions to generate useful highly energetic chemical fuels (also known as solar fuels). *Solar water splitting* (i.e. reducing protons to hydrogen) and *photoreduction of* CO_2 to organic compounds are the two major potential routes for artificial systems producing solar fuels. In this procedure, the solar energy is harvested and stored in the form of molecular bonds, in analogy to the natural photosynthesis process. The main component in any photoelectrochemical process is the semiconducting light absorber, known as the photocatalyst. A photocatalyst generates electrons and holes that can be used onsite in water splitting or other photocatalytic processes. In practice, an efficient photocatalyst structure involves close integration of the components demonstrated in figure 5.1. In particular, inorganic semiconductors are highly attractive for light harvesting as they are able to absorb solar energy across a relatively broad spectrum.

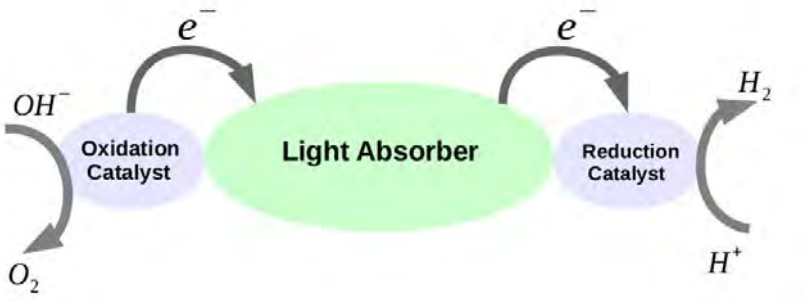

Figure 5.1: Schematic diagram of an effective photocatalyst structure. Three essential components are needed: a light harvesting material (semiconductor), an oxidation electrocatalyst, and a reduction electrocatalyst which facilitate the desired chemical reactions.

5.1.1 Solar Water Splitting

Honda and Fujishima were the first to report the photo-assisted splitting of water into hydrogen and oxygen using an inorganic semiconductor (rutile phase TiO_2) photoanode coupled to a Pt electrode (Fujishima and Honda, 1972). Since then, photocatalytic water splitting has gained considerable attention among researchers* (Ahmad et al., 2015; Ismail and Bahnemann, 2014; Chen et al., 2010; Kudo and Miseki, 2009; Navarro Y. et al., 2009) and many inorganic semiconductors were later identified as potential photocatalysts for water splitting (Osterloh, 2007).

Photocatalytic water splitting is usually associated with a harsh reaction medium (i.e. highly oxidative or reductive, highly acidic or basic). For this reason, titania (TiO_2) is the most widely investigated photocatalyst to date due its high chemical stability under these conditions in addition to its low cost and high catalytic activity (Fujishima et al., 2008).

The direct splitting of water with a semiconductor photocatalyst mainly involves four different stages discussed briefly below. These stages, demonstrated in figure 5.2, are also true for any process that requires transforming solar energy to chemical energy. Stage I is photo-excitation, at which photons of energy equal to or greater than the semiconductor bandgap is absorbed, causing electrons to be exited from the valence band to the conduction band, creating an electron-hole ($e^- - h^+$) pair. Stage II is the separation and migration of charges, at which the generated $e^- - h^+$ pair is separated and then moved to the active reaction sites on the surface of the photocatalyst/electrocatalyst. Alongside stage II, stage III could also take place, at which the produced $e^- - h^+$ pair recombine and therefore can not be utilized in further reactions. This process is one of the main sources for the low photocatalytic efficiencies reported. Stage IV is the photoelectrochemical reaction, at which the charge carriers on the active sites of the photocatalyst/electrocatalyst surface act as reducing and oxidizing agents to drive the desired redox reaction. In the case of water splitting, the holes at the photoanode or the respective electrocatalyst oxidises the water, while the electrons reduce the H^+ ions generating hydrogen gas at the cathode.

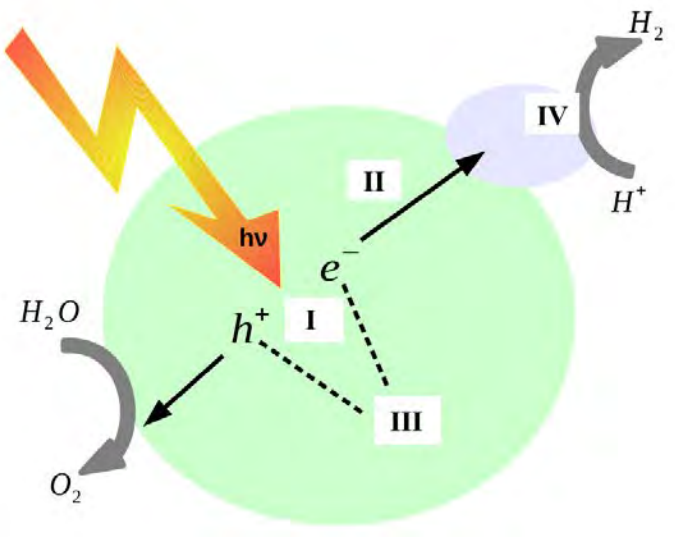

Figure 5.2: Schematic diagram illustrating the various stages of energy transmission during a photocatalytic water splitting process.

*Articles referenced are some of the recent reviews about photocatalytic water splitting.

The overall reaction for the photo-assisted water splitting is given by

$$\mathrm{H_2O} + \mathrm{h}\nu \rightarrow \mathrm{H_2} + {}^{1}\!/_{2}\,\mathrm{O_2} \tag{5.1.1}$$

Reaction 5.1.1 is a thermodynamically uphill reaction, which requires about 237 kJ mol^{-1} of the Gibbs free energy ($\Delta\mathrm{G}$) in order to decompose one molecule of water into $\mathrm{H_2}$ and ${}^{1}\!/_{2}\,\mathrm{O_2}$ under standard conditions (Bard and Fox, 1995). This $\Delta\mathrm{G}$ corresponds to $\Delta\mathrm{E}$ of about 1.23 V per electron transferred. Therefore, to drive the water splitting reaction with solar energy, the photocatalyst used must have a bandgap of a minimum 1.23 eV (practically larger amount of energy is needed to account for different losses in the used photocatalytic cell).

In addition to the above bandgap requirement, a photocatalyst structure designed for solar water splitting should satisfy the following conditions. First, there should be a match between the semiconductor bandgap and the solar spectrum to maximize light absorption. The bandgaps of several inorganic semiconductors, together with the redox potentials for proton reduction and water oxidation, are shown in figure 5.3. Second, an efficient mechanism is needed to stimulate the separation and migration of generated photo-carriers. Besides, the semiconductor should be joined with selected redox electrocatalysts for effective charge utilization in subsequent photoelectrochemical reactions. Finally, the whole structure should guarantee the photoelectrochemical stability of the system (i.e. that the semiconductor is stable or protected against photo-degradation). A single-material system is unlikely to achieve all these conditions, therefore much of the research is focusing on *heterogeneous photocatalysts*. These heterostructures combine the advantages of several constituents to overcome the difficulties associated with a single-component photocatalyst.

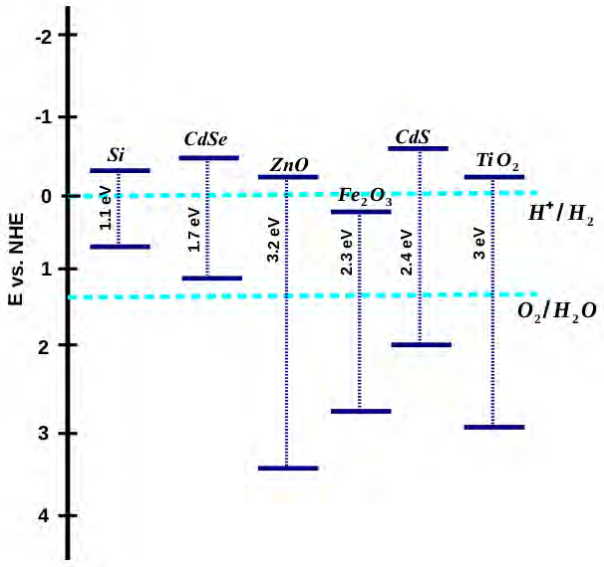

Figure 5.3: Band levels for several inorganic semiconductors relative to the water splitting redox potentials (with respect to the NHE). The levels of CB and VB should be considered corresponding to the redox pair potentials for water splitting. CB edge has to be more negative than (above) the reduction potential of ${}^{H^+}\!/_{\mathrm{H_2}}$. VB has to be more positive (below) the oxidation potential of ${}^{O_2}\!/_{\mathrm{H_2O}}$.

To date, a wide range of heterostructures have been examined for improved photocatalysts such as *metal/semiconductor*, *semiconductor/semiconductor*, and *molecule/semiconductor* (Qu and Duan,

2013, and references therein). Generally, heterogeneous photocatalysts provide the following potential benefits. Firstly, increasing the light absorption; for instance, small bandgap semiconductors or certain molecules with high absorption ability can be used to sensitize the wide bandgap semiconductors. Secondly, promoting the charge separation and migration; for example, the built-in electric fields due to the Schottky (metal/semiconductor heterostructure) or the p-n (semiconductor/semiconductor heterostructures) junctions efficiently stimulate the photo-generated electron-hole pair separation and transportation. Thirdly, enhancing the redox catalytic activity at the reaction sites. Lastly, improving the stability and the life-time of the semiconductor light absorber; protection of the semiconductor surface from the harsh electrochemical conditions causing its degradation.

5.1.2 One Dimensional Photocatalysts

Nanostructured materials have emerged as pioneering photocatalysts for various solar energy conversion processes due to their unique structures, and physical and chemical properties, which differ from their bulk counterparts (Tong et al., 2012). Diverse structures have been explored such as nanowires, nanorods, nanotubes, nanobelts, nanoparticles and other complex configurations. These structures and configurations have greatly enriched the material selection of photocatalysts and provided a new route for the design of efficient photocatalytic systems. In particular, one-dimensional nanostructured heterogeneous photocatalysts have received tremendous interest and they account for most of the research done in this area. Arrays and single nanowires have both been investigated for photocatalytic applications. Some of these examples, utilizing homogeneous and heterogeneous nanowires as building blocks for solar energy conversion, were highlighted in the review article by Qu and Daun (Qu and Duan, 2012). The properties of one-dimensional structures depending on size and morphology, such as quantum confinement characteristics in semiconducting nano-materials (Andrew Frame et al., 2008) and plasmonic effects in metallic nanostructures (Warren and Thimsen, 2012), can open a new pathway to the solar harnessing processes. Moreover, the large surface areas of one-dimensional wires, rods or tubes can provide more catalytically active sites for the oxidation and reduction reactions. Nanostructures also imply short carrier diffusion lengths compared to the bulk materials, thus reducing the losses due to the recombination. Most importantly, one-dimensional structures allow for the flexible integration of different components to achieve an effective photocatalytic system. One example of this is the Z-scheme photocatalytic system for water splitting (Maeda, 2013), in which two semiconductors are used for the photo-assisted redox reaction (i.e. one for the oxidation half reaction and the other for the reduction half reaction).

In this work, one-dimensional CdSe nanowires grown by templated electrodeposition were used as the photocatalytic material. The photocatalytic activity of one-dimensional CdSe structures (i.e. nano-wires, rods, and tubes) have been widely investigated by several researchers within various configurations. For instance, the combination of CdSe arrays with other semiconductors such as TiO_2 (Ai et al., 2011), Cu_2O (Debgupta et al., 2014), and CdS (Tongying et al., 2012) have been explored. Incorporation of metals within CdSe one-dimensional structures, forming Schottky junctions, have been also reported. For example, the photocatalytic properties of CdSe-Pt hybrids (Pt nanocrystals were loaded to CdSe nanorods and nanonets) (Elmalem et al., 2008) were examined by using the reduction of a model acceptor dye (methylene blue, MB). In addition to this, Moskovits group (Schierhorn et al., 2010; Lee et al., 2013) studied the photocatalytic performance of CdSe nanowires coupled with organic materials such as poly(3,4-ethylenedioxythiophene) poly-(styrenesulfonate) (PEDOT:PSS) and poly(3-hexylthiophene) (P3HT). The embedding of CdSe nanorods inside a matrix of these conducting polymers can enhance the overall photocatalytic activity and stability of the system.

5.2 Some Preliminary Results

In this section, we present a proof-of-concept experiment of the semiconductor nanostructures-based photocatalysis. In particular, we focus the discussion on the electrochemically grown CdSe nanowires combined with a Ni segment to form axially segmented metal-semiconductor nanowires.

These segmented nanowires can be modelled as the Schottky type photochemical diode described by Nozik (Nozik, 1977). In his paper, Nozik illustrated two configurations of photochemical diodes for energy conversion, where the Schottky type photochemical diode is achieved by forming an ohmic contact between a semiconductor and a metal as shown in figure 5.4. In this work, an ohmic contact can be formed between CdSe and Ni segments via annealing at temperatures ranging from 300 - 500 °C (Mubeen et al., 2013).

Under illumination, photons with energy higher than the bandgap of CdSe will excite electron-hole pairs. The subsequent produced photo-current, due to the generated charge carriers, depends mainly on the efficient separation of the electrons and holes at the vicinity of the Ni-CdSe contact and on the illumination intensity. Driven by the built-in electric fields due to band bending, the photo-generated electrons in the conduction band and holes in the valence band tend to move towards Ni and CdSe ends respectively as shown in figure 5.4.

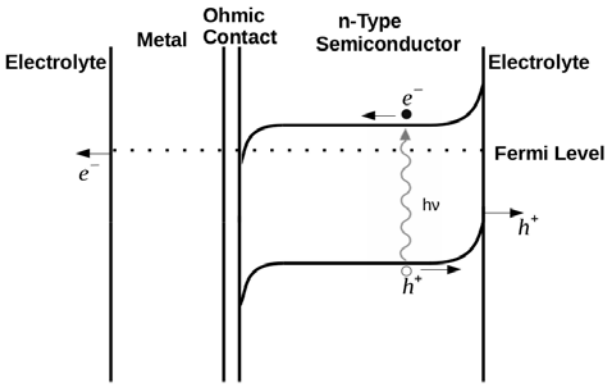

Figure 5.4: A schematic energy band diagram of the Schottky photochemical diode configuration described by Nozik (Nozik, 1977). At the CdSe/electrolyte interface band bending results in accumulation of holes which undergo the oxidative half-reaction. At the Ni/electrolyte interface electrons are accepted by the reductive half-reaction.

The activity of the Ni-CdSe nanowires in photocatalytic water splitting is tested in a methanol/water solution under white light illumination, where methanol acts as a hole scavenger. The conversion of water and methanol into hydrogen and carbon dioxide was used in this work as a model reaction to demonstrate the ability of CdSe nanowires to photocatalytically produce hydrogen. The use of a sacrificial reagent (i.e. a hole-scavenger such as alcohols or sulfide ions) is required here as water splitting is a tough reaction and CdSe would not be able to directly achieve the required energy to initiate reaction 5.1.1. By the addition of methanol, the energy required is lowered from 1.23 eV to 0.7 eV and an alternative reaction for the water splitting (rather than 5.1.1) is proposed, where methanol is oxidized to CO_2, as follows.

$$\mathrm{CH_3OH + H_2O + 6h^+ \rightarrow CO_2 + 6H^+} \tag{5.2.1}$$

The protons formed at the CdSe segment are then reduced to $\mathrm{H_2}$ at the Ni surface, following the reaction

$$\mathrm{2H^+ + 2e^- \rightarrow H_2} \tag{5.2.2}$$

This results in the overall reaction

$$\mathrm{CH_3OH}(l) + \mathrm{H_2O}(l) \rightarrow \mathrm{CO_2}(g) + 3\mathrm{H_2}(g) \tag{5.2.3}$$

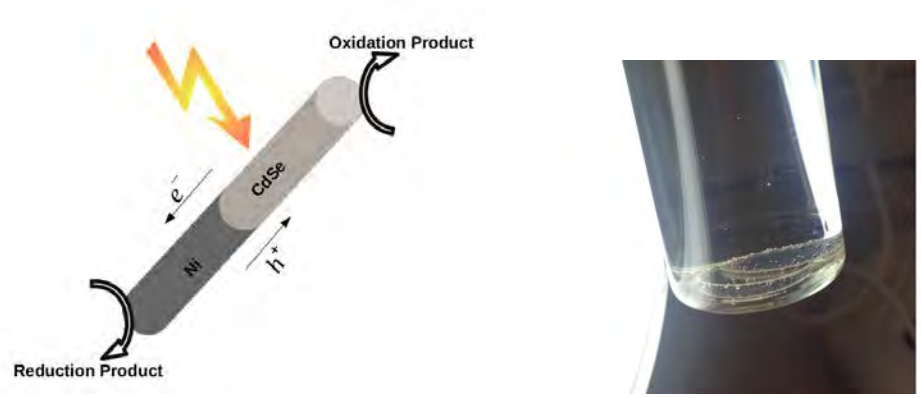

Figure 5.5: Schematic diagram of a segmented Ni-CdSe nanowire (left). Visible light is absorbed by the CdSe segment generating an $\mathrm{e^- - h^+}$ pair, which is separated at the interface followed by the hole scavenging by methanol and the reduction of protons forming $\mathrm{H_2}$. Right is an image of the templates containing the nanowires suspended in a water/methanol mixture.

The segmented nanowires utilized in this experiment were grown into the pores of AAO under the conditions specified in chapter 3. The nanowires were then suspended in a 30 mL glass vial, containing 80 vol% aqueous methanol solution, closed with a rubber septum cap. White light was then shone on the nanowires and small bubbles started to form at the surface of the templates, rising to the surface (bottom of the vial was sometimes tapped to liberate the adsorbed bubbles at the templates surface). To analyse the constituents of the created bubbles, a gas chromatography (GC) system was used[†]. The GC line was connected to the vial using a disposable hypodermic needle and the formation of hydrogen was detected. In figure 5.6, the readings from the GC analysed by a Galaxie software is presented as a plot between the thermal conductivity detector (TCD) signal and the retention time (RT). At the expected RT for hydrogen detection ($\sim$ 0.6 for this particular column), two signals appeared corresponding to two consecutive injections from the vial. The green and blue signals in figure 5.6 correspond to the first and second injections respectively. As observed, the TCD signal of the first injection is higher than the second one, which could be linked to less hydrogen being detected as the semiconductor is highly unstable.

[†]GC readings presented are for $\mathrm{H_2}$ detection only. Further quantitative experiments regarding the amount of $\mathrm{H_2}$ was not feasible due to small amounts produced and photodegeradation of the CdSe.

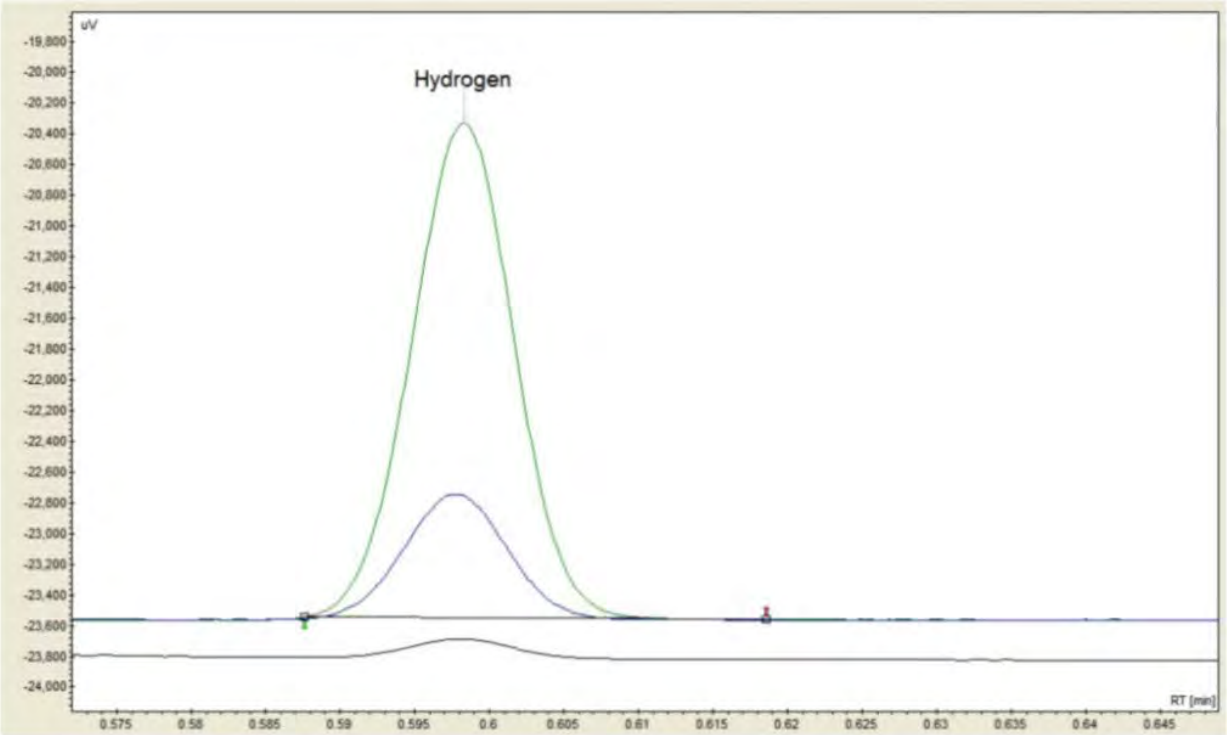

Figure 5.6: Image of TCD signal (μV) versus RT (min) plot acquired from the Galaxie software. The focused region of RT, where hydrogen is expected for this system, is displayed. The black line signal is the reference background.

After approximately 15 minutes of illumination, it was observed that the evolution of gas bubbles from the templates had stopped indicating the termination of the reaction. This could be attributed to the corrosion of CdSe which is described by the following reaction.

$$\mathrm{CdSe} + 2\mathrm{h}^{+} \rightarrow \mathrm{Cd}^{2+} + \mathrm{Se} \tag{5.2.4}$$

The Se^{2-} in the CdSe segment is oxidized by the photo-generated holes accompanied with elution of Cd^{2+} according to equation 5.2.4.

SEM and EDS investigations were done on the nanowires after the photocatalytic experiments and the results are shown in figure 5.7. The EDS spectra reflect the changes in the composition of the nanowires. The ratio between Cd and Se in the CdSe before the photocatalytic experiments is almost 1:1, but afterwards the relative intensity of the Se peak increases indicating the occurrence of the photocorrosion reaction (5.2.4) mentioned above.

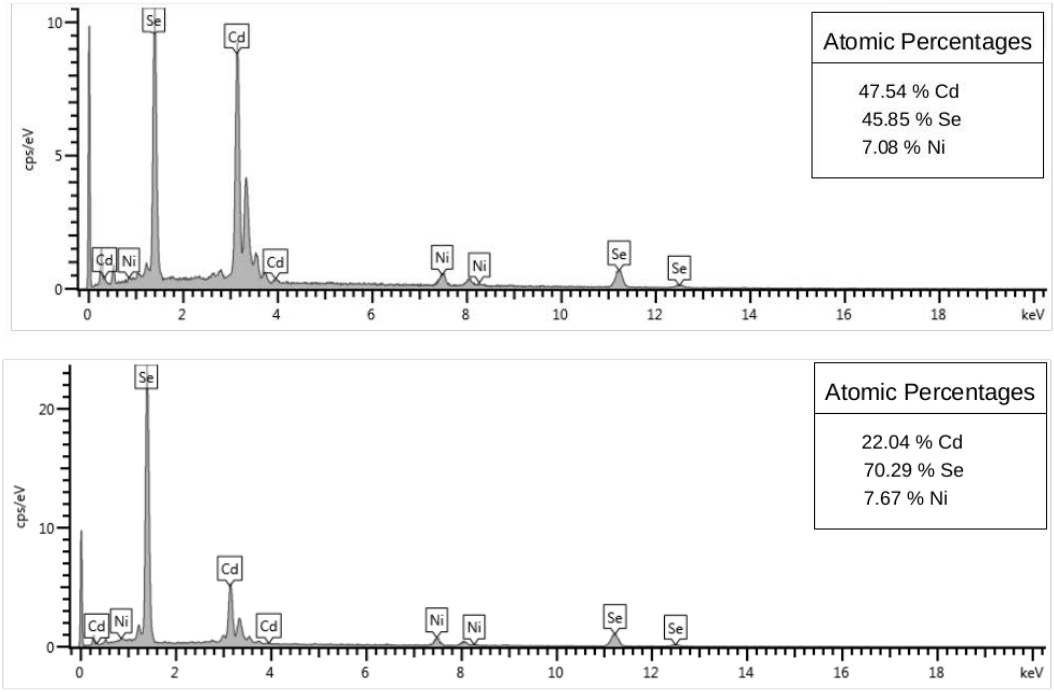

Figure 5.7: SEM-EDS analysis of Ni-CdSe nanowires before (top) and after (bottom) the photocatalytic H_2 experiment.

The poor photo-stability and short working lifetime of the CdSe nanowires, in photocatalytic water splitting experiments, restricted any further investigations on the Ni-CdSe segmented nanowires. Some of the proposed structures to overcome these limitations will be discussed in chapter 6.

6. Conclusions and Suggestions for Future Work

This thesis has discussed the fabrication of functional nanowires and their characterizations. This chapter summarizes the most important conclusions from the work that was performed. Also, suggestions are given here for future studies that are related to, and would build on, the work presented in this thesis.

We have reported the synthesis of different nanowires using the templated electrodeposition technique. The nanowires can be formed in the pores of AAO and PCTE templates under the proper electrochemical deposition conditions, mainly the solution composition and the applied potential. Nanowires produced are smooth and around 200 nm in diameter, replicating the nano-porous membranes, with lengths that depend on the duration of the deposition as confirmed by SEM studies. The research done in this thesis focused on the electrodeposition of CdSe nanowires, and the parameters recommended for creating stoichiometric CdSe deposits are as follows. First: The applied potential range should be set to (-0.35 $\rightarrow$ -0.8) V vs. Ag/AgCl. Second: The optimum ratio between Cd and Se ions in the electrolyte solution was found to be 5:1 (5 mM $\mathrm{CdSO_4}$ and 1 mM $\mathrm{SeO_2}$ is used in this work). Third: The pH of the solution is adjusted with 0.25 M $\mathrm{H_2SO_4}$. Fourth: The scan rate should be kept in the range of (10 - 50) mV/sec. The CdSe nanowires synthesized were stoichiometric, ~ 0.91 Cd:Se ratio, and polycrystalline with a cubic phase structure. Upon annealing in argon at 500 $^{\circ}\mathrm{C}$, the phase of the nanowires was changed from cubic to hexagonal as confirmed by XRD results.

Electrical contacts were defined to an array of nanowires via silver epoxy and macroscopic wires, while electron beam lithography method was employed to assemble a single CdSe nanowire into an electrical device. Pronounced photoconductivity is observed, in the presence of visible light, for the CdSe nanowires array with ca. 25 decrease in the resistivity. Transport measurements on the single CdSe nanowire devices indicated that the electrodeposited CdSe nanowires are very resistive, with current levels in few pA for few volts of applied bias.

A direct application of the nanowires was demonstrated by giving a proof-of-principle of photocatalytic hydrogen production by segmented nanowires. Ni-CdSe nanowires were used in a water splitting experiment in which hydrogen gas was produced, and confirmed by GC measurement, upon visible light illumination in a methanol/water mixture. CdSe was found to undergo photo-degradation after only a few minutes of illumination, and thus terminating the hydrogen evolution process.

From the above conclusions, the future studies could proceed in three directions as follows. Firstly, improving the stability of the photocatalytic system. Next, evaluating the efficiency of the photocatalytically active material and finally, incorporating novel materials in the photocatalytic water splitting structure. A brief discussion is given below regarding the mentioned points.

One of the proposed designs for establishing highly efficient, stable photocatalytic systems is encasing the semiconducting light absorber segment in a protective insulation with only the electrocatalysts exposed to the solution as shown in figure 6.1. Qu et al. (Qu et al., 2010; Qu and Duan, 2010) have designed a novel metal-semiconductor-metal heterostructure integrating a nanoscale Schottky diode (Pt and n-Si) with two metal electrocatalysts (Ag and Pt) protected by a silicon oxide layer. These Pt-Si-Ag exhibited photocatalytic activity for a wide range of applications including hydrogen production from formic acid (Qu and Duan, 2010). Mubeen et al. (Mubeen et al., 2013) have also reported a similar approach, where they fabricated a photocatalytically active heterostructure unit incorporating an unstable semiconductor (CdSe), together with Pt and PEDOT:PSS as reduction and oxidation electrocatalysts respectively, encased in the protective AAO membrane. The photocatalytic stability of their structure was tested through the electrolysis of HI, and reported to be stable for more than 24 hours.

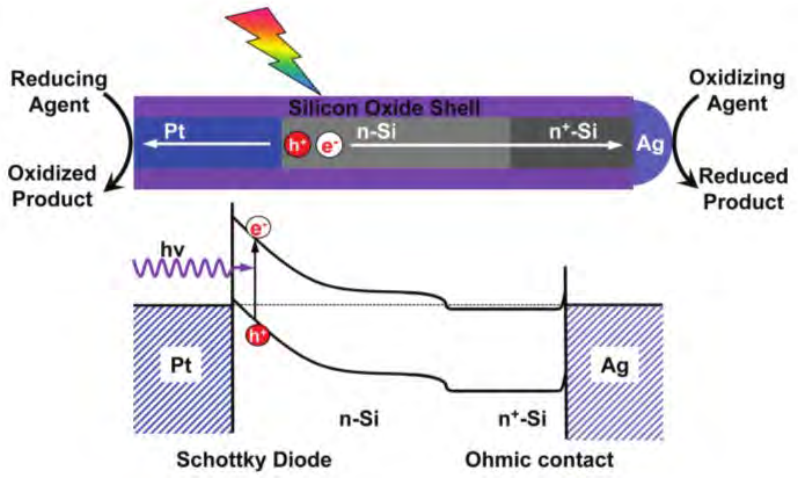

Figure 6.1: Schematic diagram of a photocatalytic heterostructure design (Qu et al., 2010). A Pt-Si-Ag nanowire encased in a silicon dioxide shell, where only Ag and Pt are exposed to the solution. The photogenerated electrons and holes are separated by the built-in potential of the Schottky diode and then quickly transported toward the two ends for the desired redox reactions.

We have attempted to incorporate PEDOT:PSS with CdSe nanowires synthesized in this work in order to protect it against photocorrosion (Lee et al., 2013). However, our trials to drop cast and/or spin coat a layer of PEDOT:PSS were not successful mainly due to the mechanical instability of the commercial AAO templates used to fabricate the nanowires. The commercial AAO templates are very brittle and could not handle the current spin coating process, whereas dropcasting resulted in very thick layers of PEDOT:PSS. Further investigations will be carried out to solve the existing problem with spin coating, and thus test the photocatalytic properties of the nanowires within this heterostrucutre. We are also aiming to fundamentally understand and control the electrical transport in these nanoscale Shocttky diodes, so additional experiments will be done on CdSe-based single nanowire devices. Another promising direction to consider is the incorporation of other materials to the CdSe-based photocatalytic structure such as graphene (Xiang et al., 2012). Graphene is a novel material with many interesting properties that could be integrated in a photocatalytic system for enhanced behaviour. The large surface area, high conductivity ($\rho = 10^{-6}\ \Omega$ cm), optical transparency (97.7%), and high stability are all promising features to consider in the water splitting process and photocatalytic systems in general.

Appendix A

Photoluminescence Analysis

Photoluminescence measurements were carried out on the electrodeposited CdSe nanowires in order to obtain the bandgap ($\mathrm{E_g}$) value. Initially, a UV-VIS absorbance measurement was done on the nanowires to determine the wavelength required for the excitation laser source. Typically, the maximum of the absorption spectrum is preferred. In these experiments, the maximum absorbance was about 733 nm as seen from figure 3.22. Hence, the excitation was chosen to be at 696 nm which is close enough to the absorbance peak but also ensures receiving a signal from the emitted spectrum only (not the excitation peak). However, in our measured data, a signal was recorded at around 710 nm, which may be due to the excitation source. Further experiments need to be carried out to verify this. PL measurements were repeated three times and for all plots the excitation baseline was subtracted and a Gaussian was fitted to get the PL peak as seen in the plots below.

The PL peaks with associated standard errors were found to be at 762.9 ± 0.2 nm, 763.4 ± 0.2 nm, and 762.8 ± 0.2 nm as indicated from the Gaussian fit parameters.

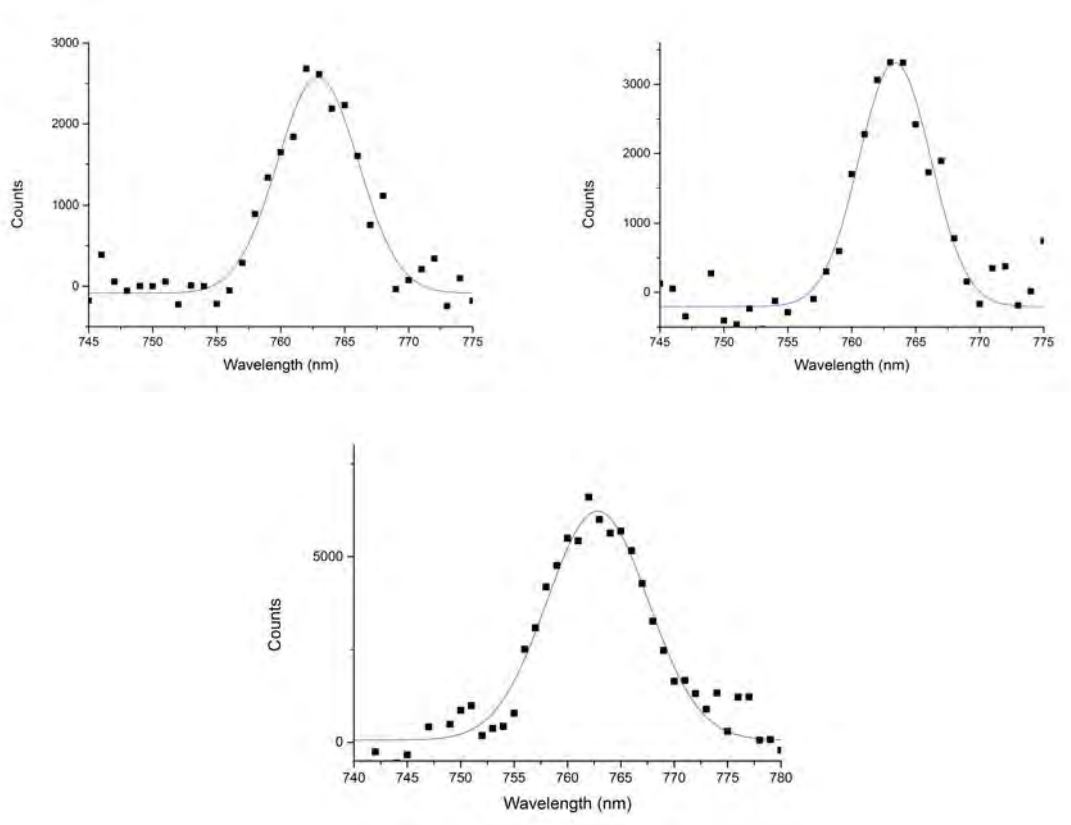

Figure 6.2: CdSe nanowires PL peaks with fitted Gaussian.

Appendix B

Materials & Instrumentation

Chemicals* & Materials

All templates used in this thesis were the commercially available Whatman templates that were sold as membrane filters under the names Anodisc 13 and Nucleopore Track-Etch for AAOs and PCTEs respectively. AAO templates are 60 μm thick with 200 nm pore-diameter, while PCTEs are 6 μm thick and with 200 nm pore-diameter.

For the fabrication of thin films, fluorine doped tin oxide coated (FTO) glass slides (surface resistivity $\sim 8\ \Omega/\mathrm{sq}$), were obtained from Sigma-Aldrich.

Chemicals used below were also purchased from Sigma-Aldrich and used without further purification; all electrodeposition solutions were prepared with Milli-Q Anopore deionized water (18 MΩ cm).

- Silver pellets
- Cadmium sulfate $^{8}/_{3}$-hydrate, ACS reagent, $\geq$ 99.0%
- Selenium dioxide, $\geq$ 99.9% trace metals basis
- Nickel(II) sulfate hexahydrate, ACS reagent, 99%
- Gold(III) chloride hydrate, 99.999% trace metals basis
- Chloroplatinic acid hexahydrate, ACS reagent, $\geq$ 37.50% Pt basis
- Boric acid, 99.999% trace metals basis
- Zinc nitrate hexahydrate, reagent grade, $\geq$ 98%
- Poly(3,4-ethylenedioxythiophene)-poly(styrenesulfonate) 1.3 wt% dispersion in $\mathrm{H_2O}$, conductive grade

Other chemicals used such as acids ($\mathrm{H_2SO_4}$ and $\mathrm{HNO_3}$), bases (NaOH), and solvents (acetone, ethanol, and methanol) were all from the Chemistry Store in house.

Adhesive copper tape and silver loaded epoxy adhesive were bought from RS Electronics.

*Working with some chemicals and heavy metals can be extremely hazardous, and suitable precautions such as; proper ventilation, and the use of protective equipments should always be taken while performing these experiments.

Instrumentation

The instruments used in all parts through this thesis are mentioned below.

Fabrication

- A rolling machine at the Centre for Materials Engineering was used to roll silver pallets to a very thin strip that could then be cut to small ($\sim$ 1 mm $\times$ 1 mm) squares for thermal evaporation.
- Thermal evaporations were done on the thermal evaporation station, equipped with suitable vacuum pumps (rotary and diffusion pumps) and a pirani cold cathode pressure gauge, at the Centre of Imaging and Analysis.
- Electrochemical depositions were preformed with a Gamry REF 300 potentiostat using the PHE200 physical electrochemistry software.
- Annealing of samples was done on an Across International (model: STF 1200) tube furnace.

Structural Characterization

Electron microscopy was done using scanning and transmission electron microscopes (SEMs & TEMs) at the Centre of Imaging and Analysis (UCT) and the Electron Microscope Unit (UWC).

SEMs used were FEI Nova NanoSEM 230 and Auriga HRSEM. Both were equipped with an EDS system for compositional analysis. Images were taken using in-lens and secondary electron detectors at an accelerating voltages of 5 keV. For acquiring EDS spectra, 20 keV was used. TEM used was the Tecnai F20. X-ray diffraction measurements were done on the D8 Advance Bruker diffractometer at iThemba Labs.

Optical Characterization

UV-VIS absorption and photoluminescence measurements were done using the Nicolet Evolution 100 UV-Visible spectrophotometer and the Nanolog Horiba JobinYvon spectrofluorometer, respectively, at the University of Western Cape.

Electrical and Photoconductivity Measurements

All electrical measurements were taken using a Keithley model 6430 Sub-Femtoamp Remote SourceMeter and custom programmed National Instruments LabVIEW software.

The uncertainty in the calculated resistances associated with electrical measurements presented in figure 4.5 are obtained from the source and measure specifications indicated in the instruction manual. The voltage sourced was in the 2 V range, this corresponds to 0.02% of the reading value + 600 μV. The currents measured in dark and under white illumination were in the 1 μA range, this corresponds to 0.05% of the reading value + 300 pA. The current measured when shinning blue laser was in the 10 μA range, this corresponds to 0.05% of the reading value + 2nA. Further uncertainties associated with all electrical measurements could be similarly attained.

Other instrumentations and materials used in fabricating the single CdSe nanowire devices were provided by University of College London, Cavendish Laboratory at University of Cambridge and the Kotelnikov Institute of Radiotechnology and Electronics of Russian Academy of Science.

Photocatalytic Production of Hydrogen

The produced hydrogen was confirmed using a Varian Micro gas chromatograph, model number CP-4900, with a thermal conductivity detector (TCD). A Varian Galaxie software was used to record and analyse data. For illumination, a 150 watt mercury vapour lamp, a white desk-magnifying lamp, and a blue laser pen were used.

References

Ahmad, H., Kamarudin, S. K., Minggu, L. J., and Kassim, M. Hydrogen from Photo-Catalytic Water Splitting Process: A Review. *Renewable and Sustainable Energy Reviews*, **43**:599–610, 2015.

Ai, G., Sun, W., Gao, X., Zhang, Y., and Peng, L. M. Hybrid CdSe/TiO_2 Nanowire Photoelectrodes: Fabrication and Photoelectric Performance. *Journal of Materials Chemistry*, **21**(24):8749–8755, 2011.

Almawlawi, D., Coombs, N., and Moskovits, M. Magnetic Properties of Fe Deposited into Anodic Aluminum Oxide Pores as a Function of Particle Size. *Journal of Applied Physics*, **70**(8):4421–4425, 1991.

Andrew Frame, F., Carroll, E. C., Larsen, D. S., Sarahan, M., Browning, N. D., and Osterloh, F. E. First Demonstration of CdSe as a Photocatalyst for Hydrogen Evolution from Water Under UV and Visible Light. *Chemical Communications*, (19):2206–2208, 2008.

Aravamudhan, S., Luongo, K., Poddar, P., Srikanth, H., and Bhansali, S. Porous Silicon Templates for Electrodeposition of Nanostructures. *Applied Physics A*, **87**(4):773–780, 2007.

Ayvazian, T., Van der Veer, W. E., Xing, W., Yan, W., and Penner, R. M. Electroluminescent, Polycrystalline Cadmium Selenide Nanowire Arrays. *ACS Nano*, **7**(10):9469–9479, 2013.

Azulai, D., Givan, U., Shpaisman, N., Belenkova, T. L., Gilon, H., Patolsky, F., and Markovich, G. On-Surface Formation of Metal Nanowire Transparent Top Electrodes on CdSe Nanowire Array-Based Photoconductive Devices. *ACS Applied Materials & Interfaces*, **4**(6):3157–3162, 2012.

Bandaranayake, R. J., Wen, G. W., Lin, J. Y., Jiang, H. X., and Sorensen, C. M. Structural Phase Behavior in II–VI Semiconductor Nanoparticles. *Applied Physics Letters*, **67**(6):831–833, 1995.

Bard, A. J. and Fox, M. A. Artificial Photosynthesis: Solar Splitting of Water to Hydrogen and Oxygen. *Accounts of Chemical Research*, **28**(3):141–145, 1995.

Bieńkowski, K., Strawski, M., Maranowski, B., and Szklarczyk, M. Studies of Stoichiometry of Electrochemically Grown CdSe Deposits. *Electrochimica Acta*, **55**(28):8908–8915, 2010.

Bocchetta, P., Santamaria, M., and Di Quarto, F. One-Step Electrochemical Synthesis and Physico-Chemical Characterization of CdSe Nanotubes. *Electrochimica Acta*, **88**:340–346, 2013.

Booker, C. J. L., Wood, J. L., and Walsh, A. Electron Micrographs from Thick Oxide Layers on Aluminium. *British Journal of Applied Physics*, **8**(9):347, 1957.

Boudreau, R. A. and Rauh, R. D. Influence of Deposition Rate on the Character of Electrodeposited CdSe Used for Photoelectrochemical Cells. *Solar Energy Materials*, **7**(3):385–391, 1982.

Cattaneo, L., Franz, S., Albertini, F., Ranzieri, P., Vicenzo, A., Bestetti, M., and Cavallotti, P. L. Electrodeposition of Hexagonal Co Nanowires with Large Magnetocrystalline Anisotropy. *Electrochimica Acta*, **85**:57–65, 2012.

Chen, X., Shen, S., Guo, L., and Mao, S. S. Semiconductor-Based Photocatalytic Hydrogen Generation. *Chemical Reviews*, **110**(11):6503–6570, 2010.

Dasgupta, N. P. and Yang, P. Semiconductor Nanowires for Photovoltaic and Photoelectrochemical Energy Conversion. *Frontiers of Physics*, **9**(3):289–302, 2014.

Debgupta, J., Devarapalli, R., Rahman, S., Shelke, M. V., and Pillai, V. K. Electrochemical Preparation of Vertically Aligned, Hollow CdSe Nanotubes and their p–n Junction Hybrids with Electrodeposited Cu_2O. *Nanoscale*, **6**(15):9148–9156, 2014.

Elmalem, E., Saunders, A. E., Costi, R., Salant, A., and Banin, U. Growth of Photocatalytic CdSe–Pt Nanorods and Nanonets. *Advanced Materials*, **20**(22):4312–4317, 2008.

Fleischer, R. L., Price, P. B., and Walker, R. M. *Nuclear Tracks in Solids: Principles and Applications*. University of California Press, 1975.

Fujishima, A. and Honda, K. Photolysis-Decomposition of Water at the Surface of an Irradiated Semiconductor. *Nature*, **238**(5385):37–38, 1972.

Fujishima, A., Zhang, X., and Tryk, D. A. TiO_2 Photocatalysis and Related Surface Phenomena. *Surface Science Reports*, **63**(12):515–582, 2008.

Gao, Z., Jin, W., Zhou, Y., Dai, Y., Yu, B., Liu, C., Xu, W., Li, Y., Peng, H., Liu, Z., and Dai, L. Self-Powered Flexible and Transparent Photovoltaic Detectors Based on CdSe Nanobelt/Graphene Schottky Junctions. *Nanoscale*, **5**(12):5576–5581, 2013.

García, M., Batalla, P., and Escarpa, A. Metallic and Polymeric Nanowires for Electrochemical Sensing and Biosensing. *Trends in Analytical Chemistry*, **57**:6–22, 2014.

Grebinski, J. W., Hull, K. L., Zhang, J., Kosel, T. H., and Kuno, M. Solution-Based Straight and Branched CdSe Nanowires. *Chemistry of Materials*, **16**(25):5260–5272, 2004.

Gu, X. W., Shadmi, N., Yarden, T. S., Cohen, H., and Joselevich, E. Photoconductive CdSe Nanowire Arrays, Serpentines, and Loops Formed by Electrodeposition on Self-Organized Carbon Nanotubes. *The Journal of Physical Chemistry C*, **116**(37):20121–20126, 2012.

Gupta, M., Sharma, V., Shrivastava, J., Solanki, A., Singh, A. P., Satsangi, V. R., Dass, S., and Shrivastav, R. Preparation and Characterization of Nanostructured ZnO Thin Films for Photoelectrochemical Splitting of Water. *Bulletin of Materials Science*, **32**(1):23–30, 2009.

Haehnel, V., Fähler, S., Schaaf, P., Miglierini, M., Mickel, C., Schultz, L., and Schlörb, H. Towards Smooth and Pure Iron Nanowires Grown by Electrodeposition in Self-Organized Alumina Membranes. *Acta Materialia*, **58**(7):2330–2337, 2010.

He, Z., Jie, J., Zhang, W., Zhang, W., Luo, L., Fan, X., Yuan, G., Bello, I., and Lee, S. T. Tuning Electrical and Photoelectrical Properties of CdSe Nanowires via Indium Doping. *Small*, **5**(3):345–350, 2009.

Hoar, T. P. and Mott, N. F. A Mechanism for the Formation of Porous Anodic Oxide Films on Aluminium. *Journal of Physics and Chemistry of Solids*, **9**(2):97–99, 1959.

Hochbaum, A. I. and Yang, P. Semiconductor Nanowires for Energy Conversion. *Chemical Reviews*, **110**(1):527–546, 2009.

Hodes, G., Manassen, J., and Cahen, D. Photoelectrochemical Energy Conversion and Storage Using Polycrystalline Chalcogenic Electrodes. *Nature*, **261**:403, 1976.

Hodes, G., Manassen, J., Neagu, S., Cahen, D., and Mirovsky, Y. Electroplated Cadmium Chalcogenide Layers: Characterization and Use in Photoelectrochemical Solar Cells. *Thin Solid Films*, **90**(4): 433–438, 1982.

Hu, J., Odom, T. W., and Lieber, C. M. Chemistry and Physics in One Dimension: Synthesis and Properties of Nanowires and Nanotubes. *Accounts of Chemical Research*, **32**(5):435–445, 1999.

Hulteen, J. C. and Martin, C. R. A General Template-Based Method for the Preparation of Nanomaterials. *Journal of Materials Chemistry*, **7**(7):1075–1087, 1997.

Hurst, S. J., Payne, E. K., Qin, L., and Mirkin, C. A. Multisegmented One-Dimensional Nanorods Prepared by Hard-Template Synthetic Methods. *Angewandte Chemie International Edition*, **45**(17): 2672–2692, 2006.

Iijima, S. Helical Microtubules of Graphitic Carbon. *Nature*, **354**(6348):56–58, 1991.

Ismail, A. A. and Bahnemann, D. W. Photochemical Splitting of Water for Hydrogen Production by Photocatalysis: A Review. *Solar Energy Materials and Solar Cells*, **128**:85–101, 2014.

Kalhori, H., Irajizad, A., Azarian, A., and Ashiri, R. Synthesis and Characterization of Electrochemically Grown CdSe Nanowires with Enhanced Photoconductivity. *Journal of Materials Science: Materials in Electronics*, **26**(3):1395–1402, 2015.

Kazacos, M. S. and Miller, B. Studies in Selenious Acid Reduction and CdSe Film Deposition. *Journal of the Electrochemical Society*, **127**(4):869–873, 1980.

Keller, F., Hunter, M. S., and Robinson, D. L. Structural Features of Oxide Coatings on Aluminum. *Journal of the Electrochemical Society*, **100**(9):411–419, 1953.

Khandelwal, A., Jena, D., Grebinski, J. W., Hull, K. L., and Kuno, M. K. Ultrathin CdSe Nanowire Field-Effect Transistors. *Journal of Electronic Materials*, **35**(1):170–172, 2006.

Kim, H.-C., Park, S.-M., and Hinsberg, W. D. Block Copolymer Based Nanostructures: Materials, Processes, and Applications to Electronics. *Chemical Reviews*, **110**(1):146–177, 2009a.

Kim, K., Kwon, N., Hong, J., and Chung, I. Fabrication and Characterization of Metal-Semiconductor-Metal Nanorod Using Template Synthesis. *Journal of Vacuum Science and Technology A*, **27**(4), 2009b.

Kim, S. H., Lee, J. Y., Han, W. K., and Lee, J. H. Electrochemical Deposition of CdSe/CdTe Multilayer Nanorods for Hybrid Solar Cell. *Thin Solid Films*, **518**(24):7222–7224, 2010.

Klein, J. D., Herrick, R. D., Palmer, D., Sailor, M. J., Brumlik, C. J., and Martin, C. R. Electrochemical Fabrication of Cadmium Chalcogenide Microdiode Arrays. *Chemistry of Materials*, **5**(7):902–904, 1993.

Kline, T. R., Tian, M., Wang, J., Sen, A., Chan, M. W. H., and Mallouk, T. E. Template-Grown Metal Nanowires. *Inorganic Chemistry*, **45**(19):7555–7565, 2006.

Kressin, A. M., Doan, V. V., Klein, J. D., and Sailor, M. J. Synthesis of Stoichiometric Cadmium Selenide Films via Sequential Monolayer Electrodeposition. *Chemistry of Materials*, **3**(6):1015–1020, 1991.

Kudo, A. and Miseki, Y. Heterogeneous Photocatalyst Materials for Water Splitting. *Chemical Society Reviews*, **38**(1):253–278, 2009.

Kum, M. C., Yoo, B. Y., Rheem, Y. W., Bozhilov, K. N., Chen, W., Mulchandani, A., and Myung, N. V. Synthesis and Characterization of Cadmium Telluride Nanowire. *Nanotechnology*, **19**(32): 325711, 2008.

Kung, S. C., Van der Veer, W. E., Yang, F., Donavan, K. C., and Penner, R. M. 20 μs Photocurrent Response from Lithographically Patterned Nanocrystalline Cadmium Selenide Nanowires. *Nano Letters*, **10**(4):1481–1485, 2010.

Kung, S. C., Xing, W., Van der Veer, W. E., Yang, F., Donavan, K. C., Cheng, M., Hemminger, J. C., and Penner, R. M. Tunable Photoconduction Sensitivity and Bandwidth for Lithographically Patterned Nanocrystalline Cadmium Selenide Nanowires. *ACS Nano*, **5**(9):7627–7639, 2011.

Lee, J., Mubeen, S., Hernandez-Sosa, G., Sun, Y., Toma, F. M., Stucky, G. D., and Moskovits, M. High-Efficiency Panchromatic Hybrid Schottky Solar Cells. *Advanced Materials*, **25**(2):256–260, 2013.

Li, Q., Brown, M. A., Hemminger, J. C., and Penner, R. M. Luminescent Polycrystalline Cadmium Selenide Nanowires Synthesized by Cyclic Electrodeposition/Stripping Coupled with Step Edge Decoration. *Chemistry of Materials*, **18**(15):3432–3441, 2006.

Li, X., Wang, Y., Song, G., Peng, Z., Yu, Y., She, X., and Li, J. Synthesis and Growth Mechanism of Ni Nanotubes and Nanowires. *Nanoscale Research Letters*, **4**(9):1015–1020, 2009.

Lin, S. W., Chang, S. C., Liu, R. S., Hu, S. F., and Jan, N. T. Fabrication and Magnetic Properties of Nickel Nanowires. *Journal of Magnetism and Magnetic Materials*, **282**:28–31, 2004.

Lincot, D. Electrodeposition of Semiconductors. *Thin Solid Films*, **487**(1):40–48, 2005.

Liu, R. *Template Synthesized Nanotubes, Nanowires and Heterogeneous Coaxial Nanowires for Electrochemical Energy Storage*. PhD thesis, University of Maryland, 2009.

Lu, W. and Lieber, C. M. Semiconductor Nanowires. *Journal of Physics D: Applied Physics*, **39**(21): R387, 2006.

Ma, C. and Wang, Z. L. Road Map for the Controlled Synthesis of CdSe Nanowires, Nanobelts, and Nanosaws - A Step Towards Nanomanufacturing. *Advanced Materials*, **17**(21):2635–2639, 2005.

Maeda, K. Z-Scheme Water Splitting Using Two Different Semiconductor Photocatalysts. *ACS Catalysis*, **3**(7):1486–1503, 2013.

Mai, L., Tian, X., Xu, X., Chang, L., and Xu, L. Nanowire Electrodes for Electrochemical Energy Storage Devices. *Chemical Reviews*, **114**(23):11828–11862, 2014.

Maijenburg, A. W., Maas, M. G., Rodijk, E. J. B., Ahmed, W., Kooij, E. S., Carlen, E. T., Blank, D. H. A., and Elshof, J. E. T. Dielectrophoretic Alignment of Metal and Metal Oxide Nanowires and Nanotubes: A Universal Set of Parameters for Bridging Prepatterned Microelectrodes. *Journal of Colloid and Interface Science*, **355**(2):486–493, 2011a.

Maijenburg, A. W., Rodijk, E. J. B., Maas, M. G., Enculescu, M., Blank, D. H. A., and Elshof, J. E. T. Hydrogen Generation from Photocatalytic Silver–Zinc Oxide Nanowires: Towards Multifunctional Multisegmented Nanowire Devices. *Small*, **7**(19):2709–2713, 2011b.

Maijenburg, A. W., George, A., Samal, D., Nijland, M., Besselink, R., Kuiper, B., Kleibeuker, J. E., and Elshof, J. E. T. Electrodeposition of Micropatterned Ni–Pt Multilayers and Segmented Ni–Pt–Ni Nanowires. *Electrochimica Acta*, **81**:123–128, 2012.

Martin, C. R. Nanomaterials: A Membrane-Based Synthetic Approach. *Science*, **266**:1961–1966, 1994.

Martin, C. R. Template Synthesis of Electronically Conductive Polymer Nanostructures. *Accounts of Chemical Research*, **28**(2):61–68, 1995.

Martin, C. R. Membrane-Based Synthesis of Nanomaterials. *Chemistry of Materials*, **8**(8):1739–1746, 1996.

Masuda, H. Highly Ordered Nanohole Arrays in Anodic Porous Alumina. In *Ordered Porous Nanostructures and Applications*, pages 37–55. Springer, 2005.

Masuda, H. and Fukuda, K. Ordered Metal Nanohole Arrays Made by a Two-Step Replication of Honeycomb Structures of Anodic Alumina. *Science*, **268**(5216):1466–1468, 1995.

Masuda, H. and Satoh, M. Fabrication of Gold Nanodot Array Using Anodic Porous Alumina as an Evaporation Mask. *Japanese Journal of Applied Physics*, **35**(1B):L126, 1996.

Masuda, H., Tanaka, H., and Baba, N. Preparation of Porous Material by Replacing Microstructure of Anodic Alumina Film with Metal. *Chemistry Letters*, (4):621–622, 1990.

Masuda, H., Nishio, K., and Baba, N. Fabrication of Porous $\mathrm{TiO_2}$ Films Using Two-Step Replication of Microstructure of Anodic Alumina. *Japanese Journal of Applied Physics*, **31**(12B):L1775, 1992.

Masuda, H., Nishio, K., and Baba, N. Preparation of Microporous Metal Membranes by Two-Step Replication of the Microstructure of Anodic Alumina. *Thin Solid Films*, **223**(1):1–3, 1993.

Masuda, H., Mizuno, T., Baba, N., and Ohmori, T. Fabrication of Pt Microporous Electrodes from Anodic Porous Alumina and Immobilization of GOD into their Micropores. *Journal of Electroanalytical Chemistry*, **368**(1):333–336, 1994.

Masuda, H., Hasegwa, F., and Ono, S. Self-Ordering of Cell Arrangement of Anodic Porous Alumina Formed in Sulfuric Acid Solution. *Journal of the Electrochemical Society*, **144**(5):L127–L130, 1997.

Masuda, H., Yada, K., and Osaka, A. Self-Ordering of Cell Configuration of Anodic Porous Alumina with Large-Size Pores in Phosphoric Acid Solution. *Japanese Journal of Applied Physics*, **37**(11A): L1340, 1998.

Menke, E. J., Li, Q., and Penner, R. M. Bismuth Telluride $(\mathrm{Bi_2Te_3})$ Nanowires Synthesized by Cyclic Electrodeposition/Stripping Coupled with Step Edge Decoration. *Nano Letters*, **4**(10):2009–2014, 2004.

Menke, E. J., Brown, M. A., Li, Q., Hemminger, J. C., and Penner, R. M. Bismuth Telluride $(\mathrm{Bi_2Te_3})$ Nanowires: Synthesis by Cyclic Electrodeposition/Stripping, Thinning by Electrooxidation, and Electrical Power Generation. *Langmuir*, **22**(25):10564–10574, 2006a.

Menke, E. J., Thompson, M. A., Xiang, C., Yang, L. C., and Penner, R. M. Lithographically Patterned Nanowire Electrodeposition. *Nature Materials*, **5**(11):914–919, 2006b.

Mishra, K. K. and Rajeshwar, K. A Re-Examination of the Mechanisms of Electrodeposition of CdX and ZnX (X= Se, Te) Semiconductors by the Cyclic Photovoltammetric Technique. *Journal of Electroanalytical Chemistry and Interfacial Electrochemistry*, **273**(1):169–182, 1989.

Mubeen, S., Singh, N., Lee, J., Stucky, G. D., Moskovits, M., and McFarland, E. W. Synthesis of Chemicals Using Solar Energy with Stable Photoelectrochemically Active Heterostructures. *Nano Letters*, **13**(5):2110–2115, 2013.

Napolskii, K. S., Eliseev, A. A., Yesin, N. V., Lukashin, A. V., Tretyakov, Y. D., Grigorieva, N. A., Grigoriev, S. V., and Eckerlebe, H. Ordered Arrays of Ni Magnetic Nanowires: Synthesis and Investigation. *Physica E: Low-dimensional Systems and Nanostructures*, **37**(1):178–183, 2007.

Navarro Y., R. M., Álvarez Galván, M. C., Del Valle, F., Villoria de la Mano, J. A., and Fierro, J. L. G. Water Splitting on Semiconductor Catalysts Under Visible-Light Irradiation. *ChemSusChem*, **2**(6): 471–485, 2009.

Nozik, A. J. Photochemical Diodes. *Applied Physics Letters*, **30**(11):567–569, 1977.

Osterloh, F. E. Inorganic Materials as Catalysts for Photochemical Splitting of Water. *Chemistry of Materials*, **20**(1):35–54, 2007.

O'sullivan, J. P. and Wood, G. C. The Morphology and Mechanism of Formation of Porous Anodic Films on Aluminium. In *Proceedings of the Royal Society of London A: Mathematical, Physical and Engineering Sciences*, volume 317, pages 511–543. The Royal Society, 1970.

Ozin, G. A. Nanochemistry: Synthesis in Diminishing Dimensions. *Advanced Materials*, **4**(10):612–649, 1992.

Pandey, R. K., Chandra, S., and Sahu, S. N. *Handbook of Semiconductor Electrodeposition*. M. Dekker, 1996.

Paunovic, M. and Schlesinger, M. *Fundamentals of Electrochemical Deposition*, chapter 5. John Wiley & sons, 2006.

Paxton, W. F., Kistler, K. C., Olmeda, C. C., Sen, A., St. Angelo, S. K., Cao, Y., Mallouk, T. E., Lammert, P. E., and Crespi, V. H. Catalytic Nanomotors: Autonomous Movement of Striped Nanorods. *Journal of the American Chemical Society*, **126**(41):13424–13431, 2004.

Pena, D. J., Razavi, B., Smith, P. A., Mbindyo, J. K., Natan, M. J., Mayer, T. S., Mallouk, T. E., and Keating, C. D. Electrochemical Synthesis of Multi-Material Nanowires as Building Blocks for Functional Nanostructures. In *MRS Proceedings*, volume 636, pages D4–6. Cambridge University Press, 2000.

Pena, D. J., Mbindyo, J. K. N., Carado, A. J., Mallouk, T. E., Keating, C. D., Razavi, B., and Mayer, T. S. Template Growth of Photoconductive Metal-CdSe-Metal Nanowires. *The Journal of Physical Chemistry B*, **106**(30):7458–7462, 2002.

Peng, Q., Dong, Y., Deng, Z., and Li, Y. Selective Synthesis and Characterization of CdSe Nanorods and Fractal Nanocrystals. *Inorganic Chemistry*, **41**(20):5249–5254, 2002.

Peng, X. S., Zhang, J., Wang, X. F., Wang, Y. W., Zhao, L. X., Meng, G. W., and Zhang, L. D. Synthesis of Highly Ordered CdSe Nanowire Arrays Embedded in Anodic Alumina Membrane by Electrodeposition in Ammonia Alkaline Solution. *Chemical Physics Letters*, **343**(5):470–474, 2001.

Penner, R. M. and Martin, C. R. Preparation and Electrochemical Characterization of Ultramicroelectrode Ensembles. *Analytical Chemistry*, **59**(21):2625–2630, 1987.

Piraux, L., Encinas, A., Vila, L., Mátéfi-Tempfli, S., Mátéfi-Tempfli, M., Darques, M., Elhoussine, F., and Michotte, S. Magnetic and Superconducting Nanowires. *Journal of Nanoscience and Nanotechnology*, **5**(3):372–389, 2005.

Possin, G. E. A Method for Forming Very Small Diameter Wires. *Review of Scientific Instruments*, **41** (5):772–774, 1970.

Preston, C. K. and Moskovits, M. Optical Characterization of Anodic Aluminum Oxide Films Containing Electrochemically Deposited Metal Particles. 1. Gold in Phosphoric Acid Anodic Aluminum Oxide Films. *The Journal of Physical Chemistry*, **97**(32):8495–8503, 1993.

Qu, Y. and Duan, X. Highly Efficient Photocatalysts from Nanoscale Metal/Semiconductor/Metal Heterojunctions. *ECS Transactions*, **33**(9):23–38, 2010.

Qu, Y. and Duan, X. One-Dimensional Homogeneous and Heterogeneous Nanowires for Solar Energy Conversion. *Journal of Materials Chemistry*, **22**(32):16171–16181, 2012.

Qu, Y. and Duan, X. Progress, Challenge and Perspective of Heterogeneous Photocatalysts. *Chemical Society Reviews*, **42**(7):2568–2580, 2013.

Qu, Y., Liao, L., Cheng, R., Wang, Y., Lin, Y. C., Huang, Y., and Duan, X. Rational Design and Synthesis of Freestanding Photoelectric Nanodevices as Highly Efficient Photocatalysts. *Nano Letters*, **10**(5):1941–1949, 2010.

Riveros, G., Gomez, H., Cortes, A., Marotti, R. E., and Dalchiele, E. A. Crystallographically-Oriented Single-Crystalline Copper Nanowire Arrays Electrochemically Grown into Nanoporous Anodic Alumina Templates. *Applied Physics A*, **81**(1):17–24, 2005.

Riveros, G., Vásquez, J., Gómez, H., Makarova, T., Silva, D., Marotti, R. E., and Dalchiele, E. A. Single-Step Electrodeposition of Polycrystalline CdSe Microwire Arrays: Structural and Optical Properties. *Applied Physics A*, **90**(3):423–430, 2008.

Roder, H., Hahn, E., Brune, H., Bucher, J. P., and Kern, K. Building One-Dimensional and 2-Dimensional Nanostructures by Diffusion-Controlled Aggregation at Surfaces. *Nature*, **366**:141–143, 1993.

Sanders, B. W. and Cocivera, M. Characterization of Cadmium Selenide Electrodeposited from Diethylene Glycol Solution Containing Tri-n-Butylphosphine Selenide. *Journal of the Electrochemical Society*, **134**(5):1075–1080, 1987.

Schierhorn, M., Boettcher, S. W., Ivanovskaya, A., Norvell, E., Sherman, J. B., Stucky, G. D., and Moskovits, M. Fabrication and Electrochemical Photovoltaic Response of CdSe Nanorod Arrays. *The Journal of Physical Chemistry C*, **112**(23):8516–8520, 2008.

Schierhorn, M., Boettcher, S. W., Kraemer, S., Stucky, G. D., and Moskovits, M. Photoelectrochemical Performance of CdSe Nanorod Arrays Grown on a Transparent Conducting Substrate. *Nano Letters*, **9**(9):3262–3267, 2009.

Schierhorn, M., Boettcher, S. W., Peet, J. H., Matioli, E., Bazan, G. C., Stucky, G. D., and Moskovits, M. CdSe Nanorods Dominate Photocurrent of Hybrid CdSe-P3HT Photovoltaic Cell. *ACS Nano*, **4** (10):6132–6136, 2010.

Schlesinger, M. and Paunovic, M. *Modern Electroplating*, volume 55. John Wiley & Sons, 2011.

Sellmyer, D. J., Zheng, M., and Skomski, R. Magnetism of Fe, Co and Ni Nanowires in Self-Assembled Arrays. *Journal of Physics: Condensed Matter*, **13**(25):R433, 2001.

Senthilkumar, S., Adisa, A., Saraswathi, R., and Dryfe, R. A. W. Electrodeposition within Zeolite Membrane Hosts. *Electrochemistry Communications*, **10**(1):141–145, 2008.

Shan, C. X., Liu, Z., and Hark, S. K. CdSe Nanowires with Controllable Growth Orientations. *Applied Physics Letters*, **90**(19):193123, 2007.

Shen, C. M., Zhang, X. G., and Li, H. L. Effect of pH on the Electrochemical Deposition of Cadmium Selenide Nanocrystal Films. *Materials Science and Engineering: B*, **84**(3):265–270, 2001.

Shen, C. M., Zhang, X. G., and Li, H. L. Influence of Different Deposition Potentials on Morphology and Structure of CdSe Films. *Applied Surface Science*, **240**(1):34–41, 2005.

Shpaisman, N., Givan, U., and Patolsky, F. Electrochemical Synthesis of Morphology-Controlled Segmented CdSe Nanowires. *ACS Nano*, **4**(4):1901–1906, 2010.

Silk, E. C. H. and Barnes, R. S. Examination of Fission Fragment Tracks with an Electron Microscope. *Philosophical Magazine*, **4**(44):970–972, 1959.

Şişman, I. Template-Assisted Electrochemical Synthesis of Semiconductor Nanowires. In *Nanowires–Implementations and Applications*, pages 41–58. InTech, 2011.

Skinner, K., Dwyer, C., and Washburn, S. Quantitative Analysis of Individual Metal-CdSe-Metal Nanowire Field-Effect Transistors. *Applied Physics Letters*, **92**(11):112105, 2008.

Strijkers, G. J., Dalderop, J. H. J., Broeksteeg, M. A. A., Swagten, H. J. M., and De Jonge, W. J. M. Structure and Magnetization of Arrays of Electrodeposited Co Wires in Anodic Alumina. *Journal of Applied Physics*, **86**(9):5141–5145, 1999.

Sun, X. Y., Xu, F. Q., Li, Z. M., and Zhang, W. H. Cyclic Voltammetry for the Fabrication of High Dense Silver Nanowire Arrays with the Assistance of AAO Template. *Materials Chemistry and Physics*, **90**(1):69–72, 2005.

Talin, A. A., Léonard, F., Katzenmeyer, A. M., Swartzentruber, B. S., Picraux, S. T., Toimil-Molares, M. E., Cederberg, J. G., Wang, X., Hersee, S. D., and Rishinaramangalum, A. Transport Characterization in Nanowires Using an Electrical Nanoprobe. *Semiconductor Science and Technology*, **25**(2): 024015, 2010.

Tang, X. T., Wang, G. C., and Shima, M. Layer Thickness Dependence of CPP Giant Magnetoresistance in Individual Co Ni/ Cu Multilayer Nanowires Grown by Electrodeposition. *Physical Review B*, **75** (13):134404, 2007.

Thelander, C., Agarwal, P., Brongersma, S., Eymery, J., Feiner, L. F., Forchel, A., Scheffler, M., Riess, W., Ohlsson, B. J., Gösele, U., and Samuelson, L. Nanowire-Based One-Dimensional Electronics. *Materials Today*, **9**(10):28–35, 2006.

Toimil-Molares, M. E. Characterization and Properties of Micro-and Nanowires of Controlled Size, Composition, and Geometry Fabricated by Electrodeposition and Ion-Track Technology. *Beilstein Journal of Nanotechnology*, **3**(1):860–883, 2012.

Tomkiewicz, M., Ling, I., and Parsons, W. S. Morphology, Properties, and Performance of Electrodeposited n-CdSe in Liquid Junction Solar Cells. *Journal of the Electrochemical Society*, **129**(9): 2016–2022, 1982.

Tong, H., Ouyang, S., Bi, Y., Umezawa, N., Oshikiri, M., and Ye, J. Nano-Photocatalytic Materials: Possibilities and Challenges. *Advanced Materials*, **24**(2):229–251, 2012.

Tongying, P., Plashnitsa, V. V., Petchsang, N., Vietmeyer, F., Ferraudi, G. J., Krylova, G., and Kuno, M. Photocatalytic Hydrogen Generation Efficiencies in One-Dimensional CdSe Heterostructures. *The Journal of Physical Chemistry Letters*, **3**(21):3234–3240, 2012.

Tonucci, R. J., Justus, B. L., Campillo, A. J., and Ford, C. E. Nanochannel Glass Arrays. *Science*, **258**: 783–785, 1992.

Vayssieres, L. Growth of Arrayed Nanorods and Nanowires of ZnO from Aqueous Solutions. *Advanced Materials*, **15**(5):464–466, 2003.

Wang, D., Zhou, W. L., McCaughy, B. F., Hampsey, J. E., Ji, X., Jiang, Y. B., Xu, H., Tang, J., Schmehl, R. H., O'Connor, C., Brinker, C. J., and Lu, Y. Electrodeposition of Metallic Nanowire Thin Films Using Mesoporous Silica Templates. *Advanced Materials*, **15**(2):130–133, 2003.

Wang, J. G., Tian, M. L., Kumar, N., and Mallouk, T. E. Controllable Template Synthesis of Superconducting Zn Nanowires with Different Microstructures by Electrochemical Deposition. *Nano Letters*, **5**(7):1247–1253, 2005.

Wang, Y., Zhao, H., Hu, Y., Ye, C., and Zhang, L. Thermal Expansion Behavior of Hexagonal Zn Nanowires. *Journal of Crystal Growth*, **305**(1):8–11, 2007.

Warren, S. C. and Thimsen, E. Plasmonic Solar Water Splitting. *Energy & Environmental Science*, **5** (1):5133–5146, 2012.

Whitney, T. M., Searson, P. C., Jiang, J. S., and Chien, C. L. Fabrication and Magnetic Properties of Arrays of Metallic Nanowires. *Science*, **261**(5126):1316–1319, 1993.

Wu, Z., Zhang, Y., and Du, K. A Simple and Efficient Combined AC–DC Electrodeposition Method for Fabrication of Highly Ordered Au Nanowires in AAO Template. *Applied Surface Science*, **265**: 149–156, 2013.

Xia, Y., Yang, P., Sun, Y., Wu, Y., Mayers, B., Gates, B., Yin, Y., Kim, F., and Yan, H. One-Dimensional Nanostructures: Synthesis, Characterization, and Applications. *Advanced Materials*, **15** (5):353–389, 2003.

Xiang, Q., Yu, J., and Jaroniec, M. Graphene-Based Semiconductor Photocatalysts. *Chemical Society Reviews*, **41**(2):782–796, 2012.

Xing, W., Kung, S. C., Van der Veer, W. E., Yan, W., Ayvazian, T., Kim, J. Y., and Penner, R. M. High-Throughput Fabrication of Photoconductors with High Detectivity, Photosensitivity, and Bandwidth. *ACS Nano*, **6**(6):5627–5634, 2012.

Yan, R., Gargas, D., and Yang, P. Nanowire Photonics. *Nature Photonics*, **3**(10):569–576, 2009.

Yang, P., Zhao, D., Margolese, D. I., Chmelka, B. F., and Stucky, G. D. Generalized syntheses of large-pore mesoporous metal oxides with semicrystalline frameworks. *Nature*, **396**(6707):152–155, 1998.

Young, D. A. Etching of Radiation Damage in Lithium Fluoride. *Nature*, **182**, 1958.

Zhang, X., Li, D., Bourgeois, L., Wang, H., and Webley, P. A. Direct Electrodeposition of Porous Gold Nanowire Arrays for Biosensing Applications. *ChemPhysChem*, **10**(2):436–441, 2009.

Zhang, Z., Yao, K., Liu, Y., Jin, C., Liang, X., Chen, Q., and Peng, L. M. Quantitative Analysis of Current–Voltage Characteristics of Semiconducting Nanowires: Decoupling of Contact Effects. *Advanced Functional Materials*, **17**(14):2478–2489, 2007.

Zhao, G. Y., Xu, C. L., Guo, D. J., Li, H., and Li, H. L. Template Preparation of Pt Nanowire Array Electrode on Ti/Si Substrate for Methanol Electro-Oxidation. *Applied Surface Science*, **253** (6):3242–3246, 2007.